Bringing service to life

serco

Thermal Analysis of the SAFKEG LS Design

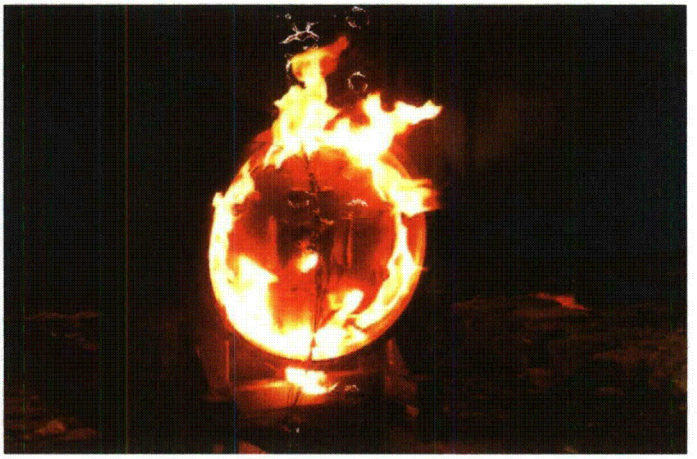

Prepared for	Croft Associates Limited
Prepared by	Serco
Your Reference	Croft Project No 06/08/10
Our Reference	SERCO/TAS/5388/001 Issue 2
Classification	SERCO COMMERCIAL

July 2009

Design | Advise | Integrate | Deliver

Title	Thermal Analysis of the SAFKEG LS Design
Prepared for	Croft Associates Limited
Your Reference	Croft Project No 06/08/10
Our Reference	SERCO/TAS/5388/001 Issue 2
Confidentiality, copyright and reproduction	SERCO COMMERCIAL This report is submitted by Serco Technical & Assurance Services (hereafter referred to as Serco) in connection with a contract to supply goods and/or services and is submitted only on the basis of strict confidentiality. The contents must not be disclosed to third parties other than in accordance with the terms of the contract. To minimise our impact on the environment, Serco prints on 100% recycled paper
Contact Details	Serco A32 Winfrith Dorchester Dorset DT2 8DH Telephone 01305 851159 Facsimile 01305 851105 E-mail chris.fry@sercoassurance.com www.serco.com/technicalassurance

	Name	Signature	Date
Author(s)	C J Fry	C J Fry	27/7/09
Reviewed by	N Butler	N Butler	27/7/09
Approved by	D W Sweet	D W Sweet	27/7/09

Executive Summary

The thermal performance of the SAFKEG LS design of transport container has been analysed using an axi-symmetric finite element model.

The model was first validated by comparison against experimental data from a self heating test and a furnace test. Good agreement was obtained with the results of the self heating test and comparison against the results of the furnace test demonstrate the model to be pessimistic.

The temperature of the container has been predicted under normal conditions of transport, both with and without solar insolation. The calculations were carried out with internal heat loads of 0W, 3W, 6W and 10W. The temperature at the inner containment vessel lid seal, with an internal heat load of 10W, is calculated to be 94°C without solar insolation and 116°C with solar insolation.

The temperature of the container has been predicted during the thermal (fire) test, with internal heat loads of 0W, 3W, 6W and 10W. The inner containment vessel lid seal, with an internal heat load of 10W, is predicted to reach a maximum temperature of 183°C.

Contents

1 Introduction

The SAFKEG LS design is a general purpose container for transporting modest quantities of radioactive material. It consists of an outer keg and an inner containment vessel, as illustrated in Figure 1. The outer keg is 'beer barrel' in shape, ~0.5m high and ~0.4m diameter and consists basically of a stainless steel shell filled with cork which provides protection from impacts and fire. The containment vessel is cylindrical in shape, ~0.20m high and ~0.12m diameter. It is also constructed from stainless steel and has a lid at the top. Both the body and lid of the containment vessel contain lead shielding. An elastomeric seal is used to provide sealing between the inner containment vessel body and lid. The inner containment vessel, when placed inside the keg, is surrounded by a further layer of cork.

The SAFKEG LS is designed as a type B(U) package and to meet all the requirements of a B(U) package as specified in the 10CFR71 Transport Regulations [1] with an internal heat load up to 10W. This report presents a thermal assessment of the SAFKEG LS design which has been performed in order to demonstrate that the package satisfies all the thermal performance requirements of the 10CFR71 Regulations.

The thermal assessment is based upon finite element modelling. The model is described in Section 2. The model has been validated by comparison against both an experimental self heating test (normal conditions of transport) and a furnace test (fire test at 800 °C). This validation is described in Section 3. The model is then used to determine temperatures both under normal conditions of transport and during the fire accident, as specified in the 10CFR71 Regulations [1]. These are described in Sections 4 and 5 respectively.

2 Description of the Model

2.1 Geometry

The SAFKEG LS package design is almost axi-symmetric. The main features which are not axi-symmetric are:

- The bolts fastening the keg lid
- The handle on the top of the keg lid
- Finger holes in the top cork
- The bolts in the containment vessel lid
- Location and lifting points in the containment vessel lid

None of these features was considered to be significant with respect to heat transfer. An axi-symmetric model has therefore been used for the thermal assessment. The axi-symmetric model is shown in Figure 2. The model explicitly represents:

- The keg outer skin
- The keg inner liner
- The cork filling the keg (between the inner liner and outer skin)
- The top cork within the keg cavity
- The side cork within the keg cavity
- The inner containment vessel
- The lead shielding in the inner containment vessel

A 3-dimensional, cut-away, view of what the model represents is shown in Figure 3.

The model, which contains 5209 nodes and 2538 elements, was generated using the Abaqus code [2]. Each of the components listed above is generated separately and joined, thermally, using tied constraints or interactions (representing narrow air gaps). The thin outer skin of the keg was

modelled using 'shell' elements while all the other components were modelled using solid elements. The drawings on which the model is based are listed in Appendix 1.

2.2 Materials

The following materials are represented in the model:

- Stainless steel
- Cork
- Lead

The thermal properties for each of these materials used in the model are described in the following sections.

2.2.1 Stainless steel

Type 304L stainless steel is used to construct the outer and inner skins and lid of the keg and the inner containment vessel and lid. The thermal properties used for type 304L stainless steel, and their sources, are shown in Table 1.

Radiation is an important heat transfer mechanism. The emissivity of the stainless steel surfaces, under different conditions, assumed in the model is shown in Table 2. The emissivity of stainless steel can vary significantly depending upon surface finish and level of oxidation. Good agreement with the measured temperatures in the steady state heating test was obtained with an assumed emissivity of the external keg surface of 0.4 (Section 3.1). This value, while well within the range of possible values, is higher than the reference value of 0.25. To ensure that the model is pessimistic, the lower, reference, value was used in the calculation of temperatures during normal conditions of transport.

2.2.2 Cork

Resin bonded cork surrounds the inner containment vessel. Croft have had measurements made at temperatures up to 108°C and the results of these are shown in Figure 4.

During the fire the cork will experience temperatures up to ~800°C. No measurements of cork properties at high temperatures are available. However, a furnace test has been performed on the SAFKEG LS container design. This test has been simulated using the model in order to validate the model and, in particular, demonstrate the acceptability of the thermal properties assumed for the cork. It was found that, in order to obtain agreement with the measured temperatures, the thermal conductivity of the cork needed to be increased by 50% This is described in Section 3.2. It should be noted that these thermal properties, validated against the furnace test, are 'effective' properties that include any effects of charring and shrinkage of the cork.

A self heating test performed on the SAFKEG LS design has also been simulated using the model. This is described in Section 3.1. It was found that, to produce the best agreement with the measured temperatures, the thermal conductivity of the cork needed to be reduced by 15% (as described in Section 3.1 and shown on Figure 4). Because cork is a natural material, this degree of variation in conductivity may well be possible. To ensure that all the calculations performed with the model are pessimistic, the lower, fitted conductivity has been assumed for the calculations of temperature during normal transport and the higher thermal conductivity assumed for the calculations of temperature during the fire accident.

2.2.3 Lead

The shielding inside the containment vessel body and lid is provided by 4% antimonial lead. The thermal properties used for this material, and their sources, are shown in Table 1.

2.3 Boundary Conditions

2.3.1 Natural Convection from Exterior Surfaces

Well established correlations for natural convection heat transfer coefficient have been applied at the outer surface of the keg. Several separate correlations were used depending upon the surface being considered and the container orientation:

- Outside of a vertical cylinder (the side of the keg when vertical)
- Horizontal plate (top of the keg when vertical)
- Vertical plate (top and bottom of the keg when horizontal)
- Outside of a horizontal cylinder (the side of the keg when horizontal)

Details of the correlation used are given in Appendix 2.

The heat transfer coefficients used to model convective heat transfer in the heating phase of the furnace test and fire accident are described in Sections 3.2 and 5 respectively.

2.3.2 Radiation from Exterior Surfaces

Heat loss by thermal radiation was modelled from all the outer surfaces. The emissivity assumed for the surface of the keg is shown in Table 2.

The top of the keg and the inner surfaces of the top skirt form an open cavity. In the calculations simulating normal transport, radiation exchange between these surfaces, and to ambient, were modelled (including the reflection of radiation). The same exchanges of radiation were modelled at the bottom of the keg when the keg was horizontal. When the keg was vertical, radiation exchange between the bottom of the keg and the skirt was again modelled but there was no net loss of heat as the keg was assumed to be sat upon an insulating surface.

In the calculations simulating the fire accident, the flames were pessimistically assumed to fill the cavity inside the skirt at either end of the keg and all surfaces were assumed to receive radiation directly from the flames. The flames were assumed to have an emissivity of 1.0 which satisfies the 'minimum average flame emissivity coefficient of 0.9' specified in the 10CFR71 Regulations [1].

2.3.3 Internal Heat Load

The heat generated by the package contents was represented in the model as a uniform heat flux applied over the side, top and bottom of the cavity inside the containment vessel. The package contents themselves were not represented in the NCT and fire accident models since:

- The assessment is intended to be general and not specific to one type and geometry of contents
- Omitting the contents from the fire accident calculation is pessimistic as it minimises the thermal capacity of the package.

In the calculations used to validate the model against the self heating test and furnace test, changes were made to the model to more accurately represent the contents (described in Section 3).

2.3.4 Narrow Gaps

Narrow air gaps are present in several locations in the model:

- Between the keg body and the cork
- Between the keg lid and the cork
- Between the keg inner liner and the cork
- Between the keg inner liner and the keg lid
- Between the cork and the containment vessel

The thickness of these gaps was obtained from the drawings. Even when surfaces are in contact (particularly a rough surfaces such as that of cork) a contact resistance will exist which can be represented as an air gap. Justification for the assumed gaps was obtained through validation of the model against test data (described in section 3).

Across each air gap heat transfer by both conduction and thermal radiation was represented in the model.

2.3.5 Radiation across Open Spaces

The package design creates a number of small cavities across which radiation heat transfer will occur (in such small cavities heat transfer by conduction and convection is expected to be negligible). In these cavities radiation exchange between all the surfaces is modelled. The view factor from each element to each other element in the cavity is determined and radiation heat transfer, including the effect of reflection, is then calculated.

2.3.6 Solar Insolation

The 10CFR71 Regulations [1] require that the effect of solar insolation is considered and specify the incident heat fluxes on various orientations of surfaces which should be assumed for a Type B(U) package. The regulations specify that the solar insolation should be considered for 12 hours each day. In order to determine the maximum temperature of the container under normal conditions of transport, a transient calculation was therefore performed with the heat flux from solar insolation turned on or off every 12 hours. The insolation flux incident on each surface is summarised in Table 3.

The Regulations specify the incident radiation flux. In order to determine the absorbed heat flux from solar insolation a surface absorptivity must also be defined. No data is readily available on the absorptivity of bead-blasted type 304 stainless steel to short wavelength radiation. A pessimistically high absorptivity to solar radiation of 0.8 was therefore assumed.

3 Validation of the Model

3.1 Normal Conditions of Transport

Measurements of container temperatures under normal conditions of transport with no solar insolation have been made by Croft [3]. The heat source in this test, 10W, was provided by cartridge heaters inside an aluminium block located inside the cavity inside the inner containment vessel. The container was placed vertically upon a wooden board covered in aluminium foil (approximating an insulating surface) in a room where the ambient temperature was relatively constant. The test ran for around three days with the temperatures being measured every minute. The measured temperatures over the final 12 hours have been averaged to obtain the 'steady state' temperatures. Further measurements were subsequently made with the container horizontal and also with a heat load of 20W (vertical).

Seven thermocouples were used to measure the temperature of the heater block, the outside of the containment vessel and the inside and outside of the keg. An additional thermocouple was used to measure the ambient temperature in the room. Once equilibrium conditions had been achieved, a contact thermometer was used to measure the temperature at various locations on the outside of the keg. Full details of the test are given in [3].

The finite element model was modified to represent the heating test. The required modification involved:

- Addition of the aluminium heater block
- Representation of heat into the heater block
- Changing the ambient temperature to that measured in the test (24.1°C)

The heater block is fitted inside the containment vessel with just a small air gap around it. Heat transfer by conduction and radiation was simulated in this air gap.

The predicted temperatures on the outside of the keg were in reasonable agreement with the measured values but the temperature of the containment vessel was initially underestimated. The calculation showed that, as expected, the majority of the temperature difference between the containment vessel and the outer surface of the keg results from heat transfer through the cork. It was therefore concluded that the low predicted containment vessel temperature was probably due to the thermal conductivity of the cork being lower than assumed in the model. The calculation was therefore repeated with the thermal conductivity of the cork reduced by 15%. Such a variation in thermal conductivity is considered possible in a natural material such as cork.

The external surface temperature was also initially moderately overestimated. The assumed value of the surface emissivity was therefore increased from the reference value of 0.25 to 0.4. The emissivity of stainless steel can vary significantly depending upon the surface condition (e.g. level of oxidation) and a value of 0.4 is well within the range of possible values.

The predicted temperatures in the repeat calculation are in good agreement with those measured in the test. The predicted temperature profile is shown in Figure 5 and it can be seen that, as expected, the highest temperatures occur in the heater block and inner containment vessel and high temperature gradients are generated in the cork. The predicted temperatures are compared against those measured in the test in Figure 6. The temperatures initially predicted by the model are also shown on this Figure. The predicted temperatures agree with the temperatures measured by the fixed thermocouples to within 1.2°C. The predicted temperature on the outside of the keg, at the bottom, is around 2°C higher than the measured values. This is probably due to the board on the which the container was sitting being modelled as perfectly insulating whereas, in practice, there is some heat loss through the board.

3.2 Fire Accident

Measurements of container temperatures under fire accident conditions have been made by Croft [3]. A SAFKEG LS container, which had first been subjected to a series of 10CFR71 Regulatory impact tests, was placed horizontally inside a furnace for 49 minutes and then removed and allowed to cool naturally. This furnace test satisfied all the requirements of the 10CFR71 Regulations [1] for a practical fire accident test.

The container was instrumented with eight thermocouples:

- Two on the inner containment vessel lid
- Four on the outside of the keg, around its 'waist'
- One on the lid of the keg
- One attached to the frame supporting the container

The inner containment vessel and inside of the keg were also instrumented with temperature sensitive strips. The inner containment vessel was filled with a tungsten insert and 42g of lead shot (to simulate the mass of the contents during the impact tests).

The finite element model was modified to represent the furnace test. The required modification involved:

- Addition of the tungsten insert and lead shot inside the inner containment vessel
- Changing the boundary conditions

The lead shot was represented as a solid material filling the cavity inside the tungsten insert. The lead shot was included in the model representing the furnace test as this will maximise the thermal capacity of the container and hence minimise the predicted temperature rise. In contrast, the contents are not represented in model used to model fire accident conditions (Section 5) in order to pessimistically maximise the predicted temperature rise under fire accident conditions. There was

assumed to be good heat transfer between the sides, top and bottom of the containment vessel and the tungsten insert and between the tungsten insert and the lead shot. These are pessimistic assumptions since they will tend to minimise the temperature increase predicted by the model (and hence reduce the level of conservatism compared to the measured data). The density of the lead shot material was adjusted to give a total mass of 42g

During the heating phase of the furnace test all exterior surfaces of the keg were assumed to receive heat by forced convection and radiation from the furnace. A convection coefficient of $10W/m^2/K$ was assumed (the value suggested in the Advisory Material for the IAEA Regulations [4]). The absorptivity of the surface of the keg was assumed to be 0.8 (the value specified in the 10CFR71 Regulations [1]). It was recognised that the predicted temperature of the inner containment vessel would be insensitive to these heat transfer boundary conditions because the exterior skin of the keg, which has very little thermal capacity, will rapidly rise to near the temperature of the furnace.

The SAFKEG LS container was placed inside the furnace by removing its lid and this resulted in the furnace being significantly cooler than 800°C when the container is first placed inside. This is why the container was inside the furnace for longer than the Regulatory 30 minutes. The temperature of the furnace increased back to 800°C over the first 19 minutes of the test. Unfortunately, the temperature provided from the furnace controller, as a function of time, was not sufficiently accurate for modelling purposes and the thermocouple attached to the support frame also gave false readings. However, the temperature of the exterior skin of the keg is expected to rapidly reach the furnace temperature. In the model, therefore, the temperature provided from the furnace controller was used as a guide but the modelled furnace temperature was actually adjusted in order to give good agreement between the predicted outer keg skin temperature and the measured skin temperatures, as a function of time. These temperatures are shown in Figure 7.

During the cooling phase, heat was modelled as being lost from all exterior surfaces of the keg by radiation and natural convection. The emissivity of the surface of the keg was assumed to remain at 0.8, the value assumed during the heating phase (pictures of the container show the surface to be blackened and oxidised by the furnace). Established correlations for natural convection were again used to derive the appropriate convection coefficient (see Appendix 2).

The predicted temperature of the containment vessel was initially much lower than the measured value. It was therefore concluded that the effective thermal conductivity of the cork was higher than had been assumed (note that significant extrapolation of the measured data had been required as shown in Figure 4). The thermal conductivity of the cork (which was initially based on a linear extrapolation of the measured values) was therefore increased by 50%. It should be noted that this thermal conductivity in the model is an effective conductivity which includes possible additional heat transfer mechanisms such as evaporation and condensation of water or waxes.

The resulting predicted temperature at the location of the thermocouples on the containment vessel lid is compared against the measured values in Figure 8. The temperatures measured while the container was inside the furnace are believed to have been influenced by the flames inside the furnace and are hence unreliable (this effect, which is observed quite often in fire and furnace tests, is most pronounced when the thermocouples are thin and the length of the thermocouple tails passing through the flames is large and is caused by a false junction being created in the thermocouple tail at high temperatures). Thermocouple 1 is located inside the lid whereas thermocouple 2 is only placed loosely against it. The temperatures measured during the cooling phase, however, are reliable and the maximum measured temperature agrees well with the temperature sensitive strip in this location. The general trend in measured temperature is predicted correctly but the predicted temperature lags behind the measured value. The maximum temperature is overestimated by 2.5°C.

It is therefore concluded that, with the adjusted cork conductivity, the finite element model is slightly pessimistic with respect to the peak inner containment seal temperature predicted during the fire test.

4 Calculation of Temperatures During Normal Transport

4.1 No Insolation

The finite element model has been used to determine the temperature of the container under normal conditions of transport in the absence of solar insolation. A steady state calculation was performed which represented the container, stood vertically on an insulating surface, with heat loads of 0W, 3W, 6W and 10W and an ambient temperature of 38°C.

Heat loss to ambient by radiation and natural convection from the sides and top of the keg were simulated. These boundary conditions (apart from the ambient temperature) were the same as used to obtain good agreement with the self heating test (see Section 3.1).

In the validation of the model against the self heating test (Section 3.1) it was found that the best agreement was obtained with the thermal conductivity of the cork reduced by 15% compared to the measured values. To ensure that the temperatures predicted under normal conditions of transport are pessimistic, the lower, adjusted, thermal conductivity value has been used. Similarly, when modelling the heat test the surface emissivity was increased to 0.4 in order to improve the agreement between predicted and measured temperatures. To ensure that the temperatures predicted under normal conditions of transport are pessimistic, the lower, reference, emissivity value has been used.

The predicted temperature profile, at a heat load of 10W, is shown in Figure 9. The temperature at the inner containment vessel lid seal is 94°C. The maximum accessible surface temperature is 43°C and occurs on the top of the keg lid. The base of the keg is predicted to reach 46°C but this surface is not readily accessible. The temperature on the outside of the keg, at mid-height, is 42°C. The maximum temperature inside the containment vessel, as a function of the heat load, is shown in Table 4.

4.2 With Insolation

The finite element model has been used to determine the temperature of the container under normal conditions of transport and subject to solar insolation. Both a vertical orientation of the container and a horizontal orientation of the container (with it stood on an insulating surface) have been considered.

The model used was the same as that used for the case of normal transport without insolation (described above in Section 4.1) except:

- Insolation was added for 12 hours each day
- The heat transfer coefficients were adjusted for horizontal orientation where appropriate
- Heat loss by natural convection and radiation from the base of the container was added (horizontal orientation only)

Transient calculations were performed covering a period of 4½ days with solar insolation incident upon the container for 12 hours each day.

Calculations were performed corresponding to both horizontal and vertical orientation of the container. It was found that, at the end of each insolation period, the temperature of the inner container was around 1°C hotter in the vertical orientation than in the horizontal orientation due to the greater insolation heat flux onto the top of the container in the vertical orientation. The temperatures corresponding to vertical orientation of the container are therefore presented and also used as the starting point for the fire test calculation.

Figure 10 shows, for a 10W heat load, the transient temperature at various locations on the outer surface of the keg. The highest temperatures occur on the top of the container because the insolation flux is greater on the top than on the side. The maximum predicted temperature, which occurs on the top, is 104°C. The bottom of keg is hotter than the side even though it does not receive any heat from solar insolation. This results from there being much less heat loss from the bottom of the keg than from the side. Figure 11 shows the transient temperature at the inner containment vessel lid seal. It can be seen that the maximum temperature has effectively been reached after 1½ days. The maximum seal temperature is predicted to be 116°C. Figure 12 shows the predicted temperature profile at the end of the transient calculation. The maximum temperature inside the containment vessel, as a function of the heat load, is shown in Table 4.

5 Calculation of Temperatures During the Fire Accident

The finite element model has been used to determine the temperature of the container during the fire accident specified in the 10CFR71 Regulations [1]. A 30 minute, 800°C fire was simulated followed by a 12 hour cooling period.

During the heating phase, the model was the same as that which was validated against the furnace test (see Section 3.2) except:

- The tungsten insert and lead shot inside the inner containment vessel were removed
- A heat load of 10W was applied to the inner surface of the inner containment vessel
- The fire temperature was fixed at a constant value of 800°C
- The convection heat transfer coefficient was increased from 10 $W/m^2/K$ to $15W/m^2/K$ to ensure that the value used is pessimistic
- The duration of the fire was reduced to 30 minutes
- The calculation started from the temperature profile obtained for normal conditions of transport with insolation (see Section 4.2)

The 10CFR71 Regulations [1] require the thermal test to be performed upon a container which has already been subjected to the regulatory impact tests. A series of impact tests, as specified by the 10CFR71 Regulations [1] have been performed upon the SAFKEG LS design. The only significant distortion or damage that occurred was to the 'skirt' at either end of the keg. These 'skirts' are not significant to the thermal performance and it is judged that the damaged 'skirt' would provide greater protection in a fire than an undamaged 'skirt' (since, when bent over, it will provide shielding of the top and bottom of the keg from the fire). The finite element model used to model the fire accident was therefore unchanged from that used to model normal conditions of transport.

Although the temperature profile at the start of the fire test calculation corresponded to that at the end of a 12 hour period of solar insolation, solar insolation was pessimistically also applied during the 12 hour cooling phase of the fire accident calculation.

During the cooling phase, the boundary conditions were the same as those used to model normal conditions of transport (with the container vertical) except that the emissivity of the keg outer surface was assumed to be 0.8 (the same as during the heating phase and specified in the 10CFR71 Regulations).

Figure 13 shows the predicted temperature profile, for a heat load of 10W, at the end of the heating phase. The external surface of the keg is, as expected, close to the temperature of the fire (800°C). At this time the temperature of the inner containment vessel is around 116°C and has hardly changed from that predicted under normal conditions of transport.

Figure 14 shows the predicted temperature, for the same case, on the exterior surface of the keg. As measured in the furnace test [3], the outer skin of the keg heats up and cools down rapidly because it is insulated from the inner containment vessel by the cork. The temperature of the keg

side changes more quickly than that of the lid or base because the outer shell is thinner than the lid or base and therefore has a lower thermal capacity.

Figure 15 shows the predicted temperature, again for the 10W heat load, of the inner containment vessel. The lid seal reaches a maximum temperature of 183°C after 3¾ hours. A similar maximum temperature is experienced by the lead shielding. The lead therefore remains well below its melting point (solidus 252°C). The maximum temperature experienced inside the containment vessel, as a function of heat load, is listed in Table 4.

6 Conclusions

The thermal performance of the SAFKEG LS design of transport container has been analysed using an axi-symmetric finite element model.

The model was first validated by comparison against experimental data from a self heating test and a furnace test.

Good agreement was obtained with the results of the self heating test but only after the thermal conductivity of the cork had been decreased by 15% compared to its measured value.

Using the lower, fitted, value of the cork conductivity in ensures that the model is pessimistic when calculating temperatures for normal conditions of transport.

Comparison of the model against the results of the furnace test initially demonstrate the model to be optimistic. However, by increasing the assumed effective thermal conductivity of the cork by 50% the model was able to reproduce the measured maximum temperature of the containment vessel lid. The resulting model was slightly pessimistic, overestimating the measured containment vessel lid temperature by 2½°C.

The temperature of the container has been predicted under normal conditions of transport, for a range of heat loads, both with and without solar insolation. When subjected to solar insolation the container is shown to be hotter in the vertical orientation than in the horizontal orientation. At a heat load of 10W, the solar insolation increases the temperature at the inner containment vessel lid seal from 94°C to a maximum of 116°C.

The temperature of the container has been predicted during the thermal (fire) test. At a heat load of 10W, the inner containment vessel lid seal is predicted to reach a maximum temperature of 183°C.

7 References

1. Title 10, Code of Federal Regulations, Part 71, Office of the Federal Register, Washington, DC, 2009.

2. Abaqus version 6.8-1, Dassault Systemes Simulia Corp.

3. 'Prototype SAFGEG LS 3979A/0002, NCT and HAC Regulatory Test Report'. Croft Report CTR 2009/21 Issue A.

4. 'Advisory Material for the IAEA Regulations for the Safe Transport of Radioactive Material', 2005 Edition, IAEA Safety Guide No. TS-G-1.1 (ST2), 2002.

Table 1 – Material Properties used in the Model

Material	Property	Temperature (°C)	Value	Reference
304 Stainless Steel	Conductivity	21	14.9 W/m/K	1
		38	15.0 W/m/K	
		93	16.1 W/m/K	
		149	16.9 W/m/K	
		205	18.0 W/m/K	
		260	18.9 W/m/K	
		316	19.5 W/m/K	
		371	20.4 W/m/K	
		427	21.1 W/m/K	
		482	22.0 W/m/K	
		538	22.8 W/m/K	
		593	23.5 W/m/K	
		649	24.2 W/m/K	
		705	25.1 W/m/K	
		760	25.8 W/m/K	
		816	26.5 W/m/K	
	Density	-	7900 kg/m^3	2
	Specific Heat	21	483 J/kg/K	1
		38	486 J/kg/K	
		93	506 J/kg/K	
		149	520 J/kg/K	
		205	535 J/kg/K	
		260	544 J/kg/K	
		316	551 J/kg/K	
		371	559 J/kg/K	
		427	562 J/kg/K	
		482	570 J/kg/K	
		538	577 J/kg/K	
		593	583 J/kg/K	
		649	585 J/kg/K	
		705	591 J/kg/K	
		760	596 J/kg/K	
		816	601 J/kg/K	
Lead	Conductivity	-	29.7 W/m/K	3
	Density	-	11040 kg/m^3	4
	Specific Heat	-	133.9 J/kg/K	3
Cork	Conductivity	-	See Figure 4	5
	Density	-	290 kg/m^3	5
	Specific Heat	-	1650 J/kg/K	5

Table 1 References

1. ASME Section II (2001), Part D, Subpart 2, Table TCD, Group J
2. 'Design Manual for Structural Stainless Steel (Second edition)', The Steel Construction Institute, Building series, Vol 3.
3. Edwards A.L, 'For Computer Heat-Conduction Calculations a Compilation of Thermal Properties Data', UCRL-50589, 1969.
4. Goodfellows data sheet, http://www.goodfellow.com/AntimonialLead.html
5. 'Summary of the Physical Properties and Composition of Resin Bonded Cork', CTR 2001/11, Issue D, 2002.

Table 2 – Emissivities used in the Model

Material	Condition	Value	Reference
304 Stainless Steel	Internal surfaces	0.2	1
	External surface – heating test	0.4	2
	External surface - NCT	0.25	1
	External surface – fire test	0.8	3
Cork	All conditions	0.95	4

Table 2 References

1. Touloukian & DeWitt, "Thermal Radiative Properties – Metallic elements and alloys", Thermophysical properties of matter, Vol 7, Pub IFI/PLENUM, 1970.
2. Fitted to measured surface temperature in heating test (see Section 3.1)
3. Title 10, Code of Federal Regulations, Part 71, Office of the Federal Register, Washington, DC, 2009.
4. 'The Emissivity of Various Materials Commonly Encountered in Industry', Land pyrometers Technical Note 101.

Table 3 – Solar Insolation Fluxes Applied to the Model

Container orientation	Surface	Insolation heat flux
Vertical	Lid end	800 W/m^2
	Side	200 W/m^2
	Bottom end	None
Horizontal	Lid end	200 W/m^2
	Side	400 W/m^2
	Bottom end	200 W/m^2

Notes
Insolation values obtained from 10CFR71 Transport Regulations [1]
Insolation flux applied for 12 hours in each day
The 'side' of the keg was taken to be the entire height of the keg plus the inside of the skirts (except the inside the bottom skirt when the container is oriented vertically)

Table 4 – Predicted Maximum Containment Vessel Temperature

Condition	Maximum containment vessel temperature (°C)			
Heat Load	0 W	3 W	6 W	10 W
Normal transport – no insolation	38.0	55.8	72.8	94.2
Normal transport – with insolation	63.7	80.4	96.4	116.4
Fire Accident	139.6	153.5	166.9	184.0

Diagram extracted from
drawing OC-6000 Issue A

Dimensions in mm

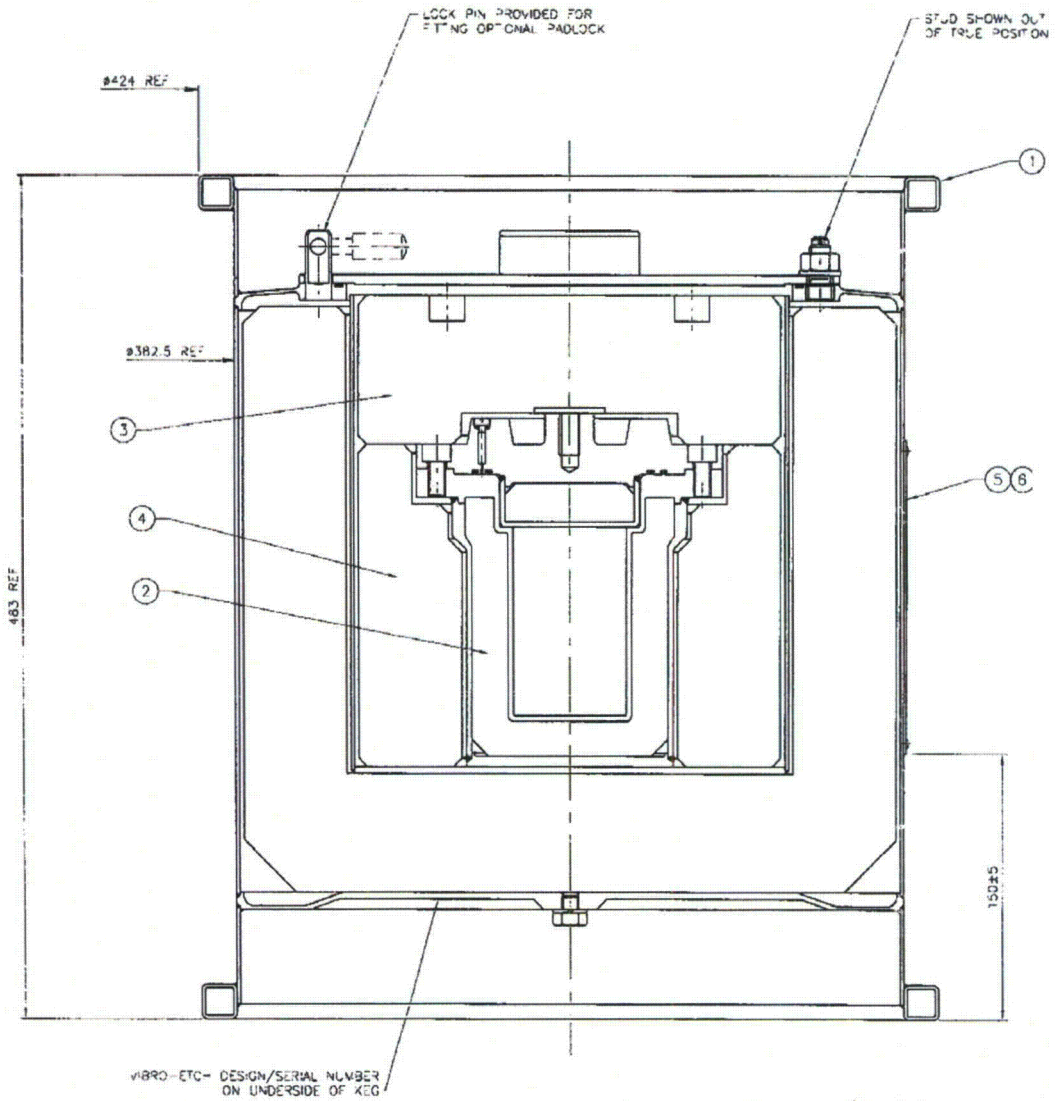

Figure 1 – The SAFKEG LS Container Design

Materials	
Grey	– stainless steel
Brown	– cork
Blue	– lead

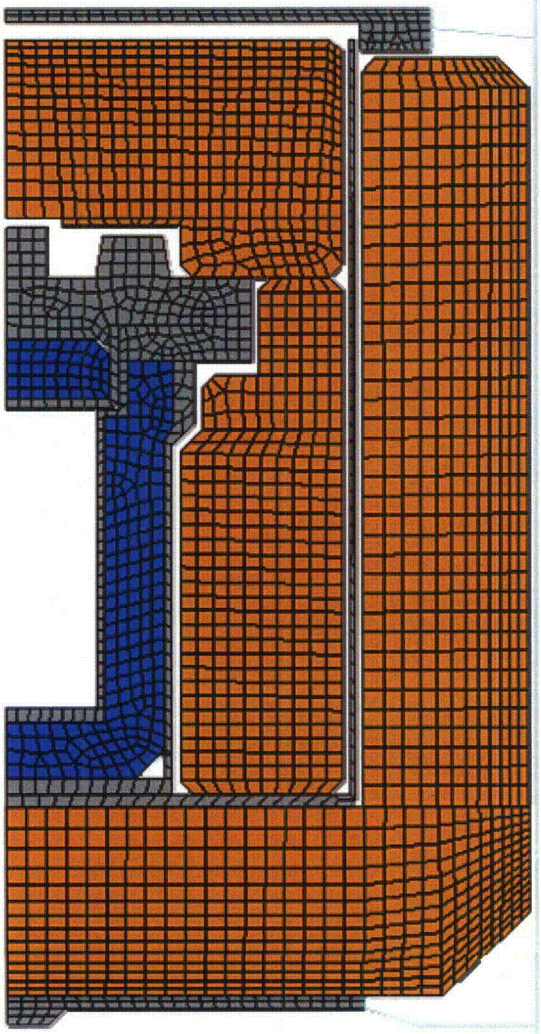

Figure 2 – The Model of the SAFKEG LS Container

Materials	
Grey	– stainless steel
Brown	– cork
Blue	– lead

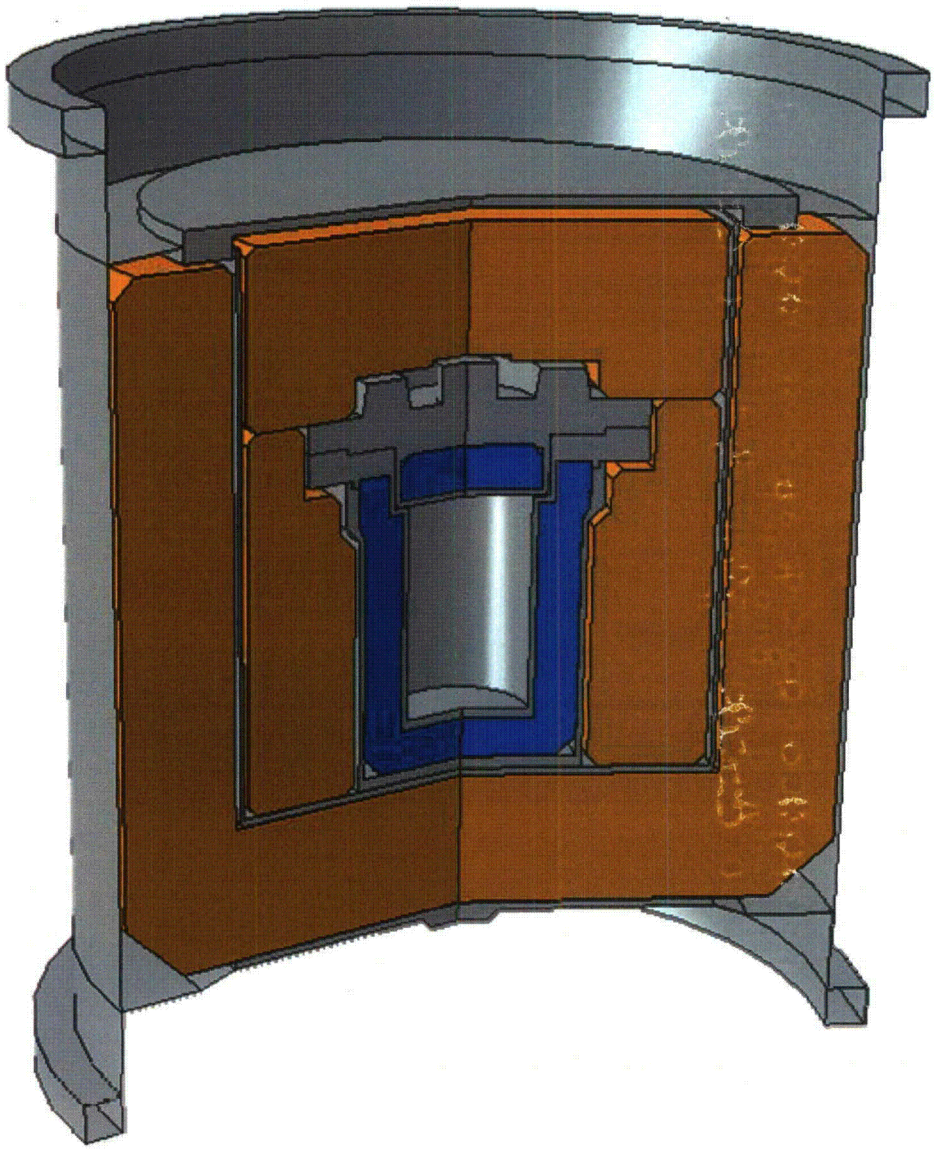

Figure 3 – 3-Dimensional View of the Axi-Symmetric Model

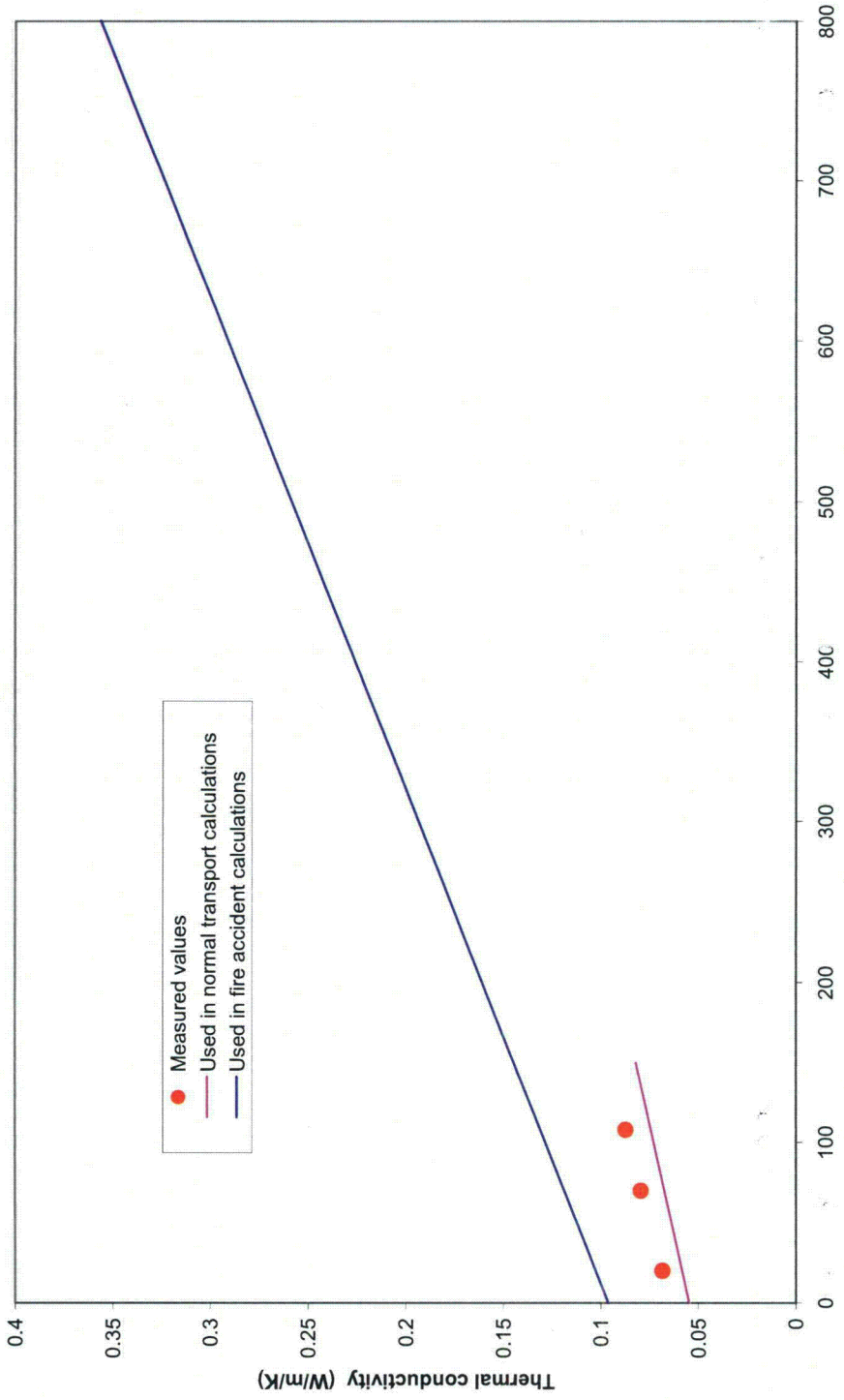

Figure 4 – Thermal Conductivity of Cork

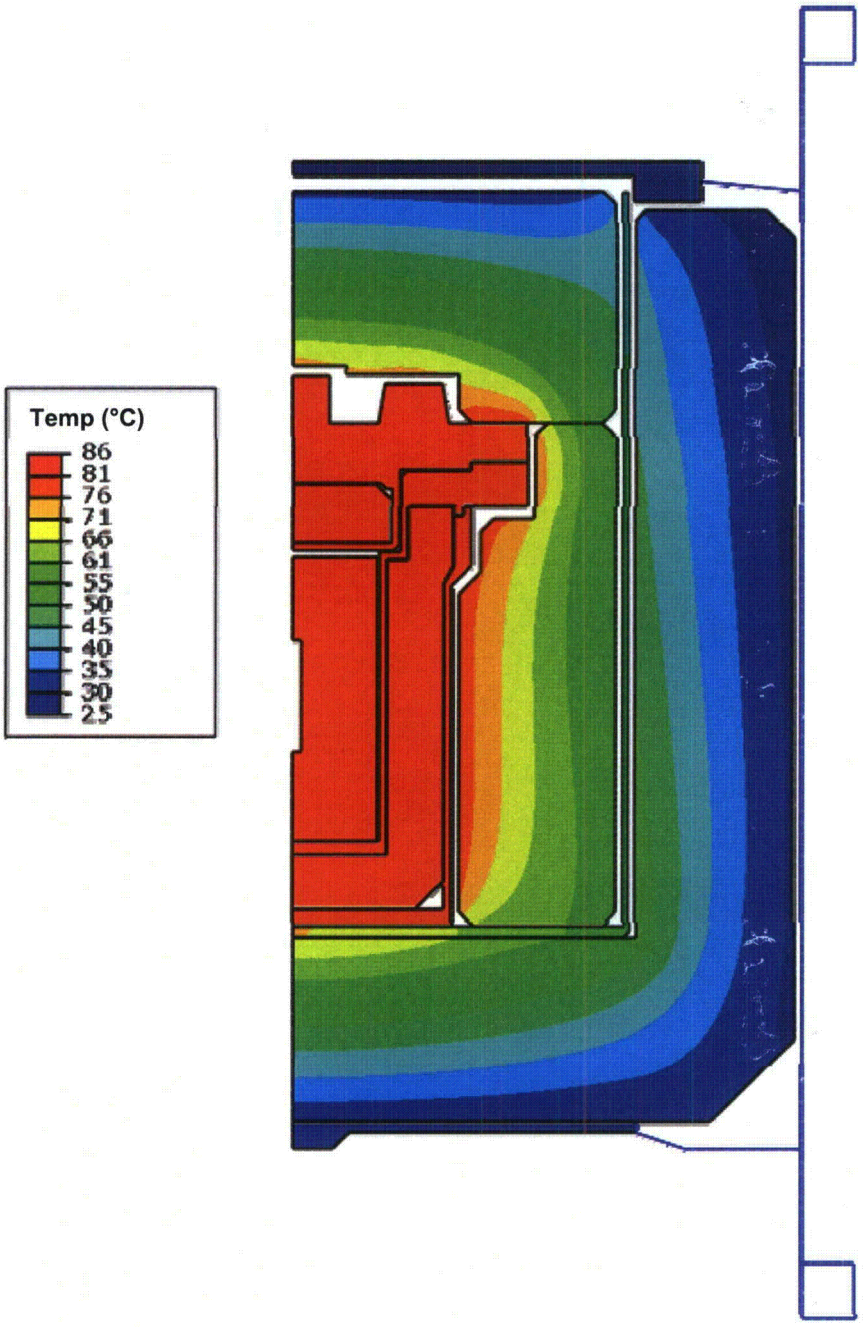

Figure 5 – Temperature Profile in the Steady-State Heating Test

Key
nn – Predicted (adjusted properties)
(nn) – Predicted (reference properties)
(nn) – Measured (fixed thermocouple)
(nn) – Measured (contact probe)

All temperatures in °C

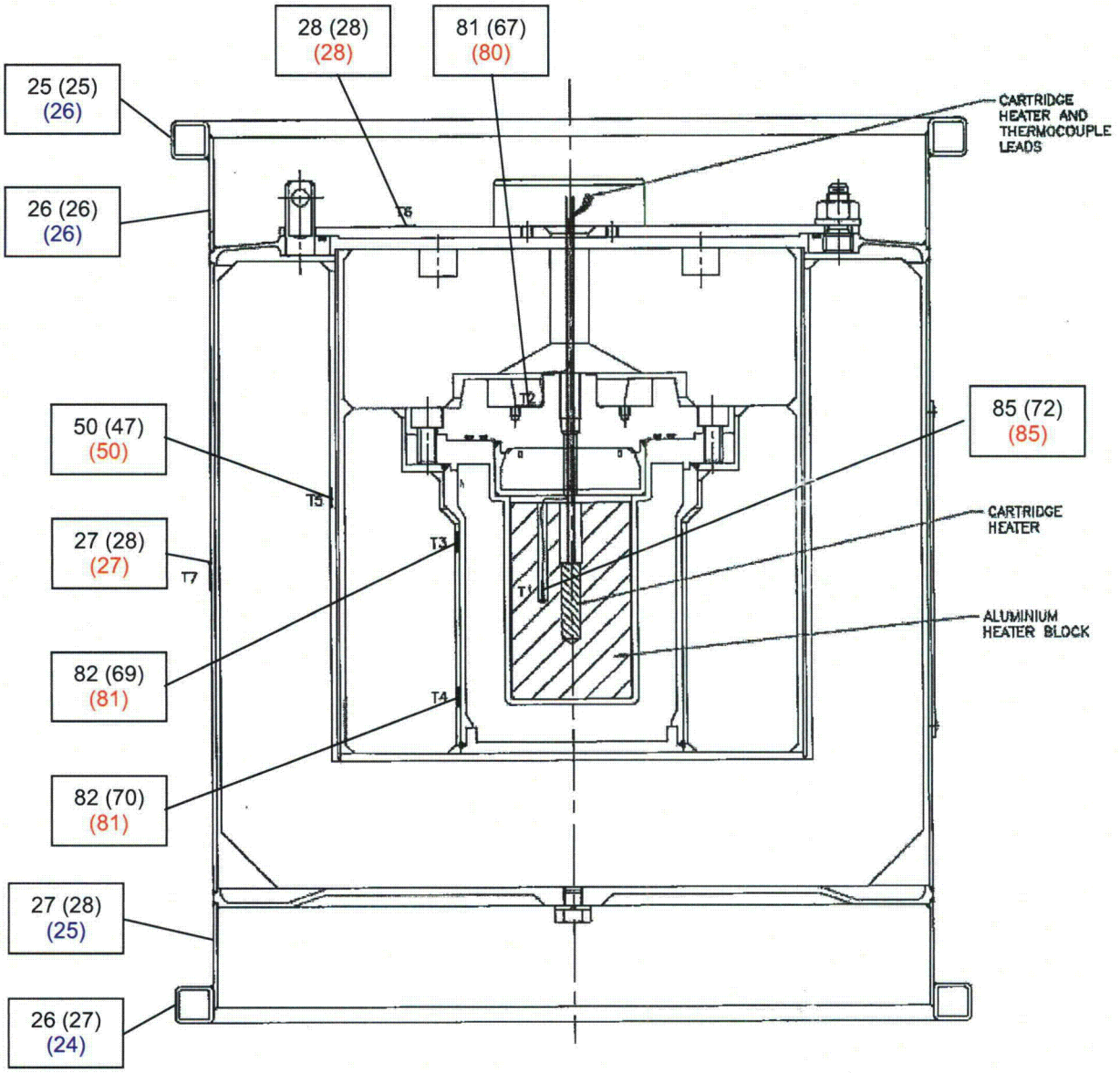

Heat load 10W
Ambient temperature 24.1°C

Figure 6 – Comparison of Measured and Predicted Temperatures in the Steady-State Heating Test

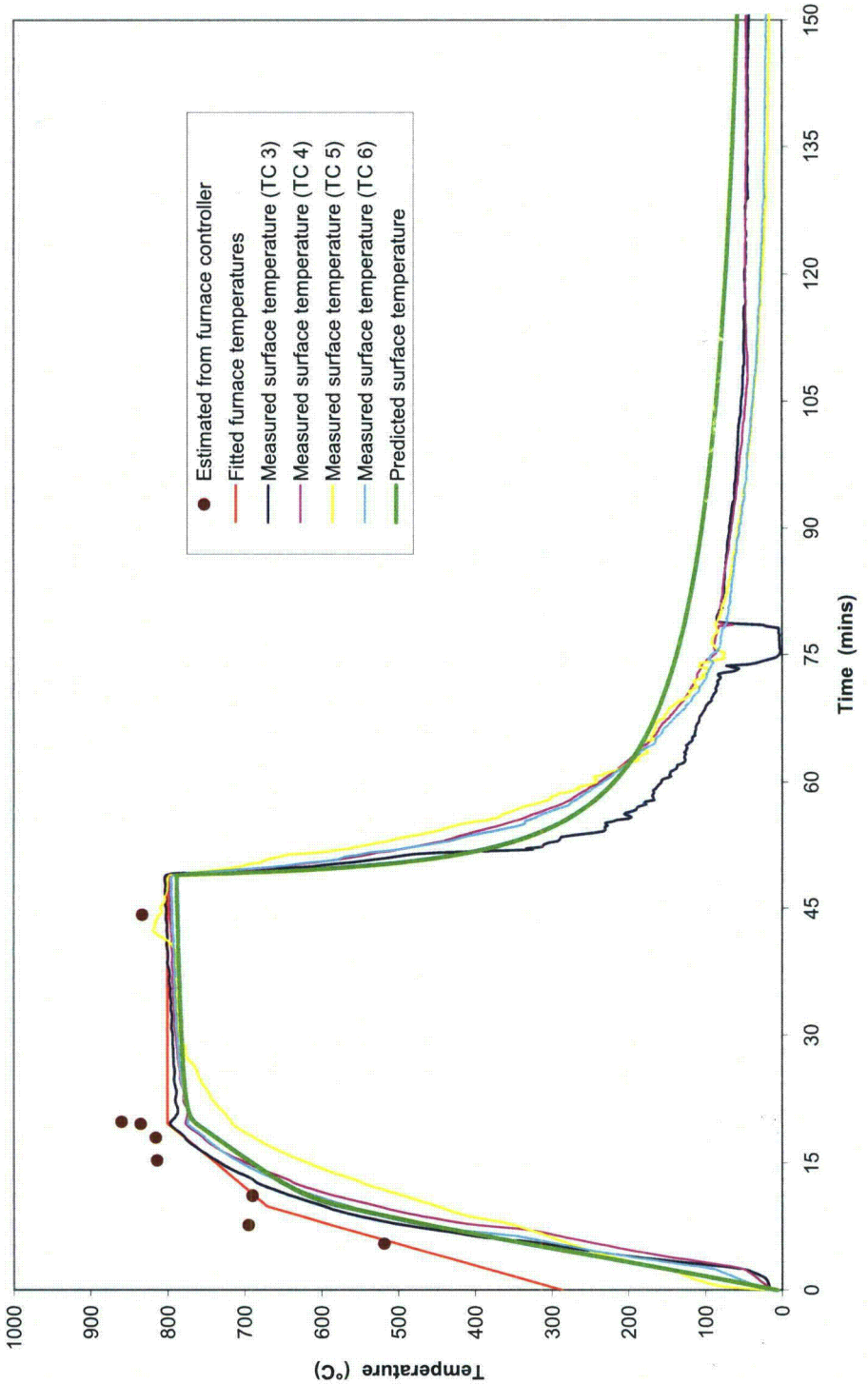

Figure 7 – Furnace Temperature and External Surface Temperature in the Furnace Test

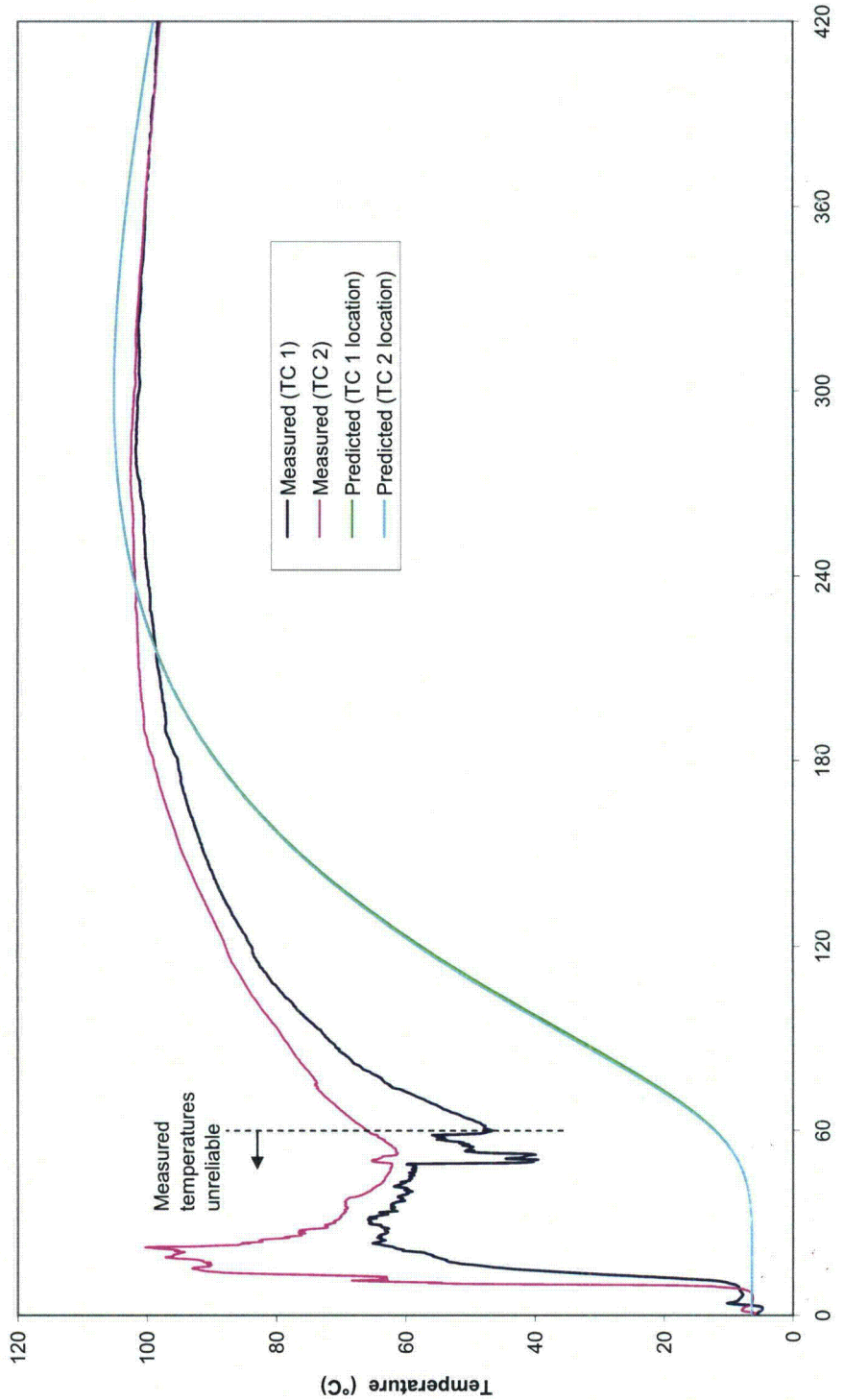

Figure 8 – Comparison of Predicted and Measured Temperature of the Inner Containment Vessel Lid in the Furnace Test

10 W heat load

Container vertical

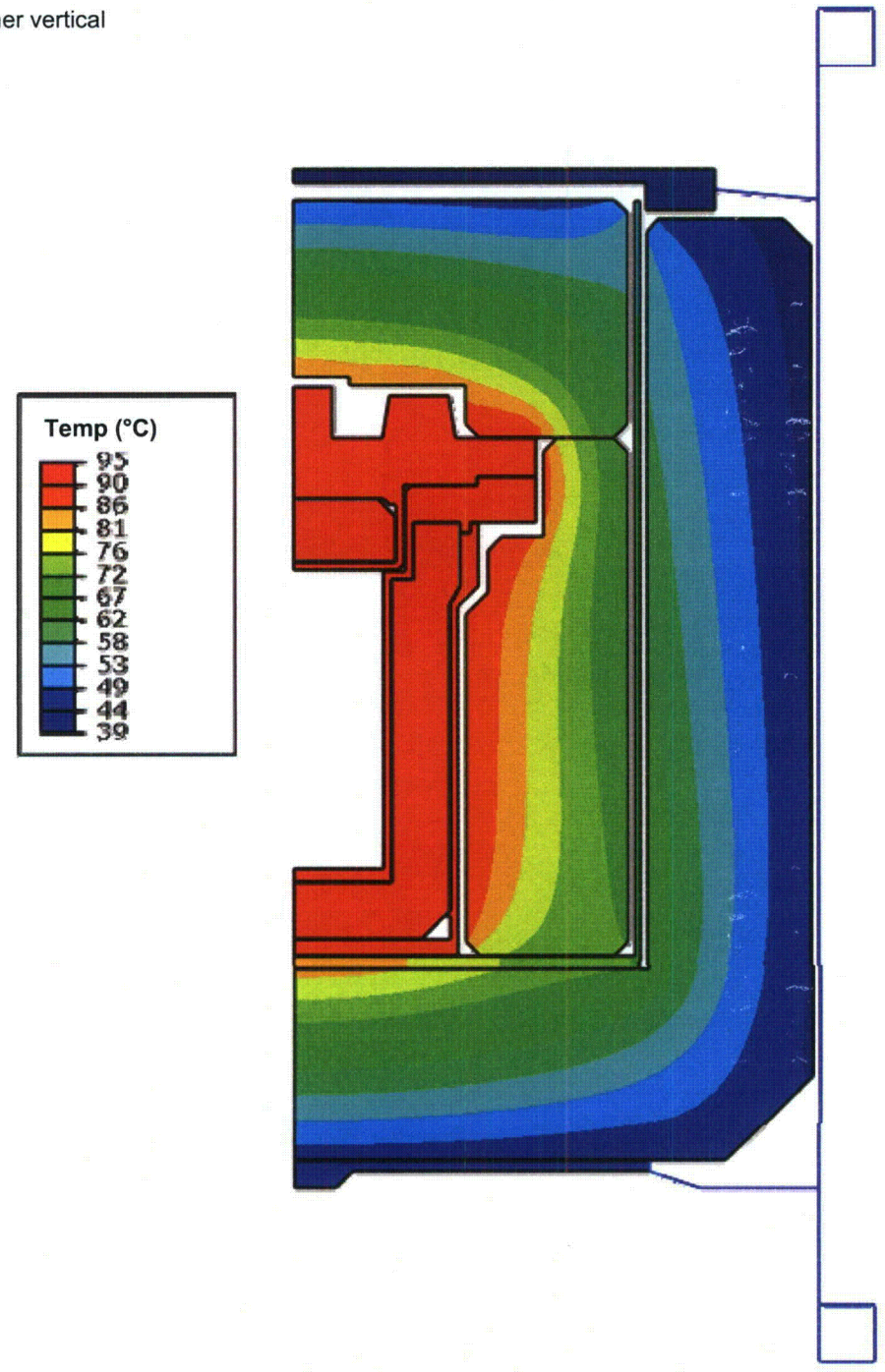

Figure 9 – Predicted Temperature Profile under Normal Conditions of Transport Without Solar Insolation

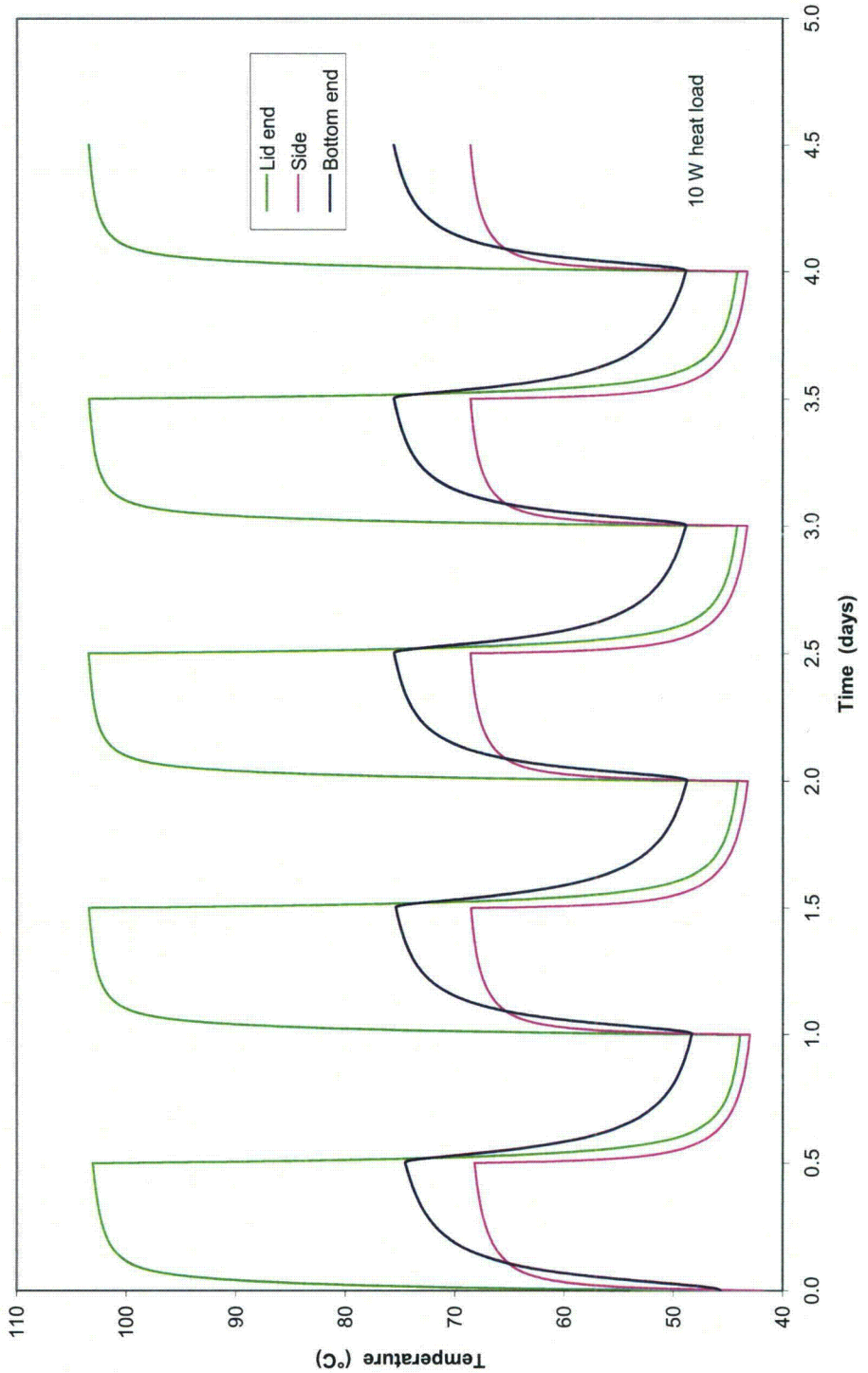

Figure 10 – Predicted Temperature on the Outside of the Keg During Normal Transport With Insolation

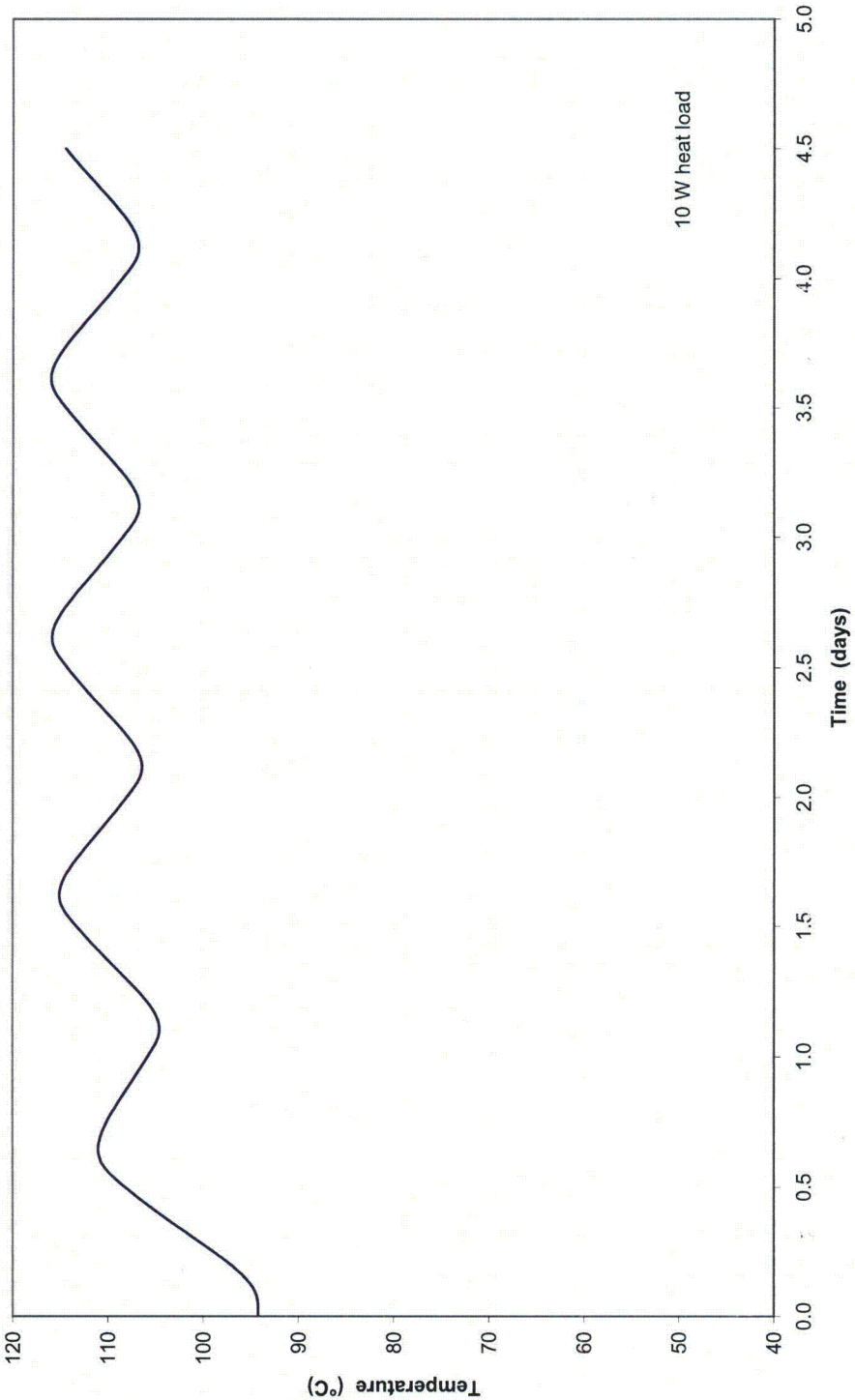

Figure 11 – Predicted Temperature at the Containment Vessel Lid Seal During Normal Transport With Insolation

10 W heat load

Container vertical

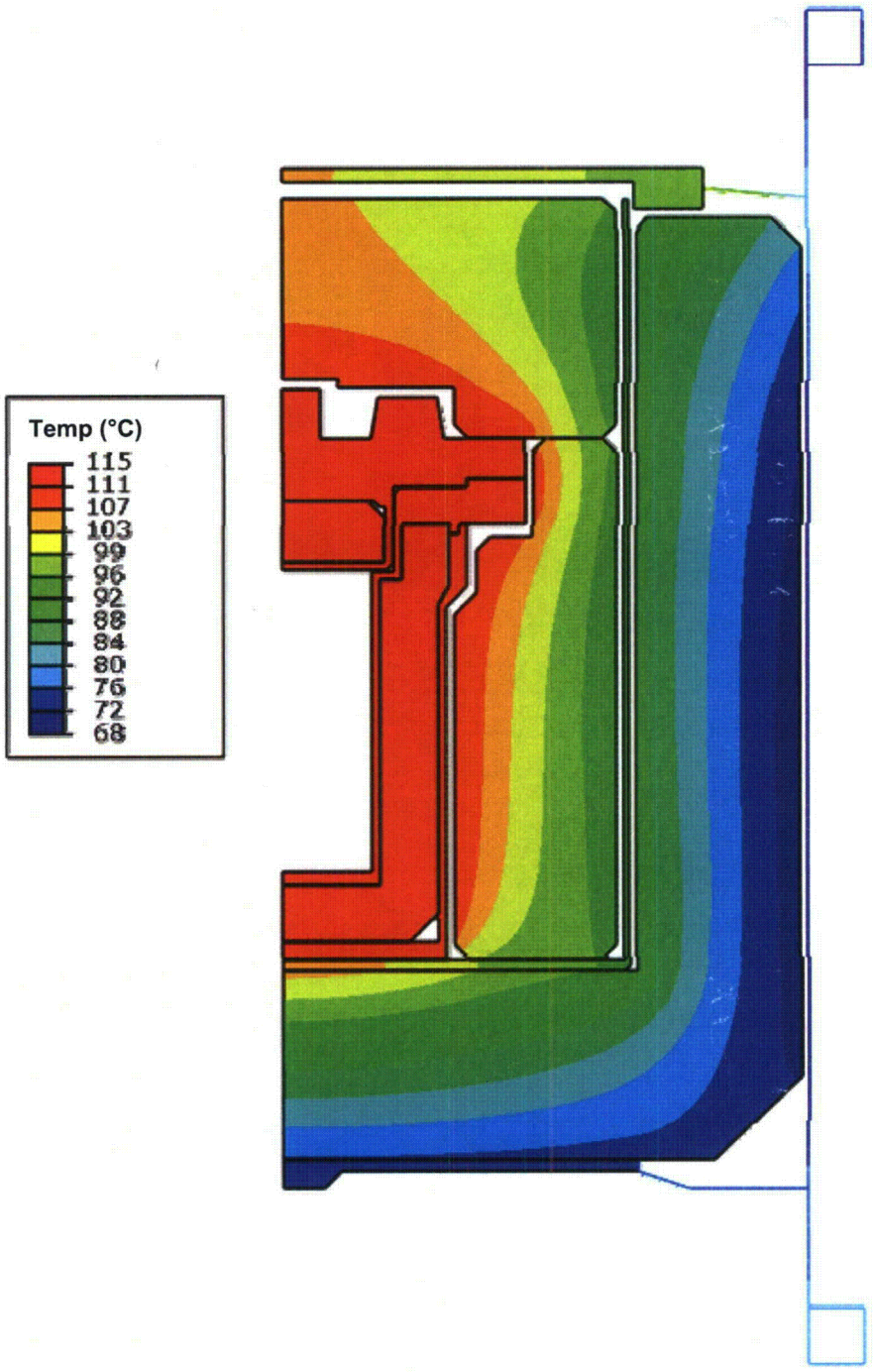

Figure 12 –Predicted Temperature Profile under Normal Conditions of Transport With Solar Insolation

10 W heat load

Container vertical

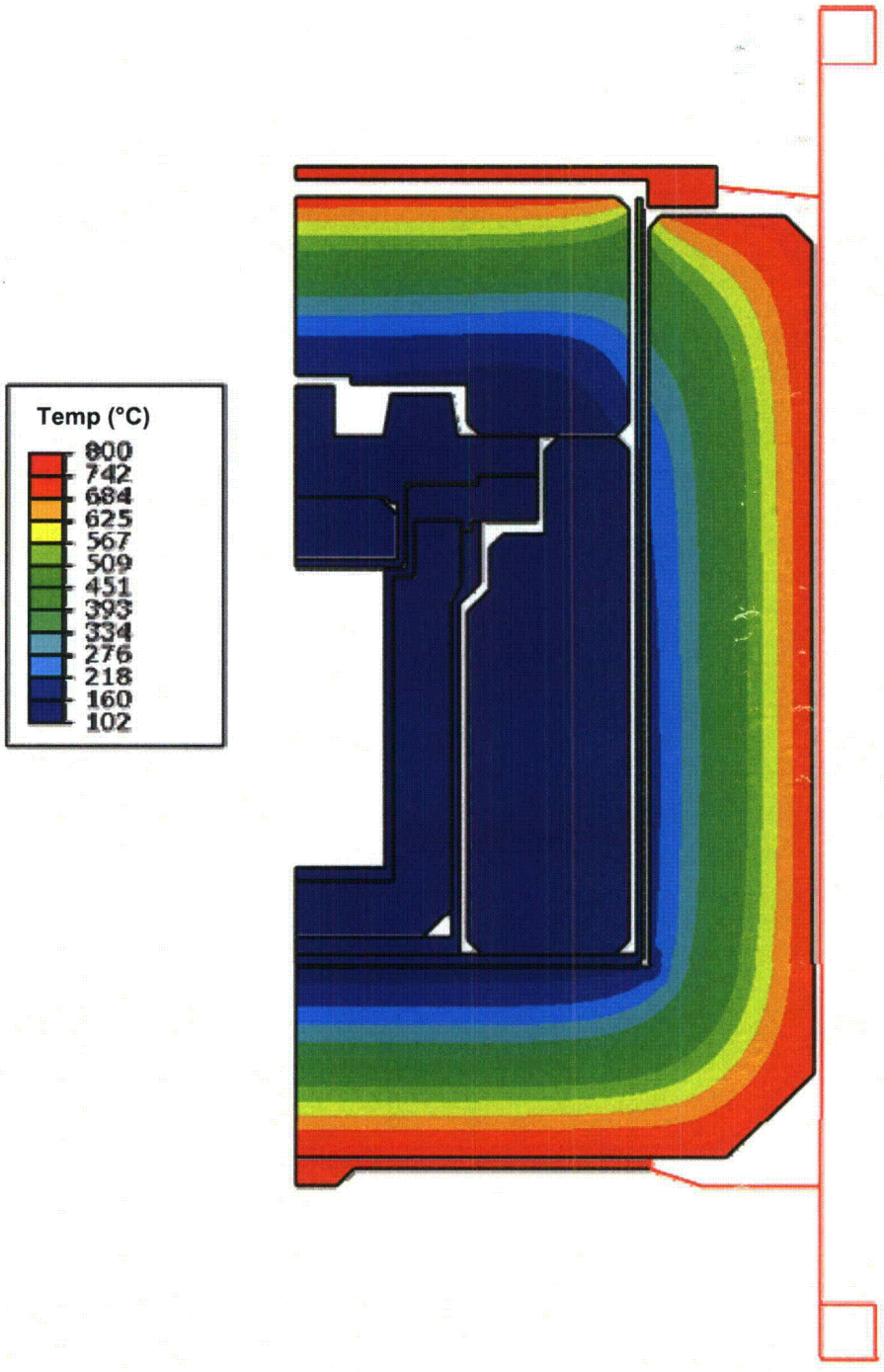

Figure 13 –Predicted Temperature Profile at the end of the Heating Phase of the Fire Accident

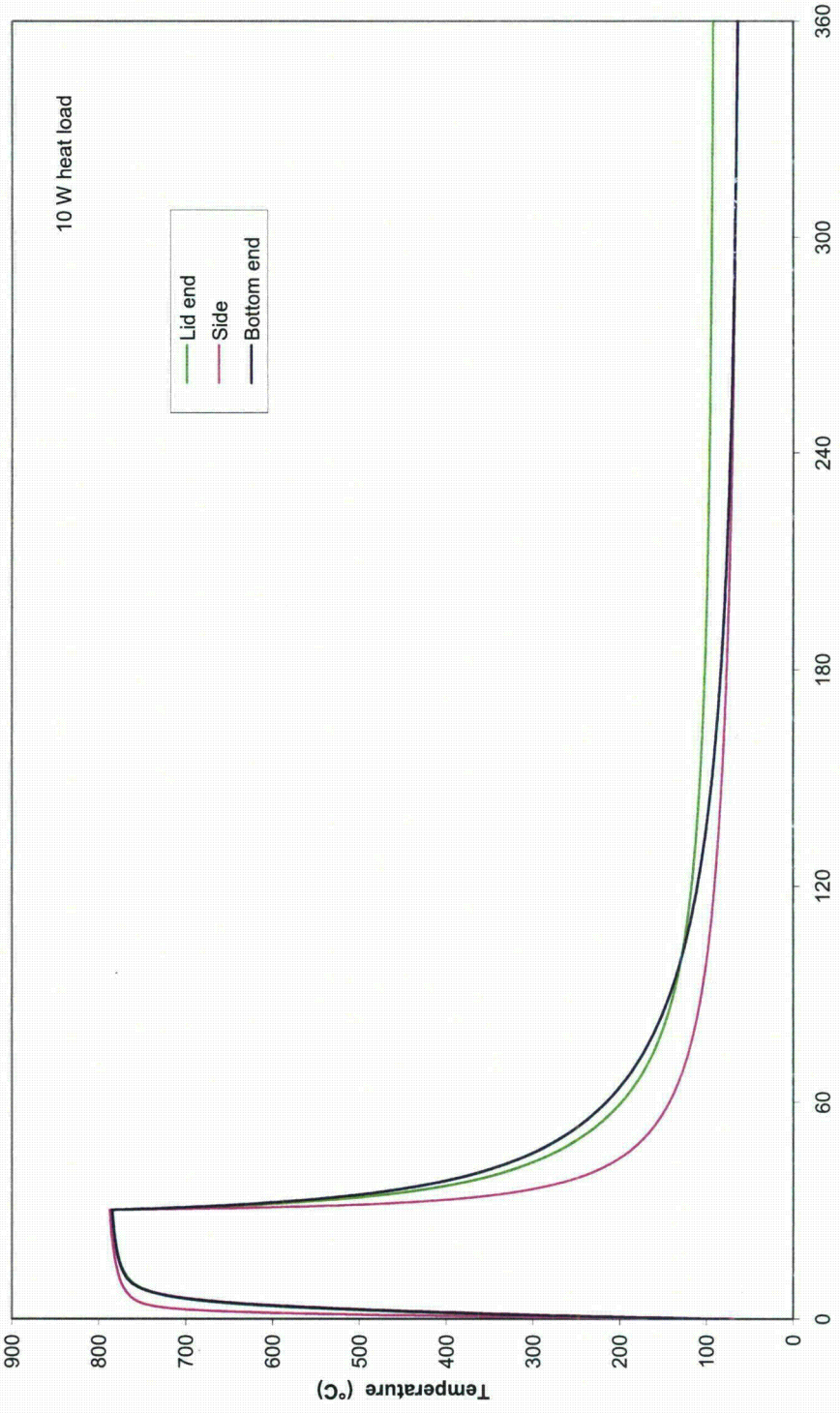

Figure 14 – Predicted Temperature on the Outside of the Keg during the Fire Accident

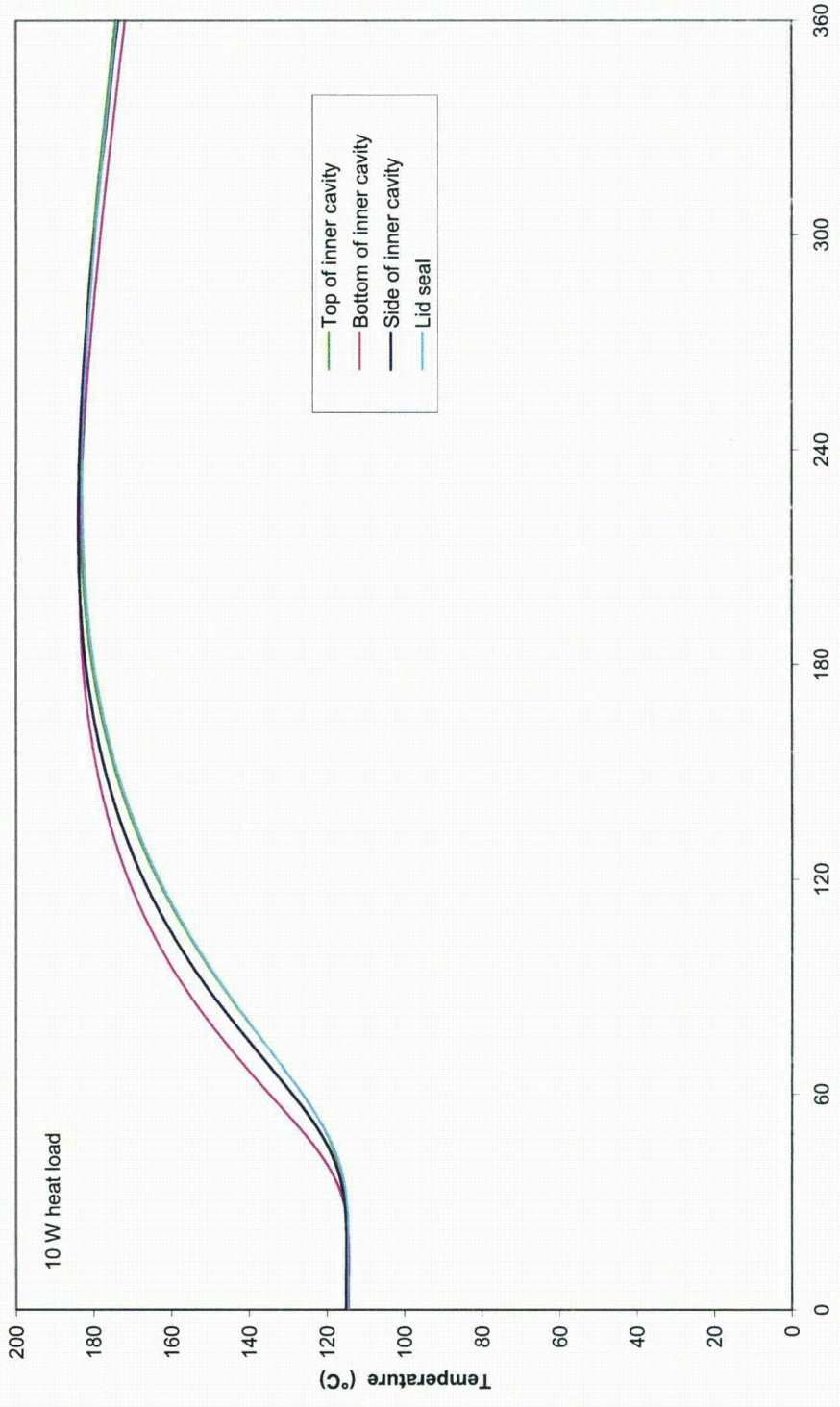

Figure 15 – Predicted Temperature of the Containment Vessel during the Fire Accident

Appendices

Contents

Appendix I
Drawings used in model generation

The engineering drawings of the SAFKEG LS design which were used to generate the finite element model are listed in the following table:

Component	Engineering Drawing Reference
Keg Body Keg Liner Keg Lid Cork	0C-6049, Issue A - Safkeg-LS Construction
Inner Container Body	1C-6099, Issue A - Containment Vessel LS Body Construction
Inner Container Lid	1C-6097, Issue A - Containment Vessel LS Lid Construction
Tungsten Insert	2C-5889, Issue A - LS-31x73-Tu Insert Design No. 3983

Appendix 2
Natural convection heat transfer correlations

Contents

Introduction

The calculations performed using the finite element model used standard correlations to determine the appropriate convection coefficient on the outside surfaces of the keg. The convection coefficients corresponding to four different geometries were required:

- vertical plate
- vertical cylinder
- horizontal plate
- horizontal cylinder

The correlations for natural convection heat transfer coefficients are all taken from [1]. In each case the correlation is for the Nusselt number, and is in the form:

$$Nu = \left({Nu_{lam}}^{m} + {Nu_{turb}}^{m} \right)^{1/m}$$

i.e. it combines a Nusselt number for fully laminar conditions with a Nusselt number for fully turbulent conditions using a power law rule with index m. The correlations for Nu_{lam}, Nu_{turb} and the corresponding values for m are given below for the four geometries used in the calculations.

Figure A2.1 compares the four correlations (expressed as heat transfer coefficients) for an ambient air temperature of 38°C.

Vertical plate

Index m = 6

Laminar part:

$$Nu_{lam} = \frac{2.8}{\ln(1 + 2.8 / Nu_{P,lam})}$$

$$Nu_{P,lam} = \frac{4}{3} \frac{0.503 Ra^{1/4}}{(1 + (0.492/\mathrm{Pr})^{9/16})^{4/9}}$$

Turbulent part:

$$Nu_{turb} = \frac{0.13 \mathrm{Pr}^{0.22} Ra^{1/3}}{(1 + 0.61 \mathrm{Pr}^{0.81})^{0.42}}$$

Vertical cylinder

Index m = 6

Laminar part:

$$Nu_{lam} = \frac{0.9 \xi_{lam}}{\ln(1 + 0.9 \xi_{lam})} Nu_{lam}^{VP}$$

$$\xi_{lam} = \frac{2L/D}{Nu_{P,lam}}$$

$$Nu_{lam}^{VP} = \frac{2.8}{\ln(1+2.8/Nu_{P,lam})}$$

$$Nu_{P,lam} = \frac{4}{3}\frac{0.503Ra^{1/4}}{(1+(0.492/\mathrm{Pr})^{9/16})^{4/9}}$$

Turbulent part:

$$Nu_{turb} = \frac{0.9\xi_{turb}Nu_{P,turb}}{\ln(1+0.9\xi_{turb})}$$

$$\xi_{turb} = \frac{2L/D}{Nu_{P,turb}}$$

$$Nu_{P,turb} = \frac{0.13\,\mathrm{Pr}^{0.22}\,Ra^{1/3}}{(1+0.61\mathrm{Pr}^{0.81})^{0.42}}$$

Horizontal plate (upward facing)

Index m = 10

Laminar part:

$$Nu_{lam} = \frac{1.4}{\ln(1+1.4/Nu_{P,lam})}$$

$$Nu_{P,lam} = 0.835\frac{4}{3}\frac{0.503Ra^{1/4}}{(1+(0.492/\mathrm{Pr})^{9/16})^{4/9}}$$

Turbulent part:

$$Nu_{turb} = 0.14Ra^{1/3}$$

Horizontal cylinder

Index m = 3.3

Laminar part:

$$Nu_{lam} = \frac{2f}{\ln(1+2f/Nu_{P,lam})}$$

where f is a constant (set to 1)

$$Nu_{P,lam} = 0.772.\frac{4}{3}\frac{0.503Ra^{1/4}}{(1+(0.492/\mathrm{Pr})^{9/16})^{4/9}}$$

Turbulent part:

$$Nu_{turb} = (0.0039\,\mathrm{Pr} + 0.1002)Ra^{1/3}$$

References

1) W M Rohsenow et al., Handbook of Heat Transfer Fundamentals, second edition.

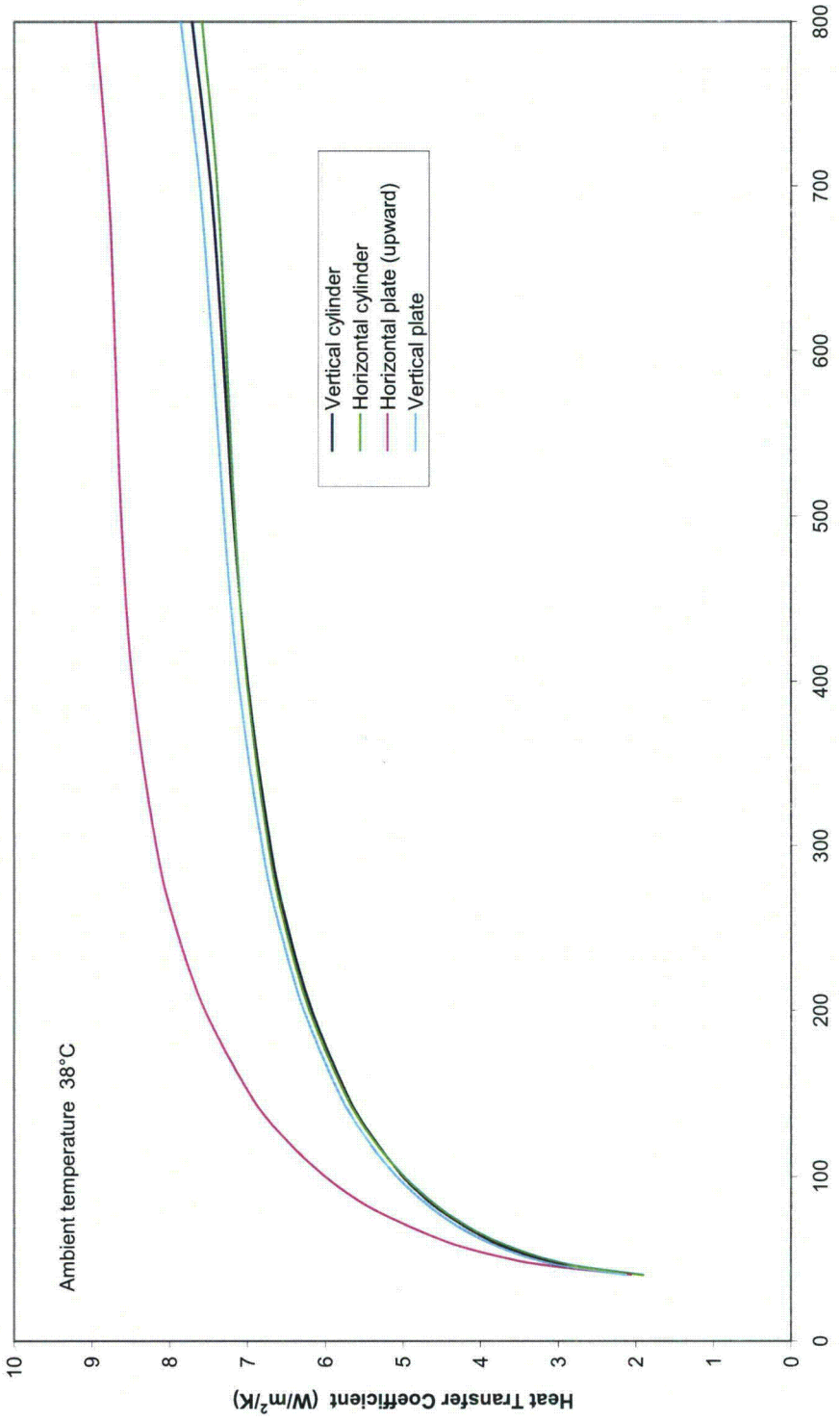

Figure A2.1 – Calculated Heat Transfer Coefficients for various Geometries and Orientations

CONTENTS

4 CONTAINMENT

The containment boundary of the Safkeg-LS 3979A package is identified and discussed in this chapter. The design, materials selected and the method of fastening are discussed with regards to meeting the containment requirements during the operation of the package. The ability of the package to provide the required containment during Normal Conditions of Transport (NCT) and Hypothetical Accident Conditions (HAC) as defined in 10 CFR 71.71 and 10 CFR 71.73 [4.1] respectively is presented. The criteria that verify the containment requirements during fabrication, maintenance and use are presented within this section.

4.1 Description of the Containment System [71.33 (a)(4)]

The containment boundary of the Safkeg-LS 3979A package is formed from the containment vessel flange/cavity wall, lid top and containment seal O-ring, as shown in Figure 4-1. The lid top is sealed to the flange/cavity wall by the containment seal O-ring which is fitted in a face seal configuration with the O-ring recessed into the flange. The lid top is held in position with 8 alloy steel closure screws which screw into the containment vessel flange/cavity wall and lid and are tightened to a torque of 10±0.5 Nm. On tightening the closure screws a uniform and repeatable compression of the O-rings is provided.

The closure screws are recessed into the lid top to physically protect them from damage. There is also a shear lip in the lid top and flange protecting the screws from shear failure due to transverse impact loads. The closure screws are positive fasteners, that cannot be opened unintentionally, or by any pressure that may arise within the package.

There are no welds, valves or pressure relief devices present in the containment boundary and the package does not rely on any filter or mechanical cooling system to meet the containment requirements.

The containment system is designed and fabricated in accordance with ASME B&PV Code Section III, Subsection NB [4.2]. The complete specifications such as closure screw torques, materials of construction, O-ring specifications and design dimensions for the containment system are given in drawings 1C-6044, 1C-6045 and 1C-6046 in Section 1.3.2.

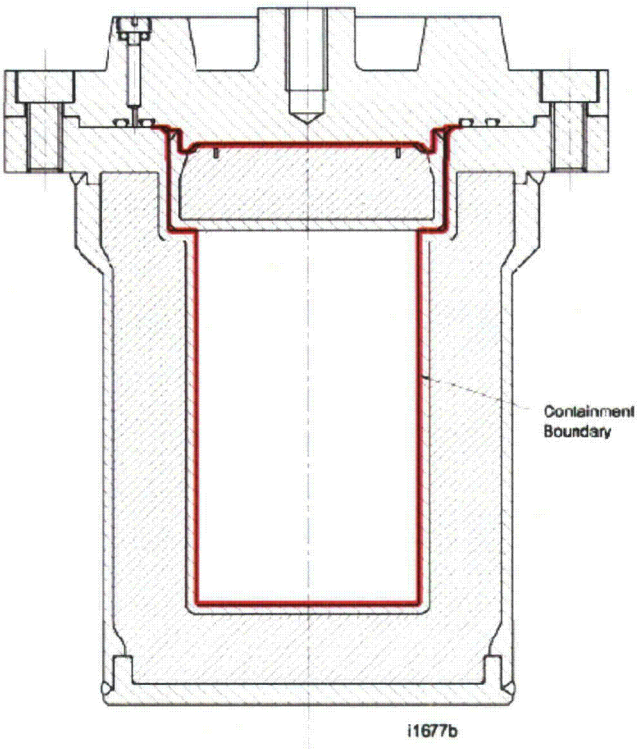

Figure 4-1 Package Containment Boundary

The flange/cavity wall and lid top are machined from solid stainless steel 304L. The containment O-ring is manufactured from Ethylene Propylene (EPM). The materials of construction of the containment system are evaluated in Section 2.2.2. All the materials have been selected for compatibility with each other, the inserts and the payload, in order to avoid chemical, galvanic or other reactions.

EPM was been selected as the containment O-ring material as EPM offers a temperature range of -40°C to 150°C and is able to withstand short excursions to 200°C for 2 hours [4.3]. Additionally a Sandia National Laboratories test program [4.4] compared several elastomeric O-ring compounds for performance under transportation package conditions and reported that EPM O-rings perform well at both low and high temperatures.

The radiation dose to the containment seal, assuming that the package is loaded with maximum contents as specified in Section 1.2.2 for a full year, is estimated to be > 10^4 Gy (10^6 rad). This estimate is based on the dose rate data presented in Section 5.4.4.1.1 for Ir-192 contents. It is judged that Ir-192 would produce the highest dose rate to the containment seal (which is outside the shielding) as it has a penetrating radiation. The maximum dose rate at the containment seal for each of the three inserts specified in Section 1.2.2 for the maximum Ir-192 contents, limited by the package maximum allowable surface dose rate, is given in Table 4-1.

Table 4-1 Safkeg-LS - Dose rate at the containment seal - based on Ir-192

Contents	CT-1				CT-2				CT-3			
Insert	LS-12x65-Tu Design No 3984				LS-31x73-Tu Design No 3983				LS-50x103-SS – Design # 3986			
	Source		Dose rate at containment seal		Source		Dose rate at containment seal		Source		Dose rate at containment seal	
			Sv/h	R/h			Sv/h	R/h			Sv/h	R/h
Calculated dose rate (1)	1000	Ci	1.46E-02	1.46E+00	1000	Ci	3.05E-01	3.05E+01	1000	Ci	3.43E+02	3.43E+04
Package limit	2.58E+01	Ci			1.16E+01	Ci			5.68E-01	Ci		
Dose rate for CT limit			3.77E-04	3.77E-02			3.54E-03	3.54E-01			1.96E-01	1.96E+01
			Sv	R								
Dose in 1 year	8760	hrs	3.30E+00	3.30E+02			3.10E+01	3.10E+03			1.71E+03	1.71E+05

Notes:
(1) From Table 5-3, Section 5.4.4.1.1

The containment O-ring seal is EPM which has good radiation resistance with compression set of <30% at an absorbed radiation level of 10^5 Gy (10^7 rad) whereas the maximum recommended compression set in the Parker Handbook is specified as 40% [4.3]. Furthermore, the Parker Handbook reports that "Practically all elastomers suffer no change of their physical properties at radiation levels up to 10^6 rad". It is concluded that the containment O-ring seal will not be unduly affected by the radiation from the contents of the package. It is noted that the containment O-ring seal is required to be replaced during the periodic maintenance activity (Section 8.2) (maximum period of 1 year).

Figure 4-2 shows the two additional O-ring seals fitted to the CV: a test point seal and a test seal. These seals are present to facilitate the leak test of the containment seal during the pre-shipment leak test. The test point is a tapped hole that allows connection of a pressure drop leak tester to the interspace volume between the test seal and the containment seal. The test seal is located close to the containment seal to provide a small interspace volume thus increasing the sensitivity of the pressure rise leakage test. The inserts as specified in Section 1.2.2 are also fitted with an O-ring seal. The test point seal, the test seal and the insert seal are not relied upon for containment.

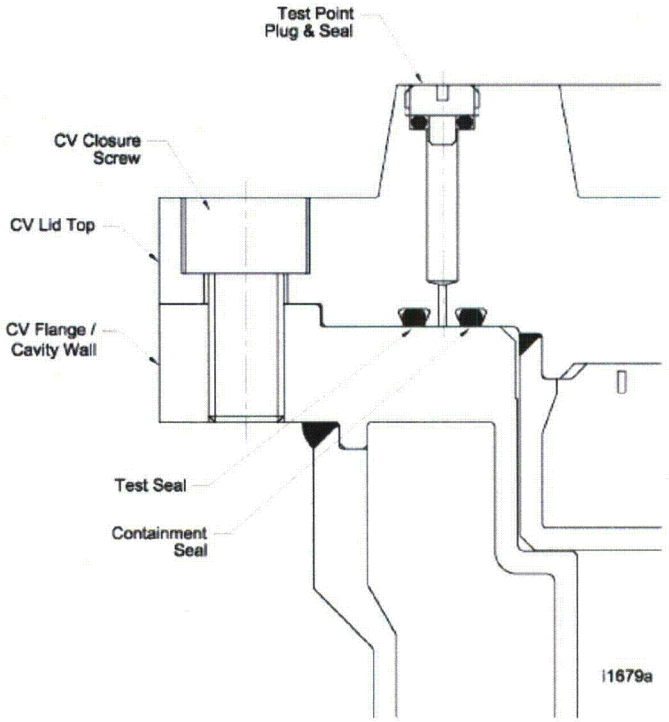

Figure 4-2 Leak Test Seal Arrangement

4.2 Containment under Normal Conditions of Transport (NCT) [71.51 (a)(1)]

4.2.1 Maximum internal pressures under NCT

The maximum internal pressure of the containment vessel under NCT is taken as the design pressure of 7 bar gauge (see Section 3.3.2).

4.2.2 NCT Containment Criterion

The Safkeg-LS 3979A package has been designed specifically to meet the criteria for leaktight during NCT and to be testable to demonstrate that the CV containment boundary is leaktight for the design, testing, fabrication, and maintenance leak tests. Leaktight is defined as demonstration of a leakage rate of $\leq 10^{-7}$ ref.cm^3/s as specified in ANSI N14.5 [4.5].

The contents are carried within inserts as specified in Section 1.2.2 which are required for all contents.

Under NCT the shielding inserts provide confinement of the radioactive material (solid, liquid or gas). Thus the shielding calculations are based on the contents being retained within the insert specified for the particular contents. However, containment is provided by the containment seal in the CV.

4.2.3 Structural Performance under NCT

The structural performance of the containment boundary of the CV has been demonstrated by prototype testing and analysis.

A prototype Safkeg-LS 3979A package was subjected to the NCT and HAC tests, as reported in Sections 2.6 and 2.7, in an uninterrupted test series, the containment seals were shown to be leaktight on conclusion of the tests.

The structural analysis reported in Sections 2.6 and 2.7 showed that there would be no permanent deformation of any of the containment system components under NCT conditions.

4.2.4 Containment of Radioactive Material under NCT

The structural performance of the containment boundary of the CV has been demonstrated by prototype testing and analysis.

A prototype Safkeg-LS 3979A package was subjected to the NCT and HAC tests, as reported in Sections 2.6 and 2.7, in an uninterrupted test series. Following the tests, the containment vessel was leakage tested in accordance with ANSI N14.5 and the containment system seals were found to be leaktight (having a leakage rate of $\leq 10^{-7}$ ref.cm^3/s).

The structural analysis reported in Sections 2.6 and 2.7 showed that there would be no permanent deformation of any of the containment system components under NCT, therefore there would be no effect which could cause any reduction in the effectiveness of the containment system.

4.3 Containment under Hypothetical Accident Conditions (HAC) [71.51 (a)(2)]

4.3.1 Maximum internal pressures under HAC

The maximum internal pressure of the containment vessel under HAC is taken as the design pressure of 10 bar gauge (see Section 3.3.2).

4.3.2 HAC Containment Criterion

The Safkeg-LS 3979A package has been designed specifically to meet the criteria for leaktight during HAC, and to be testable to demonstrate that the CV containment boundary is leaktight for the design, testing, fabrication, and maintenance leak tests. Leaktight is defined as demonstration of a leakage rate of $\leq 10^{-7}$ ref.cm^3/s as specified in ANSI N14.5 [4.5].

The contents are carried within inserts as specified in Section 1.2.2 which are required for all contents.

For solid radioactive material, under HAC the shielding inserts (together with the user defined product containers) provide confinement of the radioactive material within the shielding. Thus the shielding calculations are based on the contents being retained within the insert specified for the particular contents.

For liquid radioactive material, under HAC the liquid is assumed to leak from shielding inserts (and the user defined product containers) and flow into the space between the CV lid and CV body but is retained in the CV by the containment seal. The shielding calculations are based on the worst case configuration of the liquid contents.

For gaseous radioactive material, under HAC the gas is assumed to leak from shielding inserts (and the user defined product containers) and fill the cavity of the CV lid. The gas is assumed to leak from the CV at the containment seal at the leakage rate to which the containment is proved i.e. 10^{-7} ref.cm^3/s.

4.3.3 Structural Performance under HAC

The structural performance of the containment boundary of the CV has been demonstrated by prototype testing and analysis.

A prototype Safkeg-LS 3979A package was subjected to the NCT and HAC tests, as reported in Sections 2.6 and 2.7, in an uninterrupted test series. Following the tests, the containment vessel was leakage tested in accordance with ANSI N14.5 and the containment system seals were found to be leaktight (having a leakage rate of $\leq 10^{-7}$ ref.cm^3/s).

The structural analysis reported in Sections 2.6 and 2.7 showed that there would be no permanent deformation of any of the containment system components under HAC, therefore there would be no effect which could cause any reduction in the effectiveness of the containment system.

4.3.4 Containment of Radioactive Material under HAC

4.3.4.1 Containment of solid and liquid contents

The thermal evaluation in Section 3.4 shows that the bolts and containment system materials do not exceed their temperature limits under HAC. The seals may exceed the operational limits of the O-ring under the HAC conditions, however all batches of O-rings used in the manufacture of the containment vessel will be tested to ensure they can maintain containment under the temperatures experienced during HAC (200°C for 24 hour test as specified in the drawings in section 1.3.3).

The testing and analysis reported in Section 2 show that the containment system would be unaffected by HAC and provide complete containment for all solid and liquid contents.

The containment system has been shown to be unaffected by HAC and the seals will be tested to ensure they meet the temperature requirements under HAC: it is therefore concluded that the containment system meets the requirement for providing containment of the solid and liquid radioactive contents, within the allowable leakage limits under HAC.

4.3.4.2 Containment of gaseous contents

Containment of gases is based upon the assumption that the closure of the containment system (i.e. the containment seal and the CV lid and top flange) would leak at the leakage rate to which the containment is proved i.e. 10^{-7} ref.cm^3/s.

The maximum amount of the radioactive gases that may be carried has been calculated based upon the allowable leakage rate limits specified in 10 CFR71 and the assumed leak in the containment seals of 10^{-7} ref.cm^3/s. The calculation of the size of a single leak having a leakage rate of 10^{-7} ref.cm^3/s is given in report CS 2009/06 (Section 4.5.2). The calculated hole diameter, for a single leak path in the 3 mm O-ring, with a hole length of 0.26 cm, is 1.1 x 10^{-4} cm.

The gas leakage rates (in terms of mass flow and A_2/hr and A_2/week) are given in report CS 2009/07 (Section 4.5.2).

The allowable leakage rates under HAC are taken as no escape of Kr-85 exceeding 10 A_2, and no escape of other radioactive material exceeding a total amount of A_2 in a week, as given in 10 CFR 71.51 (a)(2) [4.1].

4.4 Leakage Rate Tests for Type B Packages

4.4.1 Fabrication Leak Rate Test

The materials and components used to manufacture the containment boundary are required to be helium leak tested during fabrication with a pass rate of 10^{-7} ref.cm^3/s. These tests ensure that the fabricated components and the materials used, meet the required level of containment prior to the approval of the package for use.

The requirements for the fabrication leak rate test are specified in Section 8.1.4.

4.4.2 Maintenance Leak Rate Test

If any maintenance activities are undertaken on the containment boundary, a helium leak rate test is required to confirm that any repairs or replacements have not degraded the containment system performance. The required leak rate has a pass rate of $\leq 10^{-7}$ ref.cm^3/s.

The requirements for the maintenance leak rate test are specified in Section 8.2.2.

4.4.3 Periodic Leak Rate Test

A periodic helium leak rate test is required to be carried out annually with a pass rate of $\leq 10^{-7}$ ref.cm^3/s. This test confirms that the containment boundary capabilities have not deteriorated over an extended period.

The requirements for the periodic leak rate test are specified in Section 8.2.2.

4.4.4 Pre-shipment Leak Rate Test

Prior to shipment, each package is required to be leak rate tested using the gas pressure rise or gas pressure drop method, with a pass rate of 10^{-3} ref.cm^3/s. This test confirms the CV is correctly assembled prior to shipment.

The requirements for the pre-shipment leak rate test are specified in Section 7.1.3.

4.5 Appendix

4.5.1 References

[4.1] Title 10, Code of Federal Regulations, Part 71, Office of the Federal Register, Washington D.C.

[4.2] ASME III Division 1 – Subsection NB, Class One Components, Rules for Construction of Nuclear Facility Components, ASME Boiler and Pressure Vessel Code, 2001 edition, the American Society of Mechanical Engineers, New York, New York

[4.3] Parker Hannifin Corporation, Parker O Ring Handbook, ORD 5700/USA, 2001

[4.4] Bronowski, D. R., Performance Testing of Elastomeric Seal Materials Under Low- and High-Temperature Conditions: Final Report, SAND94-2207, Sandia National Laboratories, June 2000

[4.5] ANSI N14.5, American National Standard for Radioactive Materials - Leakage Test on Packages for Shipment, American National Standards Institute, Inc., 1997

4.5.2 Supporting Documents

Document Reference	Title
CS 2009/06	SAFKEG-LS # 3979A - CV seal leak size for leaktight condition
CS 2009/07	SAFKEG-LS 3979A - Gas contents limit for leaktight condition

SAFKEG-LS # 3979A - CV seal leak size for leaktight condition

Scope

This calculation is to determine the size of a single leak in the CV seal that would leak at the rate for the leaktight condition specified in ANSI-N14.5-1997 as 10^{-7} ref.cm^3/s.

Calculation method

The methodology is that given in ANSI-N14.5-1997.

The equation references are those in ANSI-N14.5-1997.

$$La = (Fc+Fm)(Pu-Pd) \quad cm^3/s \tag{B.2}$$

$$Fc = 2.49 \times 10^6 \times \frac{D^4}{a \times \mu} \quad cm^3/atm.s \tag{B.3}$$

$$Fm = 3.81 \times 10^3 \times \frac{D^3}{a \times Pa} \sqrt{\frac{T}{M}} \quad cm^3/atm.s \tag{B.4}$$

$$Lu = La \times \frac{Pa}{Pu} \quad cm^3/s \tag{B.5}$$

$$Q = Lu \times Pu = La \times Pa \quad atm.cm^3/s$$

Calculation reference:-			Ref case A (a)	Ref case B (b)	CV 3980
Test gas			Air	Air	Air
Viscosity of leaking fluid at T	μ_l	cP (centipoise)	0.0185	0.0185	0.0185
Molecular weight	M	g/mol	29.0	29.0	29.0
O-ring cord diameter (c)	d	cm	-	-	0.3
Leak hole length = 0.866 x φ (c)	a	cm	1.000	1.000	0.260
Leak hole diameter	D	cm	1.0000e-04	1.0000e-04	1.1020e-04
Temperature of leaking fluid	T	K	298	298	298
Upstream pressure (mean)	Pu	atm abs	1.00	1.50	1.00
Downstream pressure (mean)	Pd	atm abs	0.01	1.00	0.01
Average stream pressure	Pa	atm abs	5.05e-01	1.25e+00	5.05e-01
Coefficient of continuum flow conductance	Fc	cm^3/s	1.35e-08	1.35e-08	7.64e-08
Coefficient of free molecular flow conductance	Fm	cm^3/s	2.42e-08	9.77e-09	1.25e-07
Volumetric leakage rate at Pa	La	cm^3/s	3.73e-08	1.16e-08	1.99e-07
Volumetric leakage rate at Pu	Lu	cm^3/s	1.88e-08	9.68e-09	1.00e-07
Mass leakage rate	Q	$ref.cm^3/s$	1.88e-08	1.45e-08	1.00e-07

Notes

a Check calc as ANSI N14.5-1997 Table B.2 - Air, Pu = 1.0 Atm abs, Pd = 0.01 Atm abs, a = 1 cm, D = 1e-4 cm

b Check calc as ANSI N14.5-1997 Table B.2 - Air, Pu = 1.5 Atm abs, Pd = 1.0 Atm abs, a = 1 cm, D = 1e-4 cm

c Chord length for an O-ring when compressed in an O-ring groove taken as 0.66 x d.

Prepared	R A Vaughan	Checked	A L Ferguson
Approved	R A Vaughan	Issue date	24 July 2009

SAFKEG-LS 3979A - Gas contents limit for leaktight condition

Scope

This calculation is to determine the maximum amount of the radioactive gases that may be carried based on the allowable leakage rates limits specified in 10 CFR71 for HAC.

The CV closure is leakage tested to demonstrate that it has a maximum leakage rate of 1 x 10-7 ref.cm³/s; for this leakage rate the calculated hole size for a single leak path in the dia 3 mm O-ring having a hole length a = 0.26 cm is D = 1.1e-4 cm (see CS 2009/06, Issue A).

Calculation method

The methodology is that given in ANSI-N14.5-1997.

The equation references are those in ANSI-N14.5-1997 (see Table 1 for definitions of symbols).

$$La = (Fc+Fm)(Pu-Pd) \quad cm^3/s \tag{B.2}$$

$$Fc = 2.49 \times 10^6 \times \frac{D^4}{a \times \mu} \quad cm^3/atm.s \tag{B.3}$$

$$Fm = 3.81 \times 10^3 \times \frac{D^3}{a \times Pa} \sqrt{\frac{T}{M}} \quad cm^3/atm.s \tag{B.4}$$

$$Lu = La \times \frac{Pa}{Pu} \quad cm^3/s \tag{B.5}$$

$$Q = Lu \times Pu = La \times Pa \quad atm.cm^3/s$$

The calculations shown in Table 1 follow the methodology on the previous page.

The principal data is taken from the sources listed in the table notes.

The free volume in the CV # 3980 is taken as 200 cc (see CS 2009/05, Issue A).

The calculation is base on the worst case condition of loading at 0°C and operating at the maximum bounding temperature of 200°C.

The mass leakage rate = Q x fluid density.

The activity leakage rate = mass leakage rate x specific activity.

The #A_2 leakage rate = activity leakage rate / A_2 value.

The #A_2 per wk = #A_2 leakage rate x 168 hr/week.

The maximum amount of each radioactive gas that may be carried is that which results in gas leakage at the allowed limit of A_2/week and "effective A2 for Kr-85" = 10 x "specified A2".

Prepared	R A Vaughan	Checked	A L Ferguson
Approved	R A Vaughan	Issue date	24 July 2009

Table 1 Gas Leakage Rates					
	Symbol	Note ref	Units	Kr79	Xe133
Free volume	Vf	1	cm3	100	100
Leakage hole diameter	D	2	cm	1.10E-04	1.10E-04
Leakage hole length	a	3	cm	0.26	0.26
Molecular weight	M		g/mol	79	133
Activity limit	Aci	4	Ci	9.35E+04	2.41E+05
	Abq		Bq	3.46E+15	8.92E+15
Specific activity	Sp		Bq/g	4.21E+16	6.90E+15
A2	A2		Bq	2.00E+12	1.00E+13
Mass of gas	m		g	8.2E-02	1.3E+00
Volume of gas @ STP	Vg		cm3	2.3E+01	2.2E+02
Density at 20degC	Dg		g/cm3	3.5E-03	5.9E-03
Temp of fluid	T	5	deg C	200	200
Volume of gas@ design limit	Vt		cm3	4.0E+01	3.8E+02
Upstream pressure	Pu	6	atm abs	4.0E-01	3.8E+00
Downstream pressure	Pd		atm abs	0.0E+00	0.0E+00
Pa	Pa		atm abs	2.0E-01	1.9E+00
Viscosity	Mu	7	cP	0.0376	0.0376
Coefficient of continuum flow	Fc		cm3/atm.s	3.7E-08	3.7E-08
Coefficient of molecular flow	Fm		cm3/atm.s	2.4E-07	2.0E-08
La	La		cm3/s	1.1E-07	2.1E-07
Lu	Lu		cm3/s	5.5E-08	1.1E-07
Q	Q		atm.cm3/s	2.2E-08	4.0E-07
Mass leakage rate	Lm		g/s	7.9E-11	2.4E-09
Activity leakage rate	La		Bq/s	3.3E+06	1.7E+07
#A2/hr leakage rate	Lhr	8	#A2 /hr	6.0E-03	6.0E-03
#A2 per wk eakage rate	Lwk	9	#A2 /wk	1.00E+00	1.00E+00

1) The free volume in the CV 3980 is taken as 100 cc which is 50% of the calculated free volume [free volume = cavity volume less volume of steel insert LS-50x103-SS and allowance of 35 cc for product container shell].
2) Leak Hole diameter is defined as that which results in a leak of 10-7 ref.cc/s (air). This is the leaktight criteria that the package is required to meet at each maintenance.
3) Leak hole length is 0.866 x the O-ring cord diameter = 0.866 x 0.3 cm= 0.26 cm.
4) Activity limit for the individual nuclide
5) Design Limit temperature is the upper bounding temperature for the package = 200 deg.C. The package is loaded at 0 deg.C.
6) Partial pressure of radioisotope in the CV calculated from gas and free volumes. The downstream partial pressure is 0.
7) Source: Chemistry and Physics Handbook @ 400K.
8) Calculated leakage rate in A2/hr.
9) Calculated leakage rate in A2/week.

CONTENTS

5 SHIELDING EVALUATION

This section of the application identifies the principal radiation shielding design features of the packaging that are important to safety and provides the results of analysis that shows the packaging meets the shielding requirements of the regulations.

5.1 Description of Shielding Design

5.1.1 Design Features

Figure 5.1 shows the gamma shielding present in the Safkeg-LS 3979A package. The materials of construction and dimensions are fully specified in the drawings in Section 1. Beta and Gamma shielding is provided principally by the lead present in the containment vessel body and lid; the steel of the CV provides some additional shielding.

The lead is cast in position inside the stainless steel cladding of the body and the lid. The only gap between the lead and the stainless steel cladding is at the outside cylindrical surface of the lead. For the CV body, the lead shrinks onto the CV cavity wall, leaving no gap while the gap between the lead and the stainless steel cladding at the outside cylindrical surface of the lead is about 0.2 mm wide. There is no axial gap at the lead onto the base of the CV cavity wall and the method of fitting the CV base leaves no gap. For the CV lid, no gap was found on fabrication of the prototype between the lead and the stainless steel cladding at the outside cylindrical surface of the lead. There is no axial gap as the lead is cast into the CV lid shielding casing and machined such that fitting to the CV lid top leaves no gap. Therefore, there are no gaps in the lead shielding of CV, or at the interface of the lead and steel parts that affect the shielding. The containment vessel is designed so that the shielding in the lid and body are stepped to reduce radiation streaming. The upstanding ring on the lid also provides some additional steel shielding to reduce the radiation streaming from the gap between the CV Lid and CV Body.

The contents of the package are defined as everything that is carried within the CV cavity. For all contents, one of the inserts shown in Figures 5.2a, 5.2b or 5.2c is used – these are fully specified in Section 1.2.2.2. These inserts provide different amounts of shielding and also provide confinement for all contents under NCT, and confinement for solid contents under HAC.

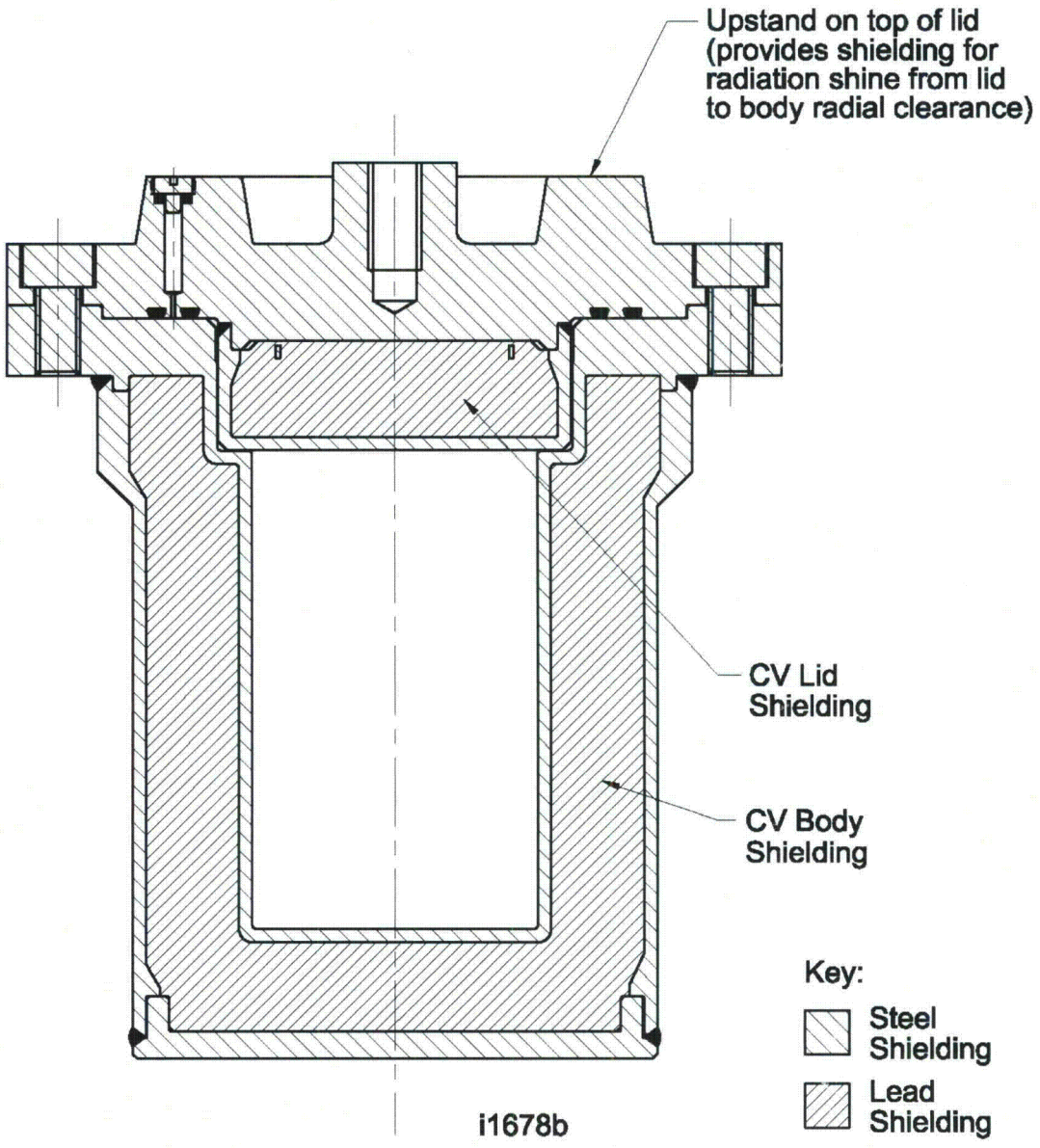

Figure 5-1 Gamma shielding present in the 3979A package

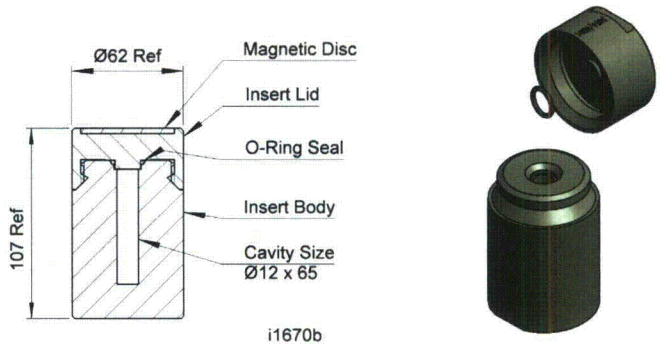

Figure 5-2a Shielding insert LS-12x65-Tu – Design # 3984

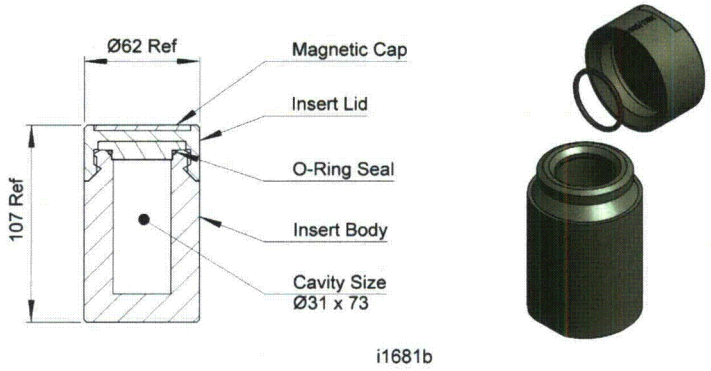

Figure 5-2b Shielding insert LS-31x73-Tu – Design # 3983

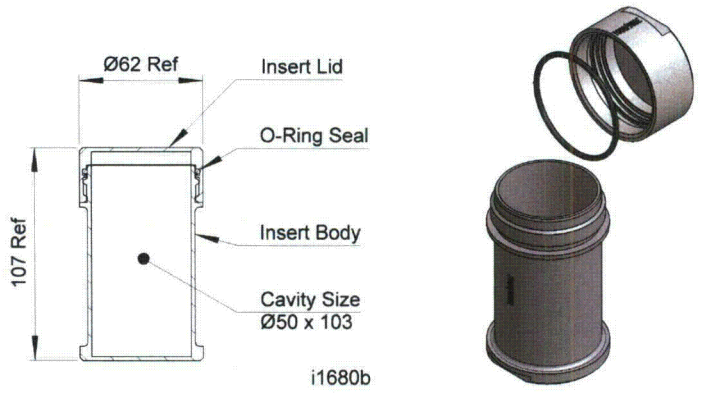

Figure 5-2c Shielding insert LS-50x103-SS – Design # 3986

5.2 Summary Table of Maximum Radiation Levels

The calculations in the shielding evaluation determined the maximum contents that could be carried whilst limiting the package surface dose rates and dose rates at 1 m from the surface (TI) to the levels shown in Table 5-1. These are the limits specified in 10 CFR 71.47(a) [3.1] for Non-Exclusive Use. Exclusive Use shipments are not planned for this package.

With regard to TI, when the the package surface dose rate is at 2 (200) mSv/h (mrem/h) the dose rate at 1m from the surface (TI) will be about 0.5 (5) mSv/h (mrem/h) because of the geometry of the package. Therefore, if the package surface dose rate is < 2 (200) mSv/h (mrem/h), then the dose rate at 1m from the surface (TI) will be < 0.5 (5) mSv/h (mrem/h).

Table 5-1 Summary Table of Maximum Radiation Levels

Normal Conditions of Transport	Package Surface mSv/h (mrem/h)			1 Meter from Package Surface mSv/h (mrem/h)		
Radiation	Top	Side	Bottom	Top	Side	Bottom
Total Gamma + Neutron	2 (200)	2 (200)	2 (200)	0.1 (10)	0.1 (10)	0.1 (10)

In practice, the surface dose rate will be less than the calculated dose rates for maximum contents of 2 (200) mSv/h (mrem/h) because the assumptions for the calculations as summarized below are inherently conservative.

The MicroShield calculations are based on the following worst case assumptions.

- Self shielding is neglected as the contents are assumed to be a point source.
- The point source is positioned in the worst position (centre of bottom of the Insert) whereas in practice it will usually be a volume distributed throughout a significant part of the cavity.
- Shielding provided by the Product containers is neglected.

The Monte Carlo calculations for liquid contents are based on the following worst case assumptions.

- The CV Lid and CV Body (see Section 5.3.1.1) have maximum gap dimensions.
- The CV Lid has maximum offset within the CV Body.
- All the liquid has leaked from the Product Container and also from the Insert.
- The package is upside down on its lid.
- The liquid has flowed to completely fill the gap between the CV Lid and CV Body.

5.3 Source Specification [71.33 (b)(1)]

5.3.1 Gamma Source

For solid, liquid and gas contents, the source (gamma, beta or alpha according to nuclide) is specified as a point source for all calculations.

For liquid contents under HAC, it has been assumed that the liquid has leaked from the product containers and insert, that the package is upside down on its lid, and that the liquid has flowed into the gap between the CV Lid and CV Body. The calculations are based on this "volume" source.

Details of source strength for the MicroShield shielding calculations is reported are CTR 2009/22 (Section 5.5.2).

Details of source strength for the Monte Carlo shielding calculations are reported in SERCO/TAS/003191 (Section 5.5.2).

5.3.2 Neutron Source

The only contents that emit neutrons are plutonium (limited to solid form).

Details of the source strength are given in report CTR 2009/22 (Section 5.5.2).

5.4 Shielding Model

5.4.1 Configuration of Source and Shielding

5.4.1.1 Model for Monte Carlo calculations for reference case (Ir-192)

For the Monte Carlo calculations, the reference case is for a 1kCi Ir-192 point source positioned all around the surface of the empty CV cavity. This includes a position that lines up with the gap between the CV lid and CV Body. Calculations were also performed with the source in similar positions within the two tungsten inserts (LS-12x65-Tu – Design # 3984, LS-31x73-Tu – Design # 3983).

5.4.1.2 Model for MicroShield calculations for Solid and Liquid Contents

For the MicroShield shielding calculations reported in CTR 2009/22 (Section 5.5.2), the contents are modeled by a point source positioned at the centre of the bottom of the insert within the CV. The calculations were restricted to the point source at this one position as the Monte Carlo calculations for the reference case (1kCi Ir-192 point source) show that this position produces the higher dose rate on

the external surface of the package (see Table 5-3). The MicroShield calculations also include point source calculations for the liquid and gaseous contents.

Full details of the configuration of the source are given in the reports referenced above.

5.4.1.3 Model for Monte Carlo calculations for Liquid Contents

For the Monte Carlo calculations for liquid contents, it has been assumed that under HAC the liquid has leaked from the insert (and that the insert is no longer present), the package is upside down on its lid, and the liquid has flowed into the gap between the CV Lid and CV Body and is of depth "X" in the CV cavity above the lid - as given in Table 5-2. The configuration of the CV body and CV Lid components and depth "X" for the liquid used for the calculations is shown in Figure 5-3.

The calculations are based on the source being the volume of liquid as given in Table 5-2.

Table 5-2 Liquid source details

Nuclide	Mo-99	Se-75	Ho-166	Lu-177	Tl-201
Specific activity	6 Ci/ml	3 Ci/ml	2 Ci/ml	3 Ci/ml	1 Ci/ml
Volume (1)	20 ml	100 ml	50 ml	100 ml	100 ml
Total activity	120 Ci	300 Ci	100 Ci	300 Ci	100 Ci
Depth in cavity "X" (2)	5.0 mm	29.4 mm	14.2 mm	29.4 mm	29.4 mm

1 Maximum volume for each nuclide
2 Calculated on basis of dimensions in Figure 5-3 (CS 2009/14 [3.3])

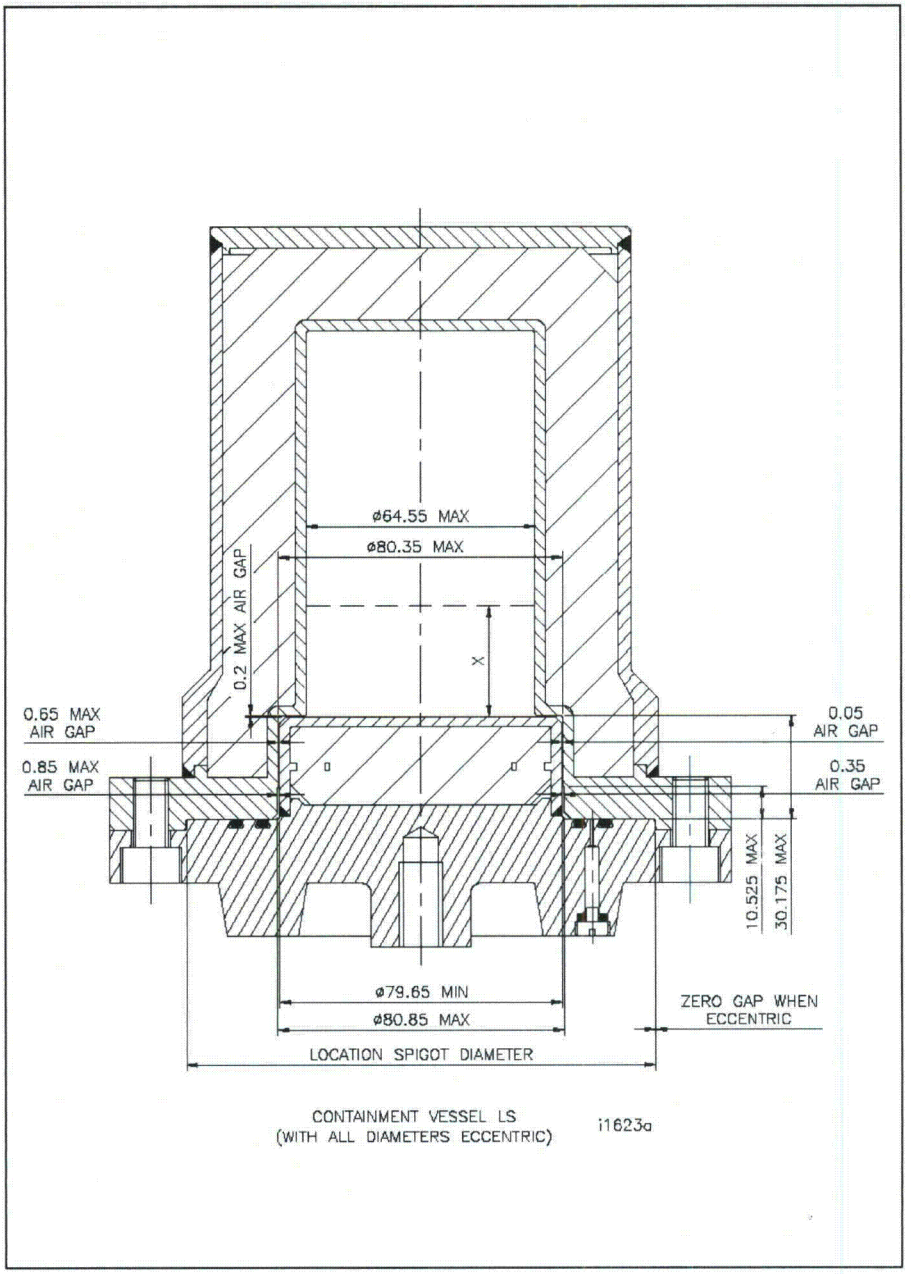

Figure 5-3 Configuration of the CV body and CV Lid components for the liquid calculations

5.4.2 Material Properties

The material properties used for the shielding evaluations are given in the reports referenced in Section 5.3.1.

5.5 Shielding Evaluation

5.5.1 Methods

The methods used for the Monte Carlo shielding calculations are reported in SERCO/TAS/003191(Section 5.5.2).

The methods used for the MicroShield shielding calculations are reported are CTR 2009/22 (Section 5.5.2). This includes the methodology for assessing gamma emitters, beta emitters and neutron emitters.

5.5.2 Input and Output Data

The input and output data for the Monte Carlo shielding calculations are reported in SERCO/TAS/003191 (Section 5.5.2).

The input and output data for the MicroShield shielding calculations is reported are CTR 2009/22 (Section 5.5.2).

5.5.3 Flux to Dose Rate Conversion

The flux to dose rate conversion data for the Monte Carlo shielding calculations reported in SERCO/TAS/003191 (Section 5.5.2) are taken from ICRP 74 [3.2].

The flux to dose rate conversion data for the MicroShield shielding calculations reported in CTR 2009/22 (Section 5.5.2) are performed by the software using ICRP-51 [3.4].

5.5.4 External Radiation Levels

5.5.4.1 Monte Carlo calculations

5.5.4.1.1 Monte Carlo calculations for reference case (Ir-192)

The results of the Monte Carlo shielding calculations reported in SERCO/TAS/003191 (Section 5.5.2) for the reference case of 1kCi Ir-192 point source, with the source positioned all around the surface of the CV, are presented in Tables 5-3 (surface radiation levels) and Table 5-4 (Radiation Levels at 1m from the Surface).

The results showed that the maximum radiation level for each surface was with the source at the centre of the correlating inner surface of the CV cavity – see Table 5-3.

The calculations also provide the dose rate at the seal O-ring position – see Table 5-3.

Table 5-3 Summary Table of External Surface Radiation Levels and Maximum O-ring Dose Rate - Monte Carlo calculations for reference case (Ir-192)

Source position in CV cavity or Insert	External Surface Radiation Levels (mSv/h)		
	No insert	LS-31x73-Tu Design No 3983	LS-12x65-Tu Design No 3984
	(least shielding)	(median shielding)	(most shielding)
Centre at the top of the cavity	9.25E+02	3.29E+01	1.50E+01
Centre at the bottom of the cavity	4.30E+03	1.67E+02	7.72E+01
Centre at side of the cavity	2.82E+03	1.21E+02	2.08E+01
Eccentred at the side of the CV cavity with the source near the top lined up with the CV Top and Body gaps	3.29E+03	Not applicable	Not applicable
CV O-ring	3.43E+05	3.05E+02	1.46E+02

The highest dose rate at the surface of the package for a point source in all positions within the CV is seen to be with the source at the centre of the bottom of the CV cavity and the highest surface dose rate is at the centre of the bottom of the Outer Keg Shell.

Table 5-4 Summary Table of External Radiation Levels at 1m from the Surface - Monte Carlo calculations for reference case (Ir-192)

Source position in CV cavity or Insert	External Surface Radiation Levels (mSv/h)		
	No insert	LS-31x73-Tu Design No 3983	LS-12x65-Tu Design No 3984
	(least shielding)	(median shielding)	(most shielding)
Centre at the top of the cavity	1.38E+01	5.33E-01	2.40E-01
Centre at the bottom of the cavity	4.22E+01	1.97E+00	9.74E-01
Centre at side of the cavity	5.08E+01	2.57E+00	4.68E-01
Eccentred at the side of the CV cavity with the source near the top lined up with the CV Top and Body gaps	3.29E+01	Not applicable	Not applicable

The dose rate at 1m from the surface of the package for a point source in all positions within the CV is seen to be with the source at the centre of the bottom or side of the CV cavity and the highest surface dose rate is at centre of the bottom or side of the outer Keg Shell respectively.

5.5.4.2 MicroShield calculations

The results of the MicroShield shielding calculations (reported in CTR 2009/22 (Section 5.5.2), consider all of the nuclides to be represented as a point source positioned at the centre of the bottom of each insert, are given in Table 5-5.

Under NCT, it is assumed that both liquids and gaseous contents are contained in sealed product containers within the applicable insert and that the liquids and gaseous contents do not leak from the insert during NCT. Therefore the NCT shielding calculations for liquid and gaseous contents are represented by the calculations for a point source positioned at the centre of the bottom of each insert, and the package limits are those given in Table 5-4.

The activities given in Table 5-4 are used to determine the package limit, taking into account mass limit, heat limit, gas limit and shielding limit – see report PCS 036 (see Section 1.3.3).

Table 5-5 Summary Table of External Radiation Levels - MicroShield calculations

		Activity for Surface Dose of 2 mSv/h		
	Insert	LS-12x65-Tu – Design # 3984	LS-31x73-Tu – Design # 3983	LS-50x103-SS – Design # 3986
Ref #	Nuclide			
1	Ac-225	1.22E+11	8.35E+10	2.08E+10
2	Ac-227	8.38E+11	4.70E+11	5.40E+10
3	Ac-228	1.07E+10	6.90E+09	1.41E+09
4	Am-241	7.07E+19	1.88E+19	1.18E+17
5	As-77	1.95E+14	7.84E+13	2.85E+12
6	Au-198	2.33E+12	1.32E+12	7.61E+10
7	Ba-131	4.52E+11	2.56E+11	2.31E+10
8	C-14	4.55E+36	4.26E+36	1.47E+29
9	Co-60	2.28E+09	1.53E+09	3.68E+08
10	Cs-131	4.85E+35	4.54E+35	3.59E+35
11	Cs-134	2.24E+10	1.29E+10	1.62E+09
12	Cs-137	1.42E+11	7.09E+10	5.85E+09
13	Cu-67	4.53E+16	1.21E+16	7.67E+13
14	Hg-203	1.06E+19	8.26E+17	6.03E+13
15	Ho-166	2.42E+11	1.66E+11	4.46E+10
17	I-125	2.61E+35	2.44E+35	1.93E+35
18	I-129	4.57E+35	4.28E+35	3.38E+35
19	I-131	1.34E+12	6.71E+11	5.03E+10
20	In-111	1.38E+22	4.81E+20	1.70E+15
21	Ir-192	9.60E+11	4.30E+11	2.10E+10
22	Ir-194	2.58E+11	1.66E+11	3.35E+10
23	Kr-79	3.34E+11	2.00E+11	2.49E+10
24	Lu-177	1.21E+19	1.73E+18	1.29E+15
26	Mo-99	2.80E+11	1.52E+11	1.70E+10
28	Na-24	7.80E+08	5.66E+08	1.79E+08
29	Np-237	6.93E+18	6.49E+18	5.02E+18
30	P-32	1.90E+10	1.35E+10	2.20E+10
31	P-33	2.37E+23	9.18E+21	1.37E+17
32	Pb-203	1.45E+13	7.34E+12	5.70E+11
33	Pb-210	3.31E+15	1.87E+15	2.39E+14
34	Pd-109	1.17E+15	4.58E+14	1.50E+13
35	Pu-238	2.99E+14	2.99E+14	2.99E+14
36	Pu-239	6.47E+21	4.64E+21	8.26E+20
37	Pu-240	1.15E+13	1.15E+13	1.15E+13
38	Pu-241	2.77E+21	7.33E+20	4.32E+18
39	Ra-223	8.46E+11	4.74E+11	5.46E+10
40	Ra-224	3.33E+09	2.44E+09	7.83E+08
41	Ra-226	3.62E+09	2.54E+09	6.81E+08
42	Re-186	1.38E+14	7.21E+13	6.93E+12
43	Re-188	5.74E+11	3.55E+11	6.02E+10
44	Rh-105	1.69E+17	2.33E+16	1.48E+13
45	Se-75	6.39E+14	1.70E+14	1.28E+12
47	Sm-153	9.33E+15	2.76E+15	3.15E+13
48	Sr-89	1.11E+14	6.64E+13	1.06E+13
49	Sr-90	1.62E+13	6.89E+12	8.94E+11
50	Tb-161	6.57E+17	2.99E+14	1.69E+13
51	Th-227	1.79E+12	1.01E+12	1.16E+11
52	Th-228	2.53E+09	1.86E+09	5.96E+08
53	Tl-201	1.11E+30	1.04E+30	1.16E+25
55	U-235	5.60E+14	3.14E+14	3.60E+13
56	W-187	1.96E+11	1.01E+11	8.88E+09
57	W-188	6.02E+11	3.72E+11	6.31E+10
58	Xe-133	3.20E+35	2.87E+35	1.61E+25
59	Y-90	8.76E+09	6.41E+09	6.02E+09
60	Yb-169	6.46E+17	9.51E+16	5.06E+13
61	Yb-175	1.41E+15	3.65E+14	2.56E+12

5.5.4.2.1 Monte Carlo calculations for liquid contents

The package external dose rates for the Monte Carlo shielding calculations reported in SERCO/TAS/003191 (Section 5.5.2) are summarized in Table 5-6 for the row titled "Max TI". From this data the maximum activity of the contents is calculated based on a dose rate at 1m from the package surface of 10 mSv/h (1000 mrem/hr), as allowed under HAC.

Table 5-6 Summary Table of External Radiation Levels - Monte Carlo calculations for liquid contents

Nuclide		Mo99	Mo99	Se75	Ho166	Lu177	Tl201
Specific activity	Ci/ml	6	60	3	2	3	1
Volume	ml	20	20	100	50	100	100
Total activity	Ci	120	1200	300	100	300	100
	Bq	4.44E+12	4.44E+13	1.11E+13	3.7E+12	1.11E+13	3.7E+12
Depth in cavity "X"	mm	5.0 mm	5.0 mm	29.4 mm	14.2 mm	29.4 mm	29.4 mm
Max TI [Mx]	µSv/hr	6.23E+03	6.23E+04	1.60E+03	1.67E+03	5.59E+01	4.41E+00
	(mrem/hr)	6.23E+02	6.23E+03	1.60E+02	1.67E+02	5.59E+00	4.41E-01
Ratio 1000/Mx = F Sp Ac		1.61E+00	1.61E-01	6.25E+00	5.99E+00	1.79E+02	2.27E+03
Act for 1000 mrem/hr @1m	Ci	1.93E+02	1.93E+02	1.88E+03	5.99E+02	5.37E+04	2.27E+05
Package limit	Bq	7.13E+12	7.13E+12	6.94E+13	2.22E+13	1.99E+15	8.39E+15

F Sp Ac = Factor by which Specific Activity could be increased for 1000 mrem/hr @ 1m

Input data Results Package

The activities given in Table 5-6 are used to determine the package limit taking into account mass limit, heat limit, gas limit and shielding limit – see PCS 036 (see Section 1.3.3).

5.6 Appendix

5.6.1 References

[3.1] Title 10, Code of Federal Regulations, Part 71, Office of the Federal Register, Washington D.C.

[3.2] ICRP Publication 74, "Conversion Coefficients for use in Radiological Protection against External Radiation", Annals of the ICRP 26 3/4, 1996

[3.3] CS 2009/14, SAFKEG-LS-3979A-Liquids shielding limits - HAC - based on TI

[3.4] ICRP Publication 51, "Data for Use in Protection against External Radiation", Annals of the ICRP, 1984

5.6.2 Supporting Documents

Document Reference	Title
CTR2009/22	SAFKEG LS 3979A: Package Activity Limits Based on Shielding
SERCO/TAS/003191/001	Monte Carlo Modelling of Safkeg LS Container

CROFT

Safkeg-LS 3979A: Package Activity Limits Based on Shielding

Title	Safkeg-LS 3979A: Package Activity Limits Based on Shielding	**Number**	CTR 2009/22
		Issue	Issue A
		File Reference	CTR2009-22-A-d4-SAFKEG LS 3979A-Package Activity Limits-Shielding.doc
Compiled	A L Ferguson	**Checked**	R A Vaughan
Approved	N Jorgensen	**Date**	21 July 2009
Croft Associates Ltd, F4 Culham Science Centre, Abingdon, Oxfordshire, OX14 3DB. 44 (0)1865 407740			

Contents

1. Introduction

The Safkeg-LS 3979A package is a general purpose container for the transport of non-fissile and fissile excepted nuclides under non exclusive use, in solid, liquid and gaseous form, via all modes of transport (road, rail, sea and air).

The Safkeg-LS 3979A package consists of an outer stainless steel double-skinned insulated keg (3979) which is 483 mm long and 424 mm in diameter. Carried within the keg is an insulating cork liner into which a single resealable containment vessel 3980 (made of lead clad in stainless steel) is located. The maximum weight of the package is 62.1 kg (137 lbs) excluding the contents. The maximum contents weight is 5.9 kg (13 lbs), therefore the gross weight of the package is 68 kg (150 lbs).

Section views of the package and the containment vessel are shown in Figure 1, 2 and 3 and the dimensions employed in the shielding models are shown in Figures 7 and 8. These figures also give the nomenclature used throughout this report.

The package is designed as a general purpose package for radioactive material that requires some shielding, however, the design includes additional optional shielding inserts, for radioactive material that requires additional shielding.

The package is designed for radioactive material that emits alpha, beta or gamma radiation. The specified contents do not include materials that emit a significant amount of neutrons.

The contents may be in solid, liquid or gaseous form and carried in various inserts: Design No's 3983, 3984 and 3986, as depicted in Figures 4, 5 and 6.

This report assesses the shielding performance of the Safkeg-LS 3979A package in complying with the non-exclusive use provisions of the 10 CFR71 transport regulations [1] (specifically, the dose limits detailed in10 CFR71.47), when transporting the nuclides detailed in Tables 3 to 6.

The package performance when carrying 1000 Ci of ^{192}Ir was assessed independently in order to establish the worst case orientation of the package in terms of shield performance, as reported in reference 2. The shielding calculations and activity for the

additional radionuclides to be carried were performed using Grove Software's code "MicroShield" [3], employing a 1 Ci point source of each nuclide.

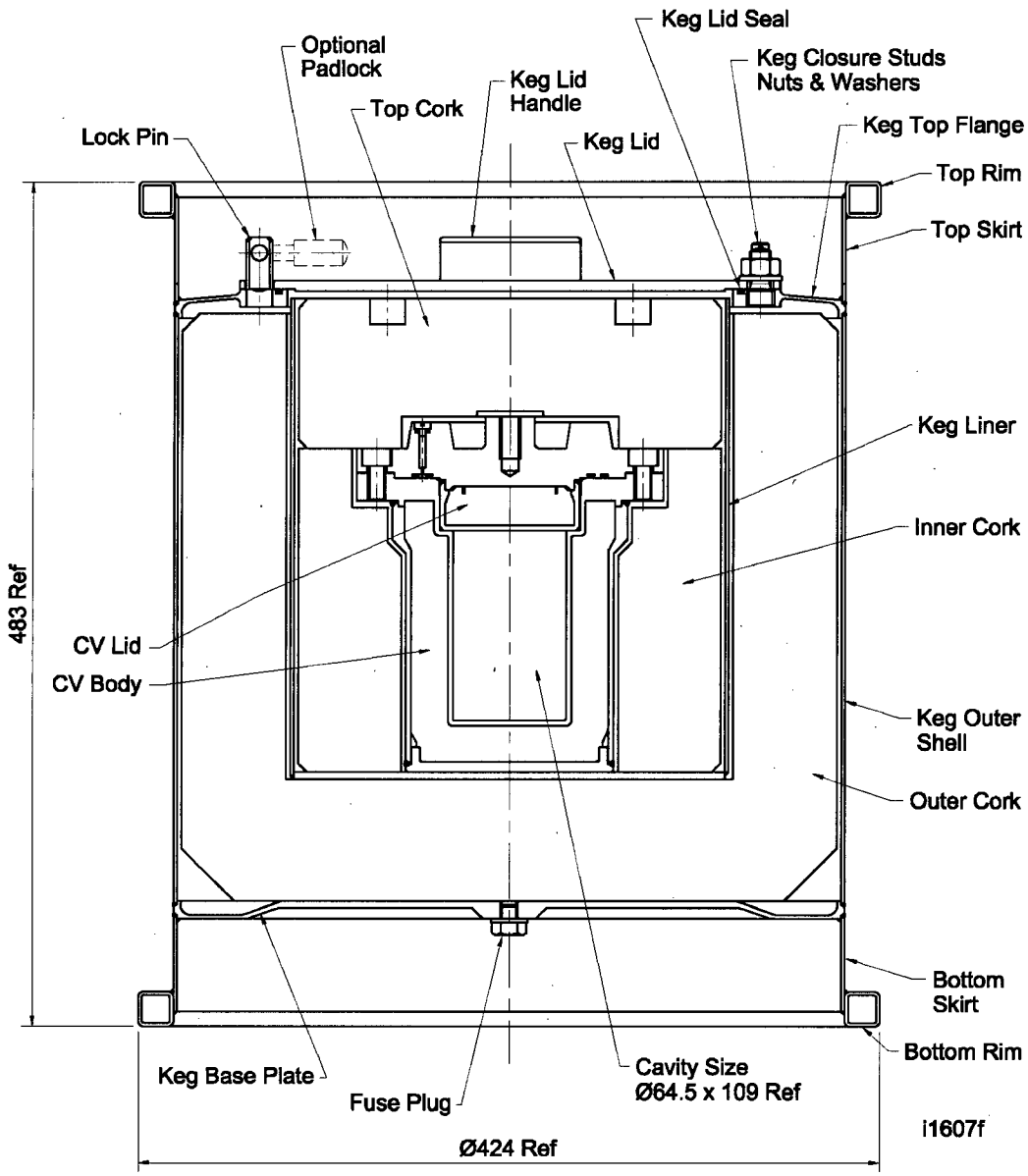

Figure 1: Safkeg-LS 3979A package - Sectional View and Nomenclature

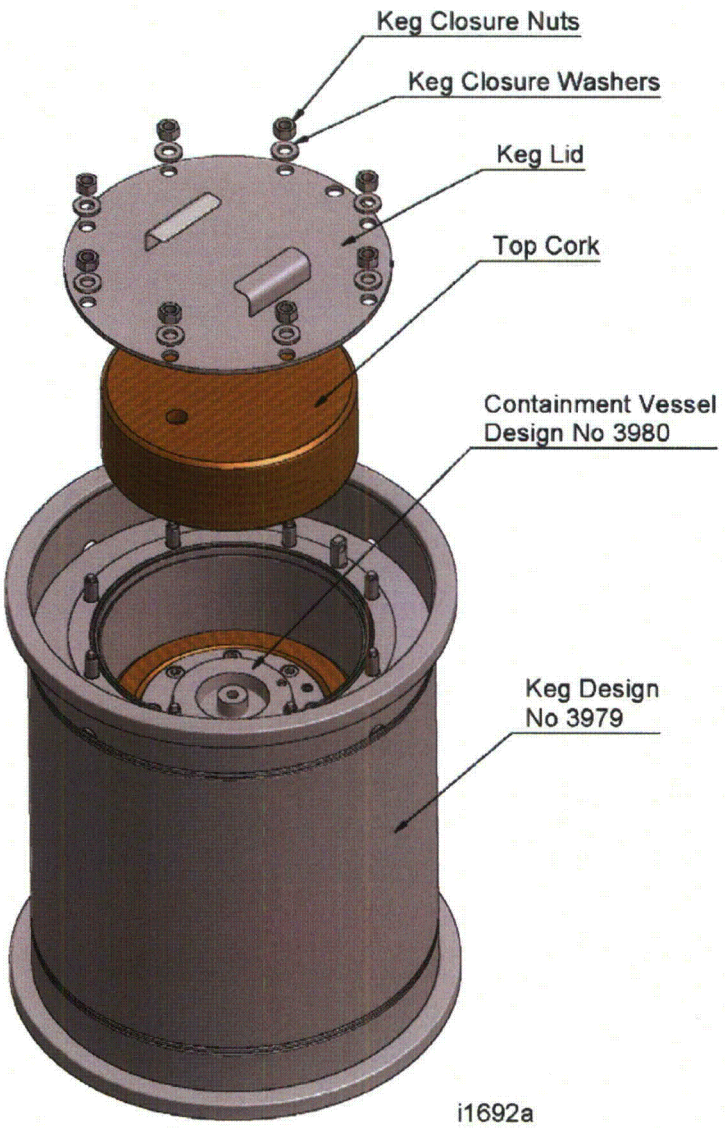

Safkeg LS Design No 3979A

Figure 2: Safkeg-LS 3979A package - Isometric View with Nomenclature

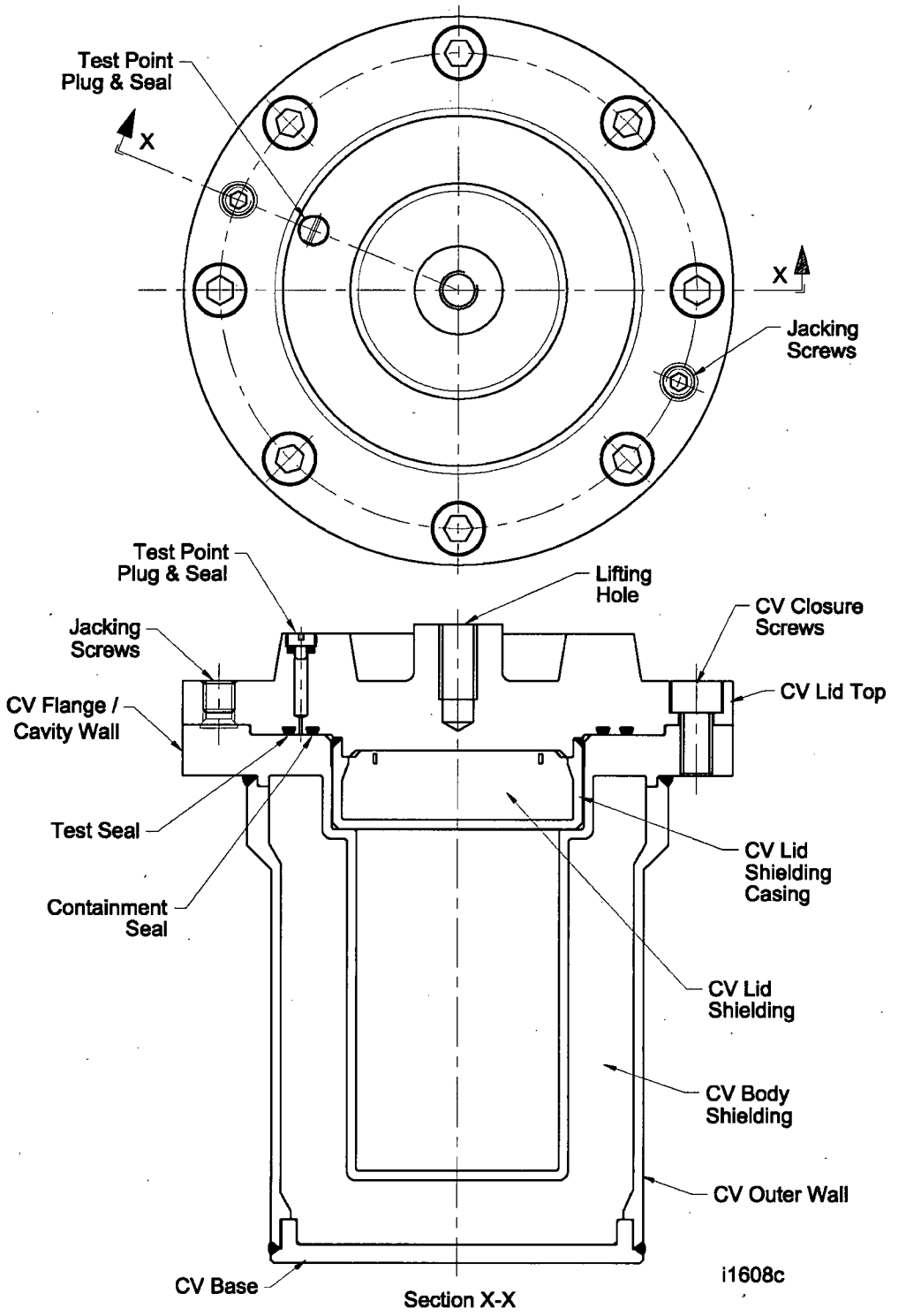

Figure 3: 3980 Containment Vessel - Top and Sectional View with Nomenclature

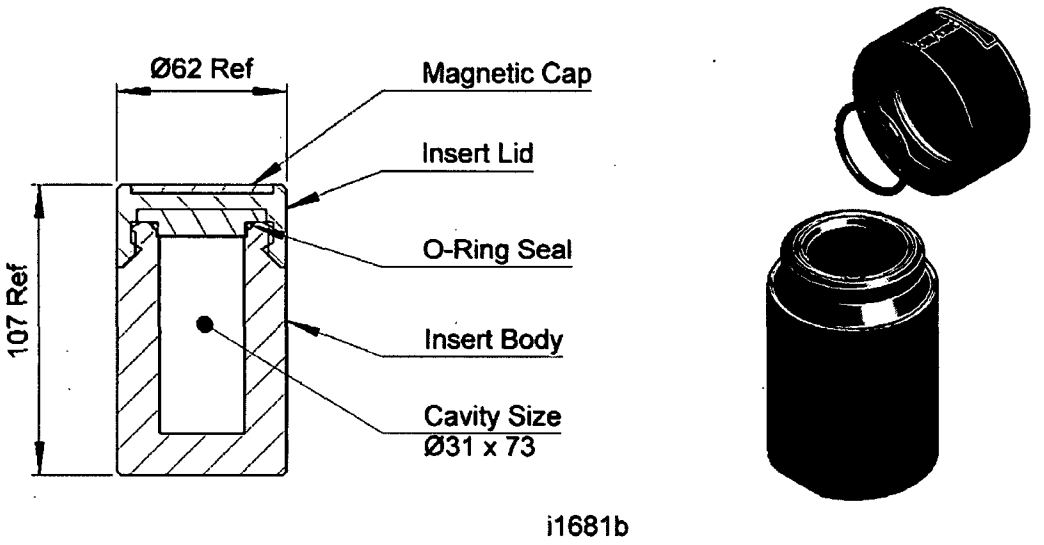

Figure 4: Shielding Insert LS-31x73-Tu, Design No 3983

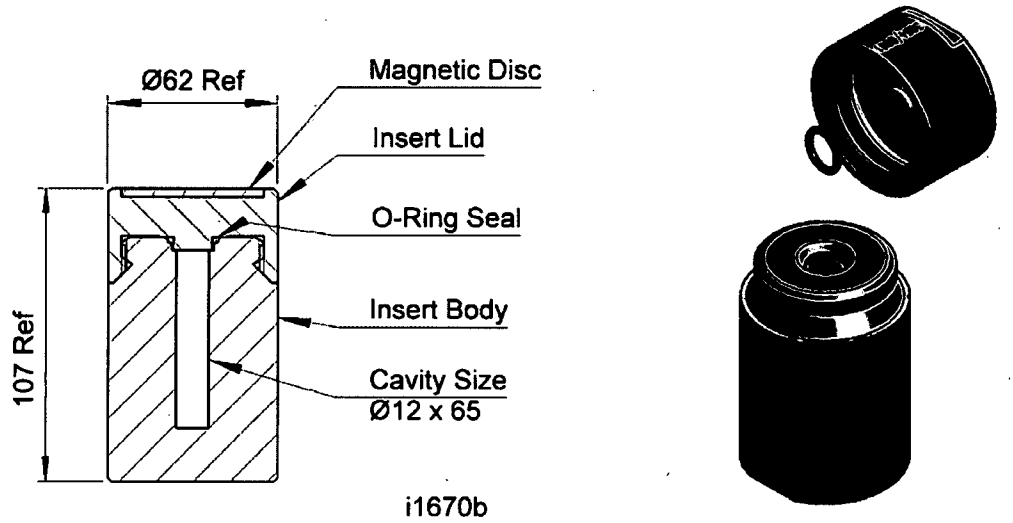

Figure 5: Shielding Insert LS-12x65-Tu, Design No 3984

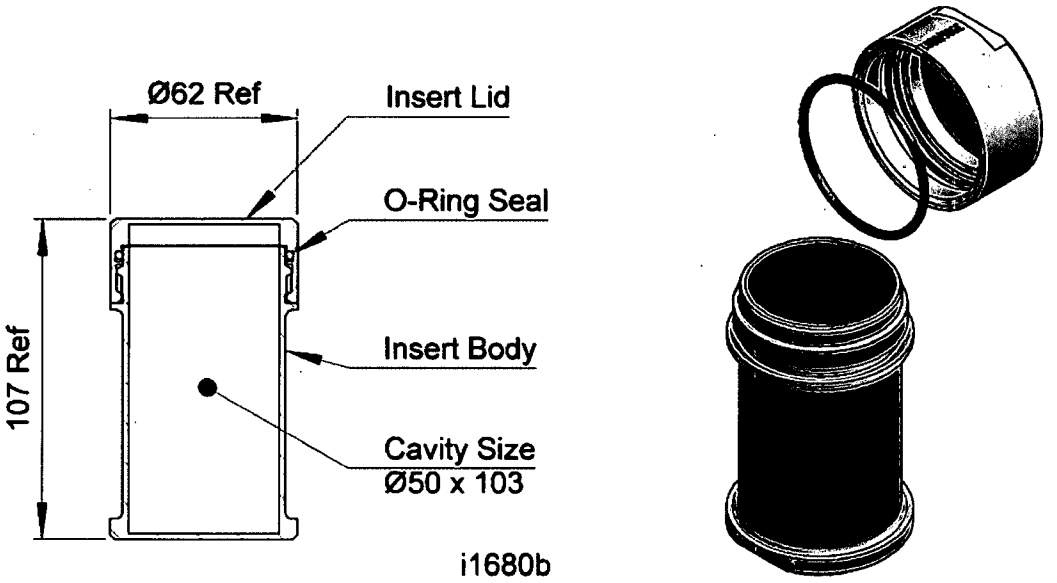

Figure 6: Shielding Insert LS-50x103-SS, Design No 3986

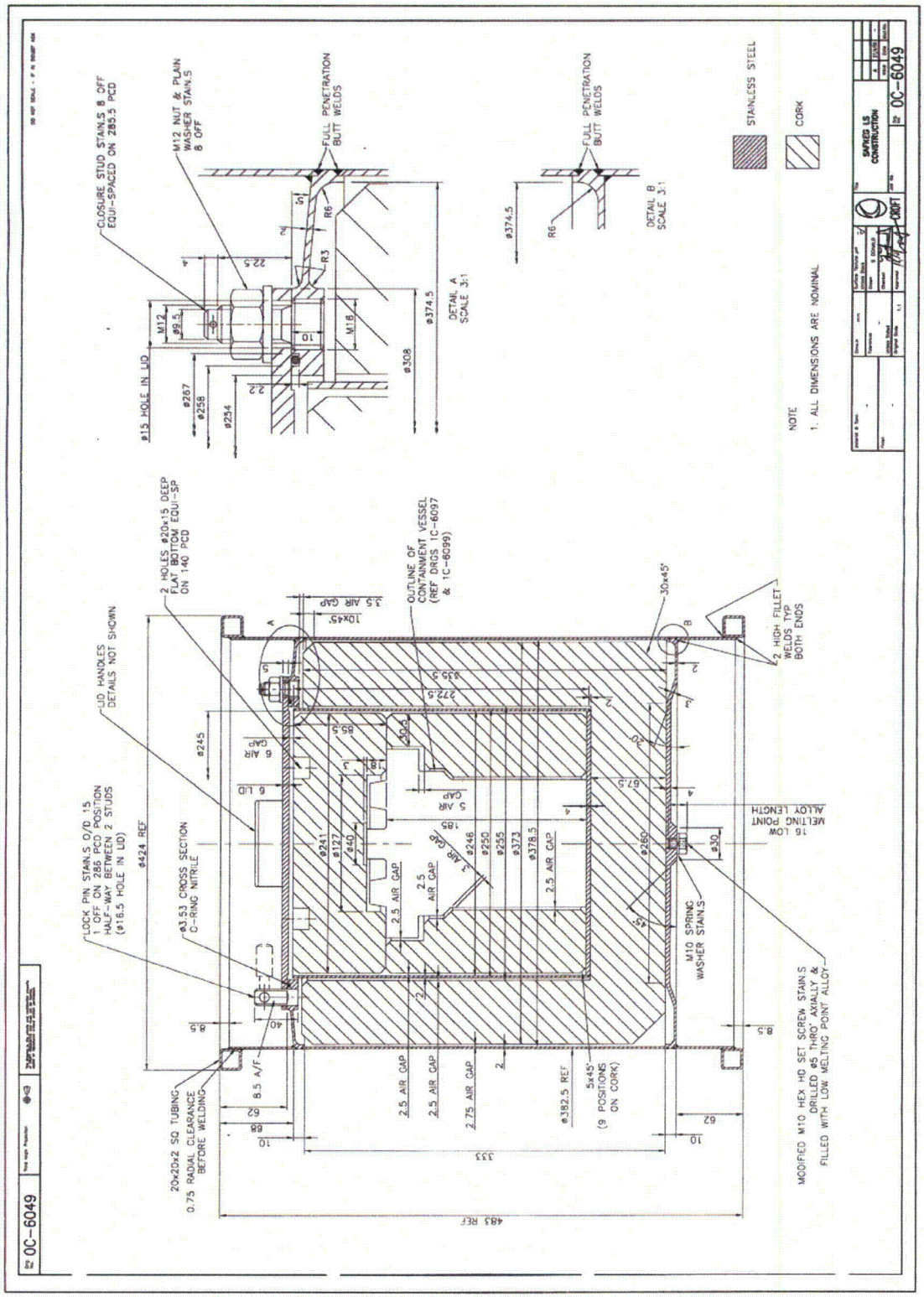

Figure 7: SAFKEG-LS 3979A PACKAGE, Design No 3979

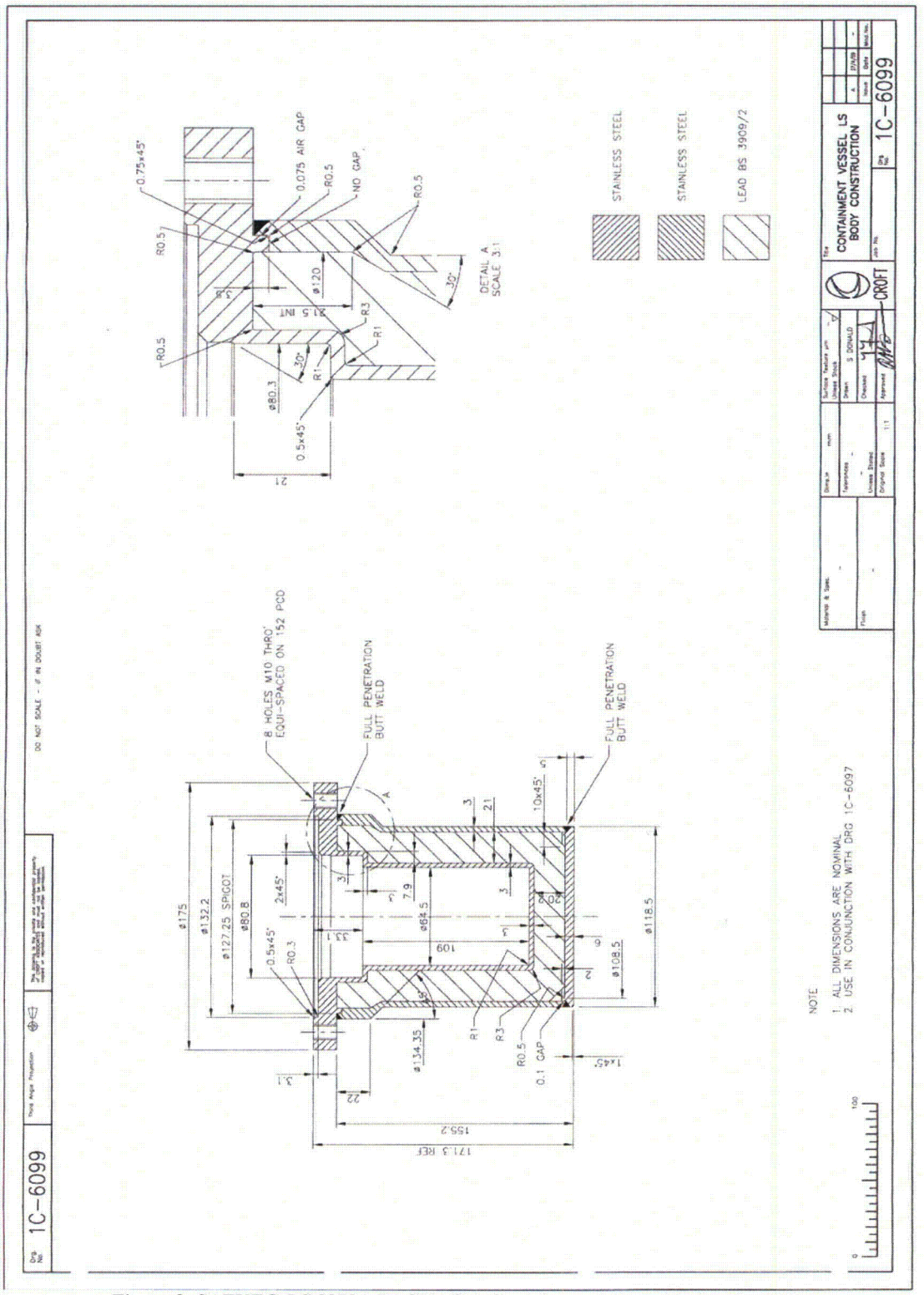

Figure 8: SAFKEG-LS 3979A PACKAGE, Containment Vessel Design No 3980

2. Shielding Assessment

2.1. Comparison with Monte Carlo Based Calculations on ^{192}Ir

The modelling performed in this assessment was validated against Monte Carlo calculations performed by Serco Assurance, using the code MCBEND. The Serco work, which is reported in reference 2, demonstrated that the worst case dose rates occur with a point source at the centre of the package base with the source at the centre of the base of CV or insert; therefore this assessment only addresses dose rates from a point source through the base of the package.

The MicroShield [3] model was initially compared with the work done by Serco in order to check the model, using a 1000 Ci point source of ^{192}Ir, with a tungsten insert (Design No 3984) located in the package cavity (as used in the Serco work [2]). The dose rates calculated by MicroShield [3] are in accordance with those calculated by Serco [2], as shown below in Table 1.

Table 1: Code Comparisons

Insert	Nuclide	Activity (Ci)	Microshield Exposure Rate mR/h	Effective Dose Equivalent (ICRP 51) mSv/h	Serco Report (Table 6 [2]) mSv/h
3984(1)	Ir-192	1000	**8.38E+03**	7.71E+01	7.72E+01
3983(1)	Ir-192	1000	**1.87E+04**	1.72E+02	1.67E+02
3986(1)	Ir-192	1000	**3.81E+05**	3.52E+03	N/A
No Insert (2)	Ir-192	1000	**4.37E+05**	4.04E+03	4.30E+03

Note

1 Microshield model adjusted to match Serco results for Insert Design No 3984 - W density reduced from 18 to 17.9
2 Microshield model - no adjustments, default material properties used.

2.2. Source and Shield Model

The Safkeg-LS 3979A package geometry employed in the shielding models together with the regional shield materials, the position of the measured dose rates (the detector position) and their properties are summarized in Table 2. To predict the maximum dose rates at the detector positions, a point source is assumed, positioned at the base of the cavity in contact with the inner surface of the cavity or insert. The use of a point source provides the greatest pessimism in the calculated dose rates as in reality, the sources used will consist of primary capsules or containers, with the source distributed within the container: additionally, using a point source takes no account of any self shielding from the distributed source or its container.

The source data employed in the calculations are incorporated within the libraries built into the MicroShield code[3], the gamma energy lines, probabilities and shield

build up factors are detailed within the MicroShield calculations for each nuclide: these calculations are provided in Appendix C.

Table 2: Shield regions and detector positions through base of package (input data)

Shield	Nomenclature	Without Insert (cm)	3983 (cm)	3984 (cm)	Material/ Regional Density (g/cm^3)	3986 (cm)	Material/ Regional Density (g/cm^3)	Comment	Drawing Reference
Source		Point						Positioned at the centerline on the base	
1	Insert	0	1.52	1.92	W/17.9	0.18	Fe/7.86		2C-5889, 2C-6180 and 2C-6160
2	CV Cavity Liner	0.3	0.3	0.3	Fe/7.86	0.3	Fe/7.86		1C-6099
3	CV Shield	2.02	2.02	2.02	Pb-Sb/ 11.04	2.02	Pb-Sb/ 11.04		1C-6099
4	CV Outer Skin	0.6	0.6	0.6	Fe/7.86	0.6	Fe/7.86		1C-6099
5	3979 Cavity Liner	0.4	0.4	0.4	Fe/7.86	0.4	Fe/7.86		0C-6049
6	Cork Base	6.75	6.75	6.75	0.25	6.75	0.25		0C-6049
7	3979 Outer Skin (base)	0.4	0.4	0.4	Fe/7.86	0.4	Fe/7.86		0C-6049
	Detector #1	**10.47**	**11.99**	**12.39**		**10.65**		At packaging surface	
	Detector #2	110.47	111.99	112.39		110.65		1 meter from packaging surface	

2.3. Dose Rates from Gamma, Neutron and Bremsstrahlung Radiation

Calculations of the radiation levels at the exterior of the as built Safkeg-LS 3979A package due to gamma radiation have been carried out using the MicroShield code [3]. The results of the calculations performed and their cumulative effect, are detailed in Tables 3 to 6: a typical output from the MicroShield code is shown in Figure 9. The MicroShield calculations are listed in Appendix C.

The dose rate at the exterior surface of the package resulting from neutron radiation is estimated based upon the neutron energy, its intensity and published dose conversion factors from IAEA SS37 [4] and Cember's Health Physics text [5]: the methodology and results of these calculations are detailed in Appendix A.

The calculations show that the dose rate from spontaneous fission from ^{238}Pu and ^{240}Pu, dominate over the gamma rates given in Tables 3 to 6. The total dose rates from these nuclides, gamma plus neutron are shown in Table 7.

A few of the nuclides carried are either pure beta emitters or emit bremsstrahlung radiation. The MicroShield code does not assess beta or x-ray radiation directly. However, Cember's Health Physics text [5] provides equations for estimating the photon flux from bremsstrahlung radiation and this can be imported into MicroShield, together with the beta energy line, to predict a worst case dose rate. The approach used and the results of the MicroShield calculations are detailed in Appendix B.

MicroShield 7.02			
Croft (7.02-0000)			
Date	By	Checked	
Filename	Run Date	Run Time	Duration
LS-3979A-Base with 3983 Insert-As-77.ms7	June 15, 2009	08:50:40	00:00:00

Project Info	
Case Title	LS 3979A
Description	Base Shielding, point source with 3983 Insert
Geometry	1 - Point

Dose Points			
A	X	Y	Z
#1	11.99 cm (4.7 in)	0.0 cm (0.0 in)	0.0 cm (0.0 in)
#2	111.99 cm (3 ft 8.1 in)	0.0 cm (0.0 in)	0.0 cm (0.0 in)

Shields			
Shield N	Dimension	Material	Density
Shield 1	1.52 cm	Tungsten	17.9
Shield 2	.3 cm	Iron	7.86
Shield 3	2.02 cm	Lead	11.04
Shield 4	.6 cm	Iron	7.86
Shield 5	.4 cm	Iron	7.86
Shield 6	6.75 cm	Cork	0.25
Shield 7	.4 cm	Iron	7.86
Air Gap		Air	0.00122

Source Input: Grouping Method - Actual Photon Energies		
Nuclide	Ci	Bq
As-77	1.00E+00	3.70E+10

Buildup: The material reference is Shield 3

Integration Parameters

Results - Dose Point # 1 - (11.99,0,0) cm

Energy (MeV)	Activity (Photons/sec)	Fluence Rate MeV/cm²/sec No Buildup	Fluence Rate MeV/cm²/sec With Buildup	Exposure Rate mR/hr No Buildup	Exposure Rate mR/hr With Buildup
0.0879	7.55E+07	3.30E-86	4.28E-23	5.10E-89	6.60E-26
0.1619	4.71E+07	3.31E-28	6.19E-23	5.56E-31	1.04E-25
0.239	5.81E+08	1.86E-08	2.72E-08	3.40E-11	4.98E-11
0.2455	3.52E+07	5.87E-09	8.61E-09	1.08E-11	1.58E-11
0.2498	1.57E+08	7.12E-08	1.05E-07	1.31E-10	1.93E-10
0.5207	2.27E+08	2.60E+01	5.18E+01	5.10E-02	1.02E-01
Totals	**1.12E+09**	**2.60E+01**	**5.18E+01**	**5.10E-02**	**1.02E-01**

Results - Dose Point # 2 - (111.99,0,0) cm

Energy (MeV)	Activity (Photons/sec)	Fluence Rate MeV/cm²/sec No Buildup	Fluence Rate MeV/cm²/sec With Buildup	Exposure Rate mR/hr No Buildup	Exposure Rate mR/hr With Buildup
0.0879	7.55E+07	3.71E-88	4.91E-25	5.73E-91	7.57E-28
0.1619	4.71E+07	3.73E-30	7.10E-25	6.27E-33	1.19E-27
0.239	5.81E+08	2.10E-10	3.08E-10	3.85E-13	5.63E-13
0.2455	3.52E+07	6.63E-11	9.73E-11	1.22E-13	1.79E-13
0.2498	1.57E+08	8.05E-10	1.18E-09	1.49E-12	2.19E-12
0.5207	2.27E+08	2.95E-01	5.88E-01	5.79E-04	1.15E-03
Totals	**1.12E+09**	**2.95E-01**	**5.88E-01**	**5.79E-04**	**1.15E-03**

Figure 9: MicroShield Output (Example)

Table 3: Insert Design No 3983 – Surface and 1m Dose Rates from gamma and bremsstrahlung

Nuclide	Microshield File Ref.	Original Activity, Bq	Dose Pt: 1.Surface	Exposure Rate, mR/hr + Buildup	Effective Dose Equivalent Rate, mSv/h	Dose Pt: 2. 1m from Surface	Exposure Rate, mR/hr + Buildup
Insert:	3983						
Ac-225	LS-3979A-Base with 3983 Insert-Ac-225.ms7	3.70E+10	1	9.94E+01	8.86E-01	2	1.13E+00
Ac-227	LS-3979A-Base with 3983 Insert-Ac-227.ms7	3.70E+10	1	1.74E+01	1.58E-01	2	1.98E-01
Ac-228	LS-3979A-Base with 3983 Insert-Ac-228.ms7	3.70E+10	1	1.20E+03	1.07E+01	2	1.37E+01
Am-241	LS-3979A-Base with 3983 Insert-Am-241.ms7	3.70E+10	1	4.14E-07	3.94E-09	2	4.69E-09
As-77	LS-3979A-Base with 3983 Insert-As-77.ms7	3.70E+10	1	1.02E-01	9.44E-04	2	1.15E-03
Au-198	LS-3979A-Base with 3983 Insert-Au-198.ms7	3.70E+10	1	6.21E+00	5.62E-02	2	7.06E-02
Ba-131	LS-3979A-Base with 3983 Insert-Ba-131.ms7	3.70E+10	1	3.19E+01	2.89E-01	2	3.63E-01
C-14	LS-3979A-Base with 3983 Insert-C-14 - Brem.ms7	3.7E+13	1	1.55E-21	1.74E-23	2	1.78E-23
Co-60	LS-3979A-Base with 3983 Insert-Co-60.ms7	3.70E+10	1	5.44E+03	4.85E+01	2	6.19E+01
Cs-131	LS-3979A-Base with 3983 Insert-Cs-131.ms7	3.70E+10	1	8.83E-23	1.63E-25	2	1.01E-24
Cs-134	LS-3979A-Base with 3983 Insert-Cs-134.ms7	3.70E+10	1	6.34E+02	5.73E+00	2	7.21E+00
Cs-137	LS-3979A-Base with 3983 Insert-Cs-137.ms7	3.70E+10	1	1.14E+02	1.04E+00	2	1.30E+00
Cu-67	LS-3979A-Base with 3983 Insert-Cu-67.ms7	3.70E+10	1	6.39E-04	6.12E-06	2	7.24E-06
Hg-203	LS-3979A-Base with 3983 Insert-Hg-203.ms7	3.70E+10	1	8.99E-06	8.96E-08	2	1.02E-07
Ho-166	LS-3979A-Base with 3983 Insert-Ho-166.ms7	3.70E+10	1	5.00E+01	4.45E-01	2	5.70E-01
I-125	LS-3979A-Base with 3983 Insert-I-125.ms7	3.70E+10	1	1.74E-22	3.03E-25	2	2.00E-24
I-129	LS-3979A-Base with 3983 Insert-I-129 - Brem.ms7	3.70E+10	1	1.65E-20	1.73E-25	2	1.89E-22
I-131	LS-3979A-Base with 3983 Insert-I-131.ms7	3.70E+10	1	1.21E+01	1.10E-01	2	1.37E-01
In-111	LS-3979A-Base with 3983 Insert-In-111.ms7	3.70E+10	1	1.52E-08	1.54E-10	2	1.72E-10
Ir-192	LS-3979A-Ir192-t0-Base with 3983 Insert.ms7	3.7E+13	1	1.87E+04	1.72E+02	2	2.12E+02
Ir-194	LS-3979A-Base with 3983 Insert-Ir-194.ms7	3.70E+10	1	4.98E+01	4.46E-01	2	5.67E-01
Kr-79	LS-3979A-Base with 3983 Insert-Kr-79.ms7	3.70E+10	1	4.10E+01	3.70E-01	2	4.67E-01
Lu-177	LS-3979A-Base with 3983 Insert-Lu-177.ms7	3.70E+10	1	4.36E-06	4.27E-08	2	4.94E-08
Mo-99	LS-3979A-Base with 3983 Insert-Mo-99.ms7	3.70E+10	1	5.34E+01	4.85E-01	2	6.07E-01
Na-24	LS-3979A-Base with 3983 Insert-Na-24.ms7	3.70E+10	1	1.46E+04	1.31E+02	2	1.66E+02
Np-237	LS-3979A-Base with 3983 Insert-Np-237.ms7	3.70E+10	1	9.00E-07	1.14E-08	2	1.03E-08
P-32	LS-3979A-Base with 3983 Insert-P-32 - Brem.ms7	3.7E+13	1	6.18E+05	5.50E+03	2	7.05E+03
P-33	LS-3979A-Base with 3983 Insert-P-33 - Brem.ms7	3.7E+13	1	7.97E-07	8.07E-09	2	9.02E-09
Pb-203	LS-3979A-Base with 3983 Insert-Pb-203.ms7	3.70E+10	1	1.10E+00	1.01E-02	2	1.25E-02
Pb-210	LS-3979A-Base with 3983 Insert-Pb-210.ms7	3.70E+10	1	4.38E-03	3.97E-05	2	4.98E-05
Pd-109	LS-3979A-Base with 3983 Insert-Pd-109.ms7	3.70E+10	1	1.74E-02	1.62E-04	2	1.97E-04
Pu-238	LS-3979A-Base with 3983 Insert-Pu-238.ms7	3.70E+10	1	4.94E-06	4.41E-08	2	5.64E-08
Pu-239	LS-3979A-Base with 3983 Insert-Pu-239.ms7	3.70E+10	1	1.56E-09	1.59E-11	2	1.77E-11
Pu-240	LS-3979A-Base with 3983 Insert-Pu-240.ms7	3.70E+10	1	3.41E-11	3.07E-13	2	3.89E-13
Pu-241	LS-3979A-Base with 3983 Insert-Pu-241.ms7	3.70E+10	1	1.06E-08	1.01E-10	2	1.20E-10
Ra-223	LS-3979A-Base with 3983 Insert-Ra-223.ms7	3.70E+10	1	1.72E+01	1.56E-01	2	1.96E-01
Ra-224	LS-3979A-Base with 3983 Insert-Ra-224.ms7	3.70E+10	1	3.36E+03	3.03E+01	2	3.84E+01
Ra-226	LS-3979A-Base with 3983 Insert-Ra-226.ms7	3.70E+10	1	3.27E+03	2.92E+01	2	3.73E+01
Re-186	LS-3979A-Base with 3983 Insert-Re-186.ms7	3.70E+10	1	1.13E-01	1.03E-03	2	1.28E-03
Re-188	LS-3979A-Base with 3983 Insert-Re-188.ms7	3.70E+10	1	2.32E+01	2.09E-01	2	2.64E-01
Rh-105	LS-3979A-Base with 3983 Insert-Rh-105.ms7	3.70E+10	1	3.24E-04	3.17E-06	2	3.67E-06
Se-75	LS-3979A-Base with 3983 Insert-Se-75.ms7	3.70E+10	1	4.58E-02	4.36E-04	2	5.19E-04
Sm-153	LS-3979A-Base with 3983 Insert-Sm-153.ms7	3.70E+10	1	2.84E-03	2.68E-05	2	3.22E-05
Sr-89	LS-3979A-Base with 3983 Insert-Sr-89.ms7	3.70E+10	1	1.24E-01	1.12E-03	2	1.41E-03
Sr-90	LS-3979A-Base with 3983 Insert-Sr-90 - Brem.ms7	3.7E+13	1	1.16E+03	1.07E+01	2	1.32E+01
Tb-161	LS-3979A-Base with 3983 Insert-Tb-161.ms7	3.70E+10	1	2.69E-02	2.47E-04	2	3.05E-04
Th-227	LS-3979A-Base with 3983 Insert-Th-227.ms7	3.70E+10	1	8.12E+00	7.36E-02	2	9.24E-02
Th-228	LS-3979A-Base with 3983 Insert-Th-228.ms7	3.70E+10	1	4.41E+03	3.98E+01	2	5.04E+01
Tl-201	LS-3979A-Base with 3983 Insert-Tl-201.ms7	3.70E+10	1	6.12E-18	7.13E-20	2	7.01E-20
U-235	LS-3979A-Base with 3983 Insert-U-235.ms7	3.70E+10	1	2.60E-02	2.36E-04	2	2.96E-04
W-187	LS-3979A-Base with 3983 Insert-W-187.ms7	3.70E+10	1	8.01E+01	7.30E-01	2	9.10E-01
W-188	LS-3979A-Base with 3983 Insert-W-188.ms7	3.70E+10	1	2.21E+01	1.99E-01	2	2.52E-01
Xe-133	LS-3979A-Base with 3983 Insert-Xe-133.ms7	3.70E+10	1	6.96E-23	2.58E-25	2	7.98E-25
Y-90	LS-3979A-Base with 3983 Insert-Y-90 - Brem.ms7	3.7E+13	1	1.29E+06	1.16E+04	2	1.47E+04
Yb-169	LS-3979A-Base with 3983 Insert-Yb-169.ms7	3.70E+10	1	7.93E-05	7.78E-07	2	8.98E-07
Yb-175	LS-3979A-Base with 3983 Insert-Yb-175.ms7	3.70E+10	1	2.13E-02	2.03E-04	2	2.41E-04

Table 4: Insert Design No 3984 – Surface and 1m Dose Rates from gamma and bremsstrahlung

Nuclide	Microshield File Ref.	Original Activity, Bq	Dose Pt: 1.Surface	Exposure Rate, mR/hr + Buildup	Effective Dose Equivalent Rate, mSv/h	Dose Pt: 2. 1m from Surface	Exposure Rate, mR/hr + Buildup
Insert:	3984						
Ac-225	LS-3979A-Base with 3984 Insert-Ac-225.ms7	3.70E+10	1	6.82E+01	6.08E-01	2	8.25E-01
Ac-227	LS-3979A-Base with 3984 Insert-Ac-227.ms7	3.70E+10	1	9.74E+00	8.83E-02	2	1.18E-01
Ac-228	LS-3979A-Base with 3984 Insert-Ac-228.ms7	3.70E+10	1	7.73E+02	6.92E+00	2	9.33E+00
Am-241	LS-3979A-Base with 3984 Insert-Am-241.ms7	3.70E+10	1	1.10E-07	1.05E-09	2	1.32E-09
As-77	LS-3979A-Base with 3984 Insert-As-77.ms7	3.70E+10	1	4.08E-02	3.79E-04	2	4.91E-04
Au-198	LS-3979A-Base with 3984 Insert-Au-198.ms7	3.70E+10	1	3.52E+00	3.18E-02	2	4.25E-02
Ba-131	LS-3979A-Base with 3984 Insert-Ba-131.ms7	3.70E+10	1	1.81E+01	1.64E-01	2	2.19E-01
C-14	LS-3979A-Base with 3984 Insert-C-14 - Brem.ms7	3.7E+13	1	1.45E-21	1.63E-23	2	1.76E-23
Co-60	LS-3979A-Base with 3984 Insert-Co-60.ms7	3.70E+10	1	3.63E+03	3.24E+01	2	4.39E+01
Cs-131	LS-3979A-Base with 3984 Insert-Cs-131.ms7	3.70E+10	1	8.27E-23	1.53E-25	2	1.01E-24
Cs-134	LS-3979A-Base with 3984 Insert-Cs-134.ms7	3.70E+10	1	3.65E+02	3.30E+00	2	4.41E+00
Cs-137	LS-3979A-Base with 3984 Insert-Cs-137.ms7	3.70E+10	1	5.72E+01	5.22E-01	2	6.89E-01
Cu-67	LS-3979A-Base with 3984 Insert-Cu-67.ms7	3.70E+10	1	1.69E-04	1.63E-06	2	2.03E-06
Hg-203	LS-3979A-Base with 3984 Insert-Hg-203.ms7	3.70E+10	1	6.98E-07	6.95E-09	2	8.37E-09
Ho-166	LS-3979A-Base with 3984 Insert-Ho-166.ms7	3.70E+10	1	3.44E+01	3.06E-01	2	4.16E-01
I-125	LS-3979A-Base with 3984 Insert-I-125.ms7	3.70E+10	1	1.63E-22	2.84E-25	2	1.98E-24
I-129	LS-3979A-Base with 3984 Insert-I-129 - Brem.ms7	3.70E+10	1	1.54E-20	1.62E-25	2	1.87E-22
I-131	LS-3979A-Base with 3984 Insert-I-131.ms7	3.70E+10	1	6.04E+00	5.52E-02	2	7.28E-02
In-111	LS-3979A-Base with 3984 Insert-In-111.ms7	3.70E+10	1	5.30E-10	5.38E-12	2	6.36E-12
Ir-192	LS-3979A-Ir192-t0-Base with 3984 Insert.ms7	3.7E+13	1	8.38E+03	7.71E+01	2	1.01E+02
Ir-194	LS-3979A-Base with 3984 Insert-Ir-194.ms7	3.70E+10	1	3.21E+01	2.87E-01	2	3.87E-01
Kr-79	LS-3979A-Base with 3984 Insert-Kr-79.ms7	3.70E+10	1	2.46E+01	2.22E-01	2	2.97E-01
Lu-177	LS-3979A-Base with 3984 Insert-Lu-177.ms7	3.70E+10	1	6.25E-07	6.11E-09	2	7.50E-09
Mo-99	LS-3979A-Base with 3984 Insert-Mo-99.ms7	3.70E+10	1	2.90E+01	2.64E-01	2	3.50E-01
Na-24	LS-3979A-Base with 3984 Insert-Na-24.ms7	3.70E+10	1	1.06E+04	9.48E+01	2	1.28E+02
Np-237	LS-3979A-Base with 3984 Insert-Np-237.ms7	3.70E+10	1	8.42E-07	1.07E-08	2	1.02E-08
P-32	LS-3979A-Base with 3984 Insert-P-32 - Brem.ms7	3.7E+13	1	4.39E+05	3.90E+03	2	5.31E+03
P-33	LS-3979A-Base with 3984 Insert-P-33 - Brem.ms7	3.7E+13	1	3.09E-08	3.13E-10	2	3.70E-10
Pb-203	LS-3979A-Base with 3984 Insert-Pb-203.ms7	3.70E+10	1	5.60E-01	5.11E-03	2	6.75E-03
Pb-210	LS-3979A-Base with 3984 Insert-Pb-210.ms7	3.70E+10	1	2.47E-03	2.24E-05	2	2.98E-05
Pd-109	LS-3979A-Base with 3984 Insert-Pd-109.ms7	3.70E+10	1	6.79E-03	6.32E-05	2	8.17E-05
Pu-238	LS-3979A-Base with 3984 Insert-Pu-238.ms7	3.70E+10	1	3.46E-06	3.09E-08	2	4.18E-08
Pu-239	LS-3979A-Base with 3984 Insert-Pu-239.ms7	3.70E+10	1	1.07E-09	1.14E-11	2	1.30E-11
Pu-240	LS-3979A-Base with 3984 Insert-Pu-240.ms7	3.70E+10	1	2.44E-11	2.19E-13	2	2.95E-13
Pu-241	LS-3979A-Base with 3984 Insert-Pu-241.ms7	3.70E+10	1	2.80E-09	2.67E-11	2	3.37E-11
Ra-223	LS-3979A-Base with 3984 Insert-Ra-223.ms7	3.70E+10	1	9.65E+00	8.75E-02	2	1.16E-01
Ra-224	LS-3979A-Base with 3984 Insert-Ra-224.ms7	3.70E+10	1	2.47E+03	2.22E+01	2	2.99E+01
Ra-226	LS-3979A-Base with 3984 Insert-Ra-226.ms7	3.70E+10	1	2.29E+03	2.04E+01	2	2.77E+01
Re-186	LS-3979A-Base with 3984 Insert-Re-186.ms7	3.70E+10	1	5.87E-02	5.35E-04	2	7.07E-04
Re-188	LS-3979A-Base with 3984 Insert-Re-188.ms7	3.70E+10	1	1.44E+01	1.29E-01	2	1.73E-01
Rh-105	LS-3979A-Base with 3984 Insert-Rh-105.ms7	3.70E+10	1	4.47E-05	4.38E-07	2	5.37E-07
Se-75	LS-3979A-Base with 3984 Insert-Se-75.ms7	3.70E+10	1	1.22E-02	1.16E-04	2	1.46E-04
Sm-153	LS-3979A-Base with 3984 Insert-Sm-153.ms7	3.70E+10	1	8.38E-04	7.93E-06	2	1.01E-05
Sr-89	LS-3979A-Base with 3984 Insert-Sr-89.ms7	3.70E+10	1	7.39E-02	6.66E-04	2	8.91E-04
Sr-90	LS-3979A-Base with 3984 Insert-Sr-90 - Brem.ms7	3.7E+13	1	4.95E+02	4.58E+00	2	5.95E+00
Tb-161	LS-3979A-Base with 3984 Insert-Tb-161.ms7	3.70E+10	1	1.23E-02	1.13E-04	2	1.48E-04
Th-227	LS-3979A-Base with 3984 Insert-Th-227.ms7	3.70E+10	1	4.55E+00	4.13E-02	2	5.49E-02
Th-228	LS-3979A-Base with 3984 Insert-Th-228.ms7	3.70E+10	1	3.24E+03	2.92E+01	2	3.92E+01
Tl-201	LS-3979A-Base with 3984 Insert-Tl-201.ms7	3.70E+10	1	5.73E-18	6.68E-20	2	6.96E-20
U-235	LS-3979A-Base with 3984 Insert-U-235.ms7	3.70E+10	1	1.46E-02	1.32E-04	2	1.76E-04
W-187	LS-3979A-Base with 3984 Insert-W-187.ms7	3.70E+10	1	4.14E+01	3.77E-01	2	4.98E-01
W-188	LS-3979A-Base with 3984 Insert-W-188.ms7	3.70E+10	1	1.37E+01	1.23E-01	2	1.65E-01
Xe-133	LS-3979A-Base with 3984 Insert-Xe-133.ms7	3.70E+10	1	6.43E-23	2.32E-25	2	7.81E-25
Y-90	LS-3979A-Base with 3984 Insert-Y-90 - Brem.ms7	3.7E+13	1	9.45E+05	8.45E+03	2	1.14E+04
Yb-169	LS-3979A-Base with 3984 Insert-Yb-169.ms7	3.70E+10	1	1.16E-05	1.15E-07	2	1.39E-07
Yb-175	LS-3979A-Base with 3984 Insert-Yb-175.ms7	3.70E+10	1	5.52E-03	5.26E-05	2	6.63E-05

Table 5: Insert Design No 3986 – Surface and 1m Dose Rates from gamma and bremsstrahlung

Nuclide	Microshield File Ref.	Original Activity, Bq	Dose Pt: 1.Surface	Exposure Rate, mR/hr + Buildup	Effective Dose Equivalent Rate, mSv/h	Dose Pt: 2. 1m from Surface	Exposure Rate, mR/hr + Buildup
Insert:	3986						
Ac-225	LS-3979A-Base with 3986 Insert-Ac-225.ms7	3.70E+10	1	3.98E+02	3.56E+00	2	3.67E+00
Ac-227	LS-3979A-Base with 3986 Insert-Ac-227.ms7	3.70E+10	1	1.51E+02	1.37E+00	2	1.38E+00
Ac-228	LS-3979A-Base with 3986 Insert-Ac-228.ms7	3.70E+10	1	5.85E+03	5.25E+01	2	5.39E+01
Am-241	LS-3979A-Base with 3986 Insert-Am-241.ms7	3.70E+10	1	6.54E-05	6.26E-07	2	5.99E-07
As-77	LS-3979A-Base with 3986 Insert-As-77.ms7	3.70E+10	1	2.79E+00	2.59E-02	2	2.56E-02
Au-198	LS-3979A-Base with 3986 Insert-Au-198.ms7	3.70E+10	1	1.04E+02	9.72E-01	2	9.57E-01
Ba-131	LS-3979A-Base with 3986 Insert-Ba-131.ms7	3.70E+10	1	3.49E+02	3.20E+00	2	3.20E+00
C-14	LS-3979A-Base with 3986 Insert-C-14 - Brem.ms7	3.7E+13	1	4.49E-14	5.03E-16	2	4.10E-16
Co-60	LS-3979A-Base with 3986 Insert-Co-60.ms7	3.70E+10	1	2.25E+04	2.01E+02	2	2.08E+02
Cs-131	LS-3979A-Base with 3986 Insert-Cs-131.ms7	3.70E+10	1	1.12E-22	2.06E-25	2	1.04E-24
Cs-134	LS-3979A-Base with 3986 Insert-Cs-134.ms7	3.70E+10	1	5.05E+03	4.58E+01	2	4.64E+01
Cs-137	LS-3979A-Base with 3986 Insert-Cs-137.ms7	3.70E+10	1	1.38E+03	1.26E+01	2	1.27E+01
Cu-67	LS-3979A-Base with 3986 Insert-Cu-67.ms7	3.70E+10	1	1.01E-01	9.65E-04	2	9.25E-04
Hg-203	LS-3979A-Base with 3986 Insert-Hg-203.ms7	3.70E+10	1	1.23E-01	1.23E-03	2	1.13E-03
Ho-166	LS-3979A-Base with 3986 Insert-Ho-166.ms7	3.70E+10	1	1.86E+02	1.66E+00	2	1.72E+00
I-125	LS-3979A-Base with 3986 Insert-I-125.ms7	3.70E+10	1	2.21E-22	3.84E-25	2	2.04E-24
I-129	LS-3979A-Base with 3986 Insert-I-129 - Brem.ms7	3.70E+10	1	3.11E-15	2.19E-25	2	2.84E-17
I-131	LS-3979A-Base with 3986 Insert-I-131.ms7	3.70E+10	1	1.60E+02	1.47E+00	2	1.47E+00
In-111	LS-3979A-Base with 3986 Insert-In-111.ms7	3.70E+10	1	4.29E-03	4.35E-05	2	3.92E-05
Ir-192	LS-3979A-Ir192-t0-Base with 3986 Insert.ms7	3.7E+13	1	3.81E+05	3.52E+03	2	3.49E+03
Ir-194	LS-3979A-Base with 3986 Insert-Ir-194.ms7	3.70E+10	1	2.46E+02	2.21E+00	2	2.27E+00
Kr-79	LS-3979A-Base with 3986 Insert-Kr-79.ms7	3.70E+10	1	3.27E+02	2.98E+00	2	3.00E+00
Lu-177	LS-3979A-Base with 3986 Insert-Lu-177.ms7	3.70E+10	1	5.88E-03	5.75E-05	2	5.38E-05
Mo-99	LS-3979A-Base with 3986 Insert-Mo-99.ms7	3.70E+10	1	4.78E+02	4.34E+00	2	4.39E+00
Na-24	LS-3979A-Base with 3986 Insert-Na-24.ms7	3.70E+10	1	4.61E+04	4.13E+02	2	4.25E+02
Np-237	LS-3979A-Base with 3986 Insert-Np-237.ms7	3.70E+10	1	1.17E-06	1.48E-08	2	1.08E-08
P-32	LS-3979A-Base with 3986 Insert-P-32 - Brem.ms7	3.7E+13	1	3.76E+05	3.36E+03	2	3.46E+03
P-33	LS-3979A-Base with 3986 Insert-P-33 - Brem.ms7	3.7E+13	1	5.33E-02	5.39E-04	2	4.87E-04
Pb-203	LS-3979A-Base with 3986 Insert-Pb-203.ms7	3.70E+10	1	1.42E+01	1.30E-01	2	1.30E-01
Pb-210	LS-3979A-Base with 3986 Insert-Pb-210.ms7	3.70E+10	1	3.42E-02	3.10E-04	2	3.14E-04
Pd-109	LS-3979A-Base with 3986 Insert-Pd-109.ms7	3.70E+10	1	5.30E-01	4.93E-03	2	4.86E-03
Pu-238	LS-3979A-Base with 3986 Insert-Pu-238.ms7	3.70E+10	1	1.84E-05	1.64E-07	2	1.69E-07
Pu-239	LS-3979A-Base with 3986 Insert-Pu-239.ms7	3.70E+10	1	9.58E-09	8.96E-11	2	8.81E-11
Pu-240	LS-3979A-Base with 3986 Insert-Pu-240.ms7	3.70E+10	1	1.19E-10	1.08E-12	2	1.10E-12
Pu-241	LS-3979A-Base with 3986 Insert-Pu-241.ms7	3.70E+10	1	1.78E-06	1.71E-08	2	1.63E-08
Ra-223	LS-3979A-Base with 3986 Insert-Ra-223.ms7	3.70E+10	1	1.49E+02	1.36E+00	2	1.37E+00
Ra-224	LS-3979A-Base with 3986 Insert-Ra-224.ms7	3.70E+10	1	1.05E+04	9.45E+01	2	9.67E+01
Ra-226	LS-3979A-Base with 3986 Insert-Ra-226.ms7	3.70E+10	1	1.22E+04	1.09E+02	2	1.12E+02
Re-186	LS-3979A-Base with 3986 Insert-Re-186.ms7	3.70E+10	1	1.17E+00	1.07E-02	2	1.08E-02
Re-188	LS-3979A-Base with 3986 Insert-Re-188.ms7	3.70E+10	1	1.36E+02	1.23E+00	2	1.25E+00
Rh-105	LS-3979A-Base with 3986 Insert-Rh-105.ms7	3.70E+10	1	5.10E-01	4.99E-03	2	4.67E-03
Se-75	LS-3979A-Base with 3986 Insert-Se-75.ms7	3.70E+10	1	6.06E+00	5.77E-02	2	5.55E-02
Sm-153	LS-3979A-Base with 3986 Insert-Sm-153.ms7	3.70E+10	1	2.48E-01	2.35E-03	2	2.27E-03
Sr-89	LS-3979A-Base with 3986 Insert-Sr-89.ms7	3.70E+10	1	7.76E-01	6.99E-03	2	7.14E-03
Sr-90	LS-3979A-Base with 3986 Insert-Sr-90 - Brem.ms7	3.7E+13	1	8.95E+03	8.28E+01	2	8.22E+01
Tb-161	LS-3979A-Base with 3986 Insert-Tb-161.ms7	3.70E+10	1	4.74E-01	4.37E-03	2	4.35E-03
Th-227	LS-3979A-Base with 3986 Insert-Th-227.ms7	3.70E+10	1	7.04E+01	6.41E-01	2	6.47E-01
Th-228	LS-3979A-Base with 3986 Insert-Th-228.ms7	3.70E+10	1	1.38E+04	1.24E+02	2	1.27E+02
Tl-201	LS-3979A-Base with 3986 Insert-Tl-201.ms7	3.70E+10	1	5.82E-13	6.39E-15	2	5.31E-15
U-235	LS-3979A-Base with 3986 Insert-U-235.ms7	3.70E+10	1	2.26E-01	2.06E-03	2	2.08E-03
W-187	LS-3979A-Base with 3986 Insert-W-187.ms7	3.70E+10	1	9.12E+02	8.34E+00	2	8.38E+00
W-188	LS-3979A-Base with 3986 Insert-W-188.ms7	3.70E+10	1	1.30E+02	1.17E+00	2	1.20E+00
Xe-133	LS-3979A-Base with 3986 Insert-Xe-133.ms7	3.70E+10	1	4.25E-13	4.60E-15	2	3.88E-15
Y-90	LS-3979A-Base with 3986 Insert-Y-90 - Brem.ms7	3.7E+13	1	1.37E+06	1.23E+04	2	1.27E+04
Yb-169	LS-3979A-Base with 3986 Insert-Yb-169.ms7	3.70E+10	1	1.49E-01	1.46E-03	2	1.36E-03
Yb-175	LS-3979A-Base with 3986 Insert-Yb-175.ms7	3.70E+10	1	3.03E+00	2.89E-02	2	2.78E-02

Table 6: Without Inserts – Surface and 1m Dose Rates from gamma and bremsstrahlung

Nuclide	Microshield File Ref.	Original Activity, Bq	Dose Pt: 1.Surface	Exposure Rate, mR/hr + Buildup	Effective Dose Equivalent Rate, mSv/h	Dose Pt: 2. 1m from Surface	Exposure Rate, mR/hr + Buildup
Insert:	No Insert						
Ac-225	LS-3979A-Base withou Insert-Ac-227.ms7	3.70E+10	1	1.79E+02	3.92E+00	2	1.60E+00
Ac-227	LS-3979A-Base without Insert-Ac-225.ms7	3.70E+10	1	4.38E+02	1.63E+00	2	3.92E+00
Ac-228	LS-3979A-Base without Insert-Ac-228.ms7	3.70E+10	1	6.49E+03	7.38E-07	2	5.79E+01
Am-241	LS-3979A-Base without Insert-Am-241.ms7	3.70E+10	1	7.70E-05	5.32E-05	2	6.84E-07
As-77	LS-3979A-Base without Insert-As-77.ms7	3.70E+10	1	3.22E+00	5.82E+01	2	2.86E-02
Au-198	LS-3979A-Base without Insert-Au-198.ms7	3.70E+10	1	1.20E+02	2.99E-02	2	1.07E+00
Ba-131	LS-3979A-Base without Insert-Ba-131.ms7	3.70E+10	1	3.97E+02	1.12E+00	2	3.54E+00
C-14	LS-3979A-Base without Insert-C-14 - Brem.ms7	3.7E+13	1	5.94E-14	6.65E-16	2	5.25E-16
Co-60	LS-3979A-Base without Insert-Co-60.ms7	3.70E+10	1	2.48E+04	3.65E+00	2	2.21E+02
Cs-131	LS-3979A-Base without Insert-Cs-131.ms7	3.70E+10	1	1.16E-22	2.21E+02	2	1.04E-24
Cs-134	LS-3979A-Base without Insert-Cs-134.ms7	3.70E+10	1	5.68E+03	2.14E-25	2	5.07E+01
Cs-137	LS-3979A-Base without Insert-Cs-137.ms7	3.70E+10	1	1.57E+03	5.16E+01	2	1.40E+01
Cu-67	LS-3979A-Base without Insert-Cu-67.ms7	3.70E+10	1	1.19E-01	1.44E+01	2	1.06E-03
Hg-203	LS-3979A-Base without Insert-Hg-203.ms7	3.70E+10	1	1.49E-01	1.14E-03	2	1.32E-03
Ho-166	LS-3979A-Base without Insert-Ho-166.ms7	3.70E+10	1	2.04E+02	1.48E-03	2	1.82E+00
I-125	LS-3979A-Base without Insert-I-125.ms7	3.70E+10	1	2.28E-22	1.82E+00	2	2.05E-24
I-129	LS-3979A-Base without Insert-I-129 - Brem.ms7	3.70E+10	1	4.09E-15	3.98E-25	2	3.62E-17
I-131	LS-3979A-Base without Insert-I-131.ms7	3.70E+10	1	1.83E+02	2.27E-25	2	1.63E+00
In-111	LS-3979A-Base without Insert-In-111.ms7	3.70E+10	1	5.25E-03	1.68E+00	2	4.65E-05
Ir-192	LS-3979A-Ir192-t0-Base without Insert.ms7	3.7E+13	1	4.37E+05	4.04E+03	2	3.89E+03
Ir-194	LS-3979A-Base without Insert-Ir-194.ms7	3.70E+10	1	2.73E+02	2.45E+00	2	2.44E+00
Kr-79	LS-3979A-Base without Insert-Kr-79.ms7	3.70E+10	1	3.69E+02	3.36E+00	2	3.29E+00
Lu-177	LS-3979A-Base without Insert-Lu-177.ms7	3.70E+10	1	7.02E-03	6.86E-05	2	6.22E-05
Mo-99	LS-3979A-Base without Insert-Mo-99.ms7	3.70E+10	1	5.40E+02	4.90E+00	2	4.81E+00
Na-24	LS-3979A-Base without Insert-Na-24.ms7	3.70E+10	1	4.99E+04	4.48E+02	2	4.47E+02
Np-237	LS-3979A-Base without Insert-Np-237.ms7	3.70E+10	1	1.22E-06	1.53E-08	2	1.09E-08
P-32	LS-3979A-Base without Insert-P-32 - Brem.ms7	3.7E+13	1	7.91E+05	7.04E+03	2	7.07E+03
P-33	LS-3979A-Base without Insert-P-33 - Brem.ms7	3.7E+13	1	6.51E-02	6.59E-04	2	5.77E-04
Pb-203	LS-3979A-Base without Insert-Pb-203.ms7	3.70E+10	1	1.61E+01	1.48E-01	2	1.44E-01
Pb-210	LS-3979A-Base without Insert-Pb-210.ms7	3.70E+10	1	3.84E-02	3.48E-04	2	3.42E-04
Pd-109	LS-3979A-Base without Insert-Pd-109.ms7	3.70E+10	1	6.12E-01	5.69E-03	2	5.44E-03
Pu-238	LS-3979A-Base without Insert-Pu-238.ms7	3.70E+10	1	2.01E-05	1.80E-07	2	1.80E-07
Pu-239	LS-3979A-Base without Insert-Pu-239.ms7	3.70E+10	1	1.08E-08	1.00E-10	2	9.59E-11
Pu-240	LS-3979A-Base without Insert-Pu-240.ms7	3.70E+10	1	1.30E-10	1.17E-12	2	1.16E-12
Pu-241	LS-3979A-Base without Insert-Pu-241.ms7	3.70E+10	1	2.10E-06	2.02E-08	2	1.87E-08
Ra-223	LS-3979A-Base without Insert-Ra-223.ms7	3.70E+10	1	1.68E+02	1.53E+00	2	1.50E+00
Ra-224	LS-3979A-Base without Insert-Ra-224.ms7	3.70E+10	1	1.13E+04	1.02E+02	2	1.01E+02
Ra-226	LS-3979A-Base without Insert-Ra-226.ms7	3.70E+10	1	1.33E+04	1.19E+02	2	1.19E+02
Re-186	LS-3979A-Base without Insert-Re-186.ms7	3.70E+10	1	1.33E+00	1.21E-02	2	1.18E-02
Re-188	LS-3979A-Base without Insert-Re-188.ms7	3.70E+10	1	1.52E+02	1.37E+00	2	1.36E+00
Rh-105	LS-3979A-Base without Insert-Rh-105.ms7	3.70E+10	1	6.09E-01	5.97E-03	2	5.40E-03
Se-75	LS-3979A-Base without Insert-Se-75.ms7	3.70E+10	1	7.11E+00	6.77E-02	2	6.32E-02
Sm-153	LS-3979A-Base without Insert-Sm-153.ms7	3.70E+10	1	2.90E-01	2.74E-03	2	2.58E-03
Sr-89	LS-3979A-Base without Insert-Sr-89.ms7	3.70E+10	1	8.66E-01	7.81E-03	2	7.73E-03
Sr-90	LS-3979A-Base without Insert-Sr-90 - Brem.ms7	3.7E+13	1	1.03E+04	9.52E+01	2	9.16E+01
Tb-161	LS-3979A-Base without Insert-Tb-161.ms7	3.70E+10	1	5.44E-01	5.01E-03	2	4.84E-03
Th-227	LS-3979A-Base without Insert-Th-227.ms7	3.70E+10	1	7.95E+01	7.24E-01	2	7.08E-01
Th-228	LS-3979A-Base without Insert-Th-228.ms7	3.70E+10	1	1.49E+04	1.34E+02	2	1.33E+02
Tl-201	LS-3979A-Base without Insert-Tl-201.ms7	3.70E+10	1	7.58E-13	8.32E-15	2	6.70E-15
U-235	LS-3979A-Base without Insert-U-235.ms7	3.70E+10	1	2.55E-01	2.32E-03	2	2.27E-03
W-187	LS-3979A-Base without Insert-W-187.ms7	3.70E+10	1	1.04E+03	9.47E+00	2	9.23E+00
W-188	LS-3979A-Base without Insert-W-188.ms7	3.70E+10	1	1.45E+02	1.31E+00	2	1.29E+00
Xe-133	LS-3979A-Base without Insert-Xe-133.ms7	3.70E+10	1	5.46E-13	5.90E-15	2	4.83E-15
Y-90	LS-3979A-Base without Insert-Y-90 - Brem.ms7	3.7E+13	1	1.49E+06	1.33E+04	2	1.33E+04
Yb-169	LS-3979A-Base without Insert-Yb-169.ms7	3.70E+10	1	1.78E-01	1.75E-03	2	1.58E-03
Yb-175	LS-3979A-Base without Insert-Yb-175.ms7	3.70E+10	1	3.56E+00	3.40E-02	2	3.17E-02

Table 7: Summation of Gamma and Neutron Dose Rates

Nuclide	Original Activity, Bq, gamma	Effective Dose Equivalent Rate, mSv/h, gamma	Dose rate at neutron Activity	Neutron Activity, Bq	Neutron Dose Rate, surface, mSv/h	Neutron+ gamma	Package Limit, Bq
Pu-238	3.70E+10	4.41E-08	3.57E-04	2.99E+14	2	2.00E+00	2.99E+14
Pu-240	3.70E+10	3.07E-13	9.54E-11	1.15E+13	2	2.00E+00	1.15E+13

3. References

1. Title 10, Code of Federal Regulations, Part 71, Office of the Federal Register, Washington, DC, 2009
2. Serco Assurance, SERCO/TAS/003191/001 Issue 1, *Monte Carlo Modelling of Safkeg LS*
3. Grove Software Inc, MicroShield v7.02, *Radiation Shielding Software Container*, June 2009
4. Advisory Material for the IAEA *Regulations for the Safe Transport of Radioactive Material* (1985 Edition, as Amended 1990), IAEA Safety Series No. 37
5. *Introduction to Health Physics*, Herman Cember, Third Edition, McGraw-Hill

Appendix A Neutron Dose Calculations

Appendix A Table 1: Package without an Insert

No Insert

3979 radius, r = 10.47 cm - distance from source centre to measurement position
Surface area = 1377.536856 cm2 - assuming a spherical source, to determine the neutron flux after a NCT damage at radius, r (cm)

A	B	C	D	E	F	G	H	I	J	K	L	
Nuclide	Element	Package Limits (Surface Transport)		Neutron emission/ transformation, SF-n (ICRP 38, 1983 [1])	MeV	Total Netrons per sec, n/s (C x E)	Neutron Flux, n/s/cm2 (G/Surface area)	SS37 [2] Conversion factor from Table A-I (cm-2.s-1 per uSv/h)	Cember [3], Table 9.5,Fluence rate producing 1mSv in 40h	Dose Rate based on I, mSv/h (H x I/1000)	Dose Rate based on J, mSv/h (H/(J*40))	Dose Rate at 1m (Based on distance squared ratio), mSv/h
		(Bq)	(g)									
		Note - adjust this limit to get surface dose of 2mSv/h										
Pu-238	Plutonium	2.89E+14	455.3	4.20E-09	1.927	1.21E+06	8.81E+02	8.08E-01	1.10E+01	7.12E-01	2.00E+00	1.80E-02
Pu-240		1.11E+13	1.31E+03	1.09E-07	1.915	1.21E+06	8.78E+02	8.08E-01	1.10E+01	7.09E-01	2.00E+00	1.79E-02

[1] ICRP 38, Radionuclide Transformations - Energy and Intensity of Emissions
[2] IAEA SS37, Third Edition, as Amended 1990.
[3] Herman Cember, Introduction to Health Physics, Third Edition.

Appendix A Table 2: Package with LS-31x73-Tu Design No 3983

3983 Insert

3979 radius, r = 11.99 cm - distance from source centre to measurement position
Surface area = 1806.542696 cm2 - assuming a spherical source, to determine the neutron flux after a NCT damage at radius, r (cm)

A	B	C	D	E	F	G	H	I	J	K	L	
Nuclide	Element	Package Limits (Surface Transport)		Neutron emission/ transformation, SF-n (ICRP 38, 1983 [1])	MeV	Total Netrons per sec, n/s (C x E)	Neutron Flux, n/s/cm2 (G/Surface area)	SS37 [2] Conversion factor from Table A-I (cm-2.s-1 per uSv/h)	Cember [3], Table 9.5,Fluence rate producing 1mSv in 40h	Dose Rate based on I, mSv/h (H x I/1000)	Dose Rate based on J, mSv/h (H/(J*40))	Dose Rate at 1m (Based on distance squared ratio), mSv/h
		(Bq)	(g)									
		Note - adjust this limit to get surface dose of 2mSv/h										
Pu-238	Plutonium	3.79E+14	597.1	4.20E-09	1.927	1.59E+06	8.81E+02	8.08E-01	1.10E+01	7.12E-01	2.00E+00	2.30E-02
Pu-240		1.46E+13	1.73E+03	1.09E-07	1.915	1.59E+06	8.81E+02	8.08E-01	1.10E+01	7.11E-01	2.00E+00	2.29E-02

[1] ICRP 38, Radionuclide Transformations - Energy and Intensity of Emissions
[2] IAEA SS37, Third Edition, as Amended 1990.
[3] Herman Cember, Introduction to Health Physics, Third Edition.

Appendix A Table 3: Package with insert LS-12x65-Tu Design No 3984

3984 Insert

3979 radius, r = 12.39 cm - distance from source centre to measurement position
Surface area = 1929.089942 cm2 - assuming a spherical source, to determine the neutron flux after a NCT damage at radius, r (cm)

A	B	C	D	E	F	G	H	I	J	K	L	
Nuclide	Element	Package Limits (Surface Transport)		Neutron emission/ transformation, SF-n (ICRP 38, 1983 [1])	MeV	Total Netrons per sec, n/s (C x E)	Neutron Flux, n/s/cm2 (G/Surface area)	SS37 [2] Conversion factor from Table A-I (cm-2.s-1 per uSv/h)	Cember [3], Table 9.5,Fluence rate producing 1mSv in 40h	Dose Rate based on I, mSv/h (H x I/1000)	Dose Rate based on J, mSv/h (H/(J*40))	Dose Rate at 1m (Based on distance squared ratio), mSv/h
		(Bq)	(g)									
		Note - adjust this limit to get surface dose of 2mSv/h										
Pu-238	Plutonium	4.04E+14	636.5	4.20E-09	1.927	1.70E+06	8.80E+02	8.08E-01	1.10E+01	7.10E-01	2.00E+00	2.43E-02
Pu-240		1.56E+13	1.85E+03	1.09E-07	1.915	1.70E+06	8.81E+02	8.08E-01	1.10E+01	7.12E-01	2.00E+00	2.43E-02

[1] ICRP 38, Radionuclide Transformations - Energy and Intensity of Emissions
[2] IAEA SS37, Third Edition, as Amended 1990.
[3] Herman Cember, Introduction to Health Physics, Third Edition.

Appendix A Table 4: Package with insert LS-50x103-SS Design No 3986

3986 Insert

3979 radius, r = 10.65 cm - distance from source centre to measurement position
Surface area = 1425.309171 cm2 - assuming a spherical source, to determine the neutron flux after a NCT damage at radius, r (cm)

A	B	C	D	E	F	G	H	I	J	K	L	
Nuclide	Element	Package Limits (Surface Transport)		Neutron emission/ transformation, SF-n (ICRP 38, 1983 [1])	MeV	Total Netrons per sec, n/s (C x E)	Neutron Flux, n/s/cm2 (G/Surface area)	SS37 [2] Conversion factor from Table A-I (cm-2.s-1 per uSv/h)	Cember [3], Table 9.5,Fluence rate producing 1mSv in 40h	Dose Rate based on I, mSv/h (H x I/1000)	Dose Rate based on J, mSv/h (H/(J*40))	Dose Rate at 1m (Based on distance squared ratio), mSv/h
		(Bq)	(g)									
		Note - adjust this limit to get surface dose of 2mSv/h										
Pu-238	Plutonium	2.99E+14	471.1	4.20E-09	1.927	1.26E+06	8.81E+02	8.08E-01	1.10E+01	7.11E-01	2.00E+00	1.86E-02
Pu-240		1.15E+13	1.36E+03	1.09E-07	1.915	1.25E+06	8.79E+02	8.08E-01	1.10E+01	7.10E-01	2.00E+00	1.85E-02

[1] ICRP 38, Radionuclide Transformations - Energy and Intensity of Emissions
[2] IAEA SS37, Third Edition, as Amended 1990.
[3] Herman Cember, Introduction to Health Physics, Third Edition.

Appendix B Bremsstrahlung Dose Rates

3979A Bremsstrahlung Calculations

Introduction to Health Physics, 3rd Edition - Herman Cember
p130, formula 5.11a.

$F_B = 3.5 \times 10^{-4} Z E_M$

Primary Shield, Steel, Z = 26 (Cavity is Stain.S lined)
E_M = 2.28 MeV

F_B = 2.07E-02

Flux = $F_B E_B A/E$ = **1.87E+12** photons/sec A = 3.70E+13 Bq 1000 Ci
E = 9.35E-01 Mev

Where:
Z = Atomic Number of the absorber
A = Activity, Bq
E_B = Em = Maximum Beta erergy, MeV (Kaye & Laby, 16th Edition)
E = Average Beta Energy, MeV (ICRP 38, 1983)

Photon Flux
Using the above formula, the total flux for each beta emitter can be calculated, as shown below:

Steel Insert

Nuclide	Z	E_M	F_B	A	E	Flux, photons/s
C-14	26	0.156	0.00142	3.70E+13	4.95E-02	1.66E+11
I-129	26	0.15	0.001365	3.70E+13	4.89E-02	1.55E+11
P-32	26	1.71	0.015561	3.70E+13	0.6947	1.42E+12
P-33	26	0.249	0.002266	3.70E+13	7.66E-02	2.73E+11
Sr-90	26	0.55	0.005005	3.70E+13	1.96E-01	5.20E+11
Y-90	26	2.28	0.020748	3.70E+13	9.35E-01	1.87E+12

Tungsten Insert

Nuclide	Z	E_M	F_B	A	E	Flux, photons/s
C-14	74	0.156	0.00404	3.70E+13	4.95E-02	4.72E+11
I-129	74	0.15	0.003885	3.70E+13	4.89E-02	4.41E+11
P-32	74	1.71	0.044289	3.70E+13	0.6947	4.03E+12
P-33	74	0.249	0.006449	3.70E+13	7.66E-02	7.76E+11
Sr-90	74	0.55	0.014245	3.70E+13	1.96E-01	1.48E+12
Y-90	74	2.28	0.059052	3.70E+13	9.35E-01	5.33E+12

Dose Rates
Importing the Photon Flux derived above into Microshield, the following dose rates are derived.

No Insert	Exposure Rate mR/h		Effective Dose Equivalent Rate	
Microshield Case No	Surface	1m	Surface, mSv/h	1m, mSv/h
LS-3979A-Base without Insert-C-14 - Brem.ms7	5.94E-14	5.25E-16	6.65E-16	5.88E-18
LS-3979A-Base without Insert-I-129 - Brem.ms7	4.09E-15	3.62E-17	4.64E-17	4.10E-19
LS-3979A-Base without Insert-P-32 - Brem.ms7	7.91E+05	7.07E+03	7.04E+03	6.30E+01
LS-3979A-Base without Insert-P-33 - Brem.ms7	6.51E-02	5.77E-04	6.59E-04	5.84E-06
LS-3979A-Base without Insert-Sr-90 - Brem.ms7	1.03E+04	9.16E+01	9.52E+01	8.47E-01
LS-3979A-Base without Insert-Y-90 - Brem.ms7	1.49E+06	1.33E+04	1.33E+04	1.19E+02

3986 Steel Insert	Exposure Rate mR/h		Effective Dose Equivalent Rate	
Microshield Case No	Surface	1m	Surface, mSv/h	1m, mSv/h
LS-3979A-Base with 3986 Insert-C-14 - Brem.ms7	4.49E-14	4.10E-16	5.03E-16	4.59E-18
LS-3979A-Base with 3986 Insert-I-129 - Brem.ms7	3.11E-15	2.84E-17	3.52E-17	3.21E-19
LS-3979A-Base with 3986 Insert-P-32 - Brem.ms7	3.76E+05	3.46E+03	3.36E+03	3.10E+01
LS-3979A-Base with 3986 Insert-P-33 - Brem.ms7	5.33E-02	4.87E-04	5.39E-04	4.93E-06
LS-3979A-Base with 3986 Insert-Sr-90 - Brem.ms7	8.95E+03	8.22E+01	8.28E+01	7.60E-01
LS-3979A-Base with 3986 Insert-Y-90 - Brem.ms7	1.37E+06	1.27E+04	1.23E+04	1.13E+02

3983 Tungsten Insert	Exposure Rate mR/h		Effective Dose Equivalent Rate	
Microshield Case No	Surface	1m	Surface, mSv/h	1m, mSv/h
LS-3979A-Base with 3983 Insert-C-14 - Brem.ms7	1.55E-21	1.78E-23	1.74E-23	1.99E-25
LS-3979A-Base with 3983 Insert-I-129 - Brem.ms7	1.65E-20	1.89E-22	1.86E-22	2.14E-24
LS-3979A-Base with 3983 Insert-P-32 - Brem.ms7	6.18E+05	7.05E+03	5.50E+03	6.27E+01
LS-3979A-Base with 3983 Insert-P-33 - Brem.ms7	7.97E-07	9.02E-09	8.07E-09	9.12E-11
LS-3979A-Base with 3983 Insert-Sr-90 - Brem.ms7	1.16E+03	1.32E+01	1.07E+01	1.22E-01
LS-3979A-Base with 3983 Insert-Y-90 - Brem.ms7	1.29E+06	1.47E+04	1.16E+04	1.32E+02

3984 Tungsten Insert	Exposure Rate mR/h		Effective Dose Equivalent Rate	
Microshield Case No	Surface	1m	Surface, mSv/h	1m, mSv/h
LS-3979A-Base with 3984 Insert-C-14 - Brem.ms7	1.45E-21	1.76E-23	1.63E-23	1.98E-25
LS-3979A-Base with 3984 Insert-I-129 - Brem.ms7	1.54E-20	1.87E-22	1.75E-22	2.12E-24
LS-3979A-Base with 3984 Insert-P-32 - Brem.ms7	4.39E+05	5.31E+03	3.90E+03	4.72E+01
LS-3979A-Base with 3984 Insert-P-33 - Brem.ms7	3.09E-08	3.70E-10	3.13E-10	3.75E-12
LS-3979A-Base with 3984 Insert-Sr-90 - Brem.ms7	4.95E+02	5.95E+00	4.58E+00	5.51E-02
LS-3979A-Base with 3984 Insert-Y-90 - Brem.ms7	9.45E+05	1.14E+04	8.45E+03	1.02E+02

From Cember, p131: "For Helth Physics purposes, it is assumed that all bremsstrahlung photons are of the maximum energy".

Appendix C: MicroShield Calculations

Contents

#	Microshield File Ref.
	3983
1	LS-3979A-Base with 3983 Insert-Ac-225.ms7
2	LS-3979A-Base with 3983 Insert-Ac-227.ms7
3	LS-3979A-Base with 3983 Insert-Ac-228.ms7
4	LS-3979A-Base with 3983 Insert-Am-241.ms7
5	LS-3979A-Base with 3983 Insert-As-77.ms7
6	LS-3979A-Base with 3983 Insert-Au-198.ms7
7	LS-3979A-Base with 3983 Insert-Ba-131.ms7
8	LS-3979A-Base with 3983 Insert-C-14 - Brem.ms7
9	LS-3979A-Base with 3983 Insert-Co-60.ms7
10	LS-3979A-Base with 3983 Insert-Cs-131.ms7
11	LS-3979A-Base with 3983 Insert-Cs-134.ms7
12	LS-3979A-Base with 3983 Insert-Cs-137.ms7
13	LS-3979A-Base with 3983 Insert-Cu-67.ms7
14	LS-3979A-Base with 3983 Insert-Hg-203.ms7
15	LS-3979A-Base with 3983 Insert-Ho-166.ms7
16	LS-3979A-Base with 3983 Insert-I-125.ms7
17	LS-3979A-Base with 3983 Insert-I-129 - Brem.ms7
18	LS-3979A-Base with 3983 Insert-I-131.ms7
19	LS-3979A-Base with 3983 Insert-In-111.ms7
20	LS-3979A-Ir192-t0-Base with 3983 Insert.ms7
21	LS-3979A-Base with 3983 Insert-Ir-194.ms7
22	LS-3979A-Base with 3983 Insert-Kr-79.ms7
23	LS-3979A-Base with 3983 Insert-Lu-177.ms7
24	LS-3979A-Base with 3983 Insert-Mo-99.ms7
25	LS-3979A-Base with 3983 Insert-Na-24.ms7
26	LS-3979A-Base with 3983 Insert-Np-237.ms7
27	LS-3979A-Base with 3983 Insert-P-32 - Brem.ms7
28	LS-3979A-Base with 3983 Insert-P-33 - Brem.ms7
29	LS-3979A-Base with 3983 Insert-Pb-203.ms7
30	LS-3979A-Base with 3983 Insert-Pb-210.ms7
31	LS-3979A-Base with 3983 Insert-Pd-109.ms7
32	LS-3979A-Base with 3983 Insert-Pu-238.ms7
33	LS-3979A-Base with 3983 Insert-Pu-239.ms7
34	LS-3979A-Base with 3983 Insert-Pu-240.ms7
35	LS-3979A-Base with 3983 Insert-Pu-241.ms7
36	LS-3979A-Base with 3983 Insert-Ra-223.ms7
37	LS-3979A-Base with 3983 Insert-Ra-224.ms7
38	LS-3979A-Base with 3983 Insert-Ra-226.ms7
39	LS-3979A-Base with 3983 Insert-Re-186.ms7
40	LS-3979A-Base with 3983 Insert-Re-188.ms7
41	LS-3979A-Base with 3983 Insert-Rh-105.ms7
42	LS-3979A-Base with 3983 Insert-Se-75.ms7
43	LS-3979A-Base with 3983 Insert-Sm-153.ms7
44	LS-3979A-Base with 3983 Insert-Sr-89.ms7
45	LS-3979A-Base with 3983 Insert-Sr-90 - Brem.ms7
46	LS-3979A-Base with 3983 Insert-Tb-161.ms7
47	LS-3979A-Base with 3983 Insert-Th-227.ms7
48	LS-3979A-Base with 3983 Insert-Th-228.ms7
49	LS-3979A-Base with 3983 Insert-Tl-201.ms7
50	LS-3979A-Base with 3983 Insert-U-235.ms7
51	LS-3979A-Base with 3983 Insert-W-187.ms7
52	LS-3979A-Base with 3983 Insert-W-188.ms7
53	LS-3979A-Base with 3983 Insert-Xe-133.ms7
54	LS-3979A-Base with 3983 Insert-Y-90 - Brem.ms7
55	LS-3979A-Base with 3983 Insert-Yb-169.ms7
56	LS-3979A-Base with 3983 Insert-Yb-175.ms7

#	Microshield File Ref.
	3984
57	LS-3979A-Base with 3984 Insert-Ac-225.ms7
58	LS-3979A-Base with 3984 Insert-Ac-227.ms7
59	LS-3979A-Base with 3984 Insert-Ac-228.ms7
60	LS-3979A-Base with 3984 Insert-Am-241.ms7
61	LS-3979A-Base with 3984 Insert-As-77.ms7
62	LS-3979A-Base with 3984 Insert-Au-198.ms7
63	LS-3979A-Base with 3984 Insert-Ba-131.ms7
64	LS-3979A-Base with 3984 Insert-C-14 - Brem.ms7
65	LS-3979A-Base with 3984 Insert-Co-60.ms7
66	LS-3979A-Base with 3984 Insert-Cs-131.ms7
67	LS-3979A-Base with 3984 Insert-Cs-134.ms7
68	LS-3979A-Base with 3984 Insert-Cs-137.ms7
69	LS-3979A-Base with 3984 Insert-Cu-67.ms7
70	LS-3979A-Base with 3984 Insert-Hg-203.ms7
71	LS-3979A-Base with 3984 Insert-Ho-166.ms7
72	LS-3979A-Base with 3984 Insert-I-125.ms7
73	LS-3979A-Base with 3984 Insert-I-129 - Brem.ms7
74	LS-3979A-Base with 3984 Insert-I-131.ms7
75	LS-3979A-Base with 3984 Insert-In-111.ms7
76	LS-3979A-Ir192-t0-Base with 3984 Insert.ms7
77	LS-3979A-Base with 3984 Insert-Ir-194.ms7
78	LS-3979A-Base with 3984 Insert-Kr-79.ms7
79	LS-3979A-Base with 3984 Insert-Lu-177.ms7
80	LS-3979A-Base with 3984 Insert-Mo-99.ms7
81	LS-3979A-Base with 3984 Insert-Na-24.ms7
82	LS-3979A-Base with 3984 Insert-Np-237.ms7
83	LS-3979A-Base with 3984 Insert-P-32 - Brem.ms7
84	LS-3979A-Base with 3984 Insert-P-33 - Brem.ms7
85	LS-3979A-Base with 3984 Insert-Pb-203.ms7
86	LS-3979A-Base with 3984 Insert-Pb-210.ms7
87	LS-3979A-Base with 3984 Insert-Pd-109.ms7
88	LS-3979A-Base with 3984 Insert-Pu-238.ms7
89	LS-3979A-Base with 3984 Insert-Pu-239.ms7
90	LS-3979A-Base with 3984 Insert-Pu-240.ms7
91	LS-3979A-Base with 3984 Insert-Pu-241.ms7
92	LS-3979A-Base with 3984 Insert-Ra-223.ms7
93	LS-3979A-Base with 3984 Insert-Ra-224.ms7
94	LS-3979A-Base with 3984 Insert-Ra-226.ms7
95	LS-3979A-Base with 3984 Insert-Re-186.ms7
96	LS-3979A-Base with 3984 Insert-Re-188.ms7
97	LS-3979A-Base with 3984 Insert-Rh-105.ms7
98	LS-3979A-Base with 3984 Insert-Se-75.ms7
99	LS-3979A-Base with 3984 Insert-Sm-153.ms7
100	LS-3979A-Base with 3984 Insert-Sr-89.ms7
101	LS-3979A-Base with 3984 Insert-Sr-90 - Brem.ms7
102	LS-3979A-Base with 3984 Insert-Tb-161.ms7
103	LS-3979A-Base with 3984 Insert-Th-227.ms7
104	LS-3979A-Base with 3984 Insert-Th-228.ms7
105	LS-3979A-Base with 3984 Insert-Tl-201.ms7
106	LS-3979A-Base with 3984 Insert-U-235.ms7
107	LS-3979A-Base with 3984 Insert-W-187.ms7
108	LS-3979A-Base with 3984 Insert-W-188.ms7
109	LS-3979A-Base with 3984 Insert-Xe-133.ms7
110	LS-3979A-Base with 3984 Insert-Y-90 - Brem.ms7
111	LS-3979A-Base with 3984 Insert-Yb-169.ms7
112	LS-3979A-Base with 3984 Insert-Yb-175.ms7

#	Microshield File Ref.
	3986
113	LS-3979A-Base with 3986 Insert-Ac-225.ms7
114	LS-3979A-Base with 3986 Insert-Ac-227.ms7
115	LS-3979A-Base with 3986 Insert-Ac-228.ms7
116	LS-3979A-Base with 3986 Insert-Am-241.ms7
117	LS-3979A-Base with 3986 Insert-As-77.ms7
118	LS-3979A-Base with 3986 Insert-Au-198.ms7
119	LS-3979A-Base with 3986 Insert-Ba-131.ms7
120	LS-3979A-Base with 3986 Insert-C-14 - Brem.ms7
121	LS-3979A-Base with 3986 Insert-Co-60.ms7
122	LS-3979A-Base with 3986 Insert-Cs-131.ms7
123	LS-3979A-Base with 3986 Insert-Cs-134.ms7
124	LS-3979A-Base with 3986 Insert-Cs-137.ms7
125	LS-3979A-Base with 3986 Insert-Cu-67.ms7
126	LS-3979A-Base with 3986 Insert-Hg-203.ms7
127	LS-3979A-Base with 3986 Insert-Ho-166.ms7
128	LS-3979A-Base with 3986 Insert-I-125.ms7
129	LS-3979A-Base with 3986 Insert-I-129 - Brem.ms7
130	LS-3979A-Base with 3986 Insert-I-131.ms7
131	LS-3979A-Base with 3986 Insert-In-111.ms7
132	LS-3979A-Ir192-t0-Base with 3986 Insert.ms7
133	LS-3979A-Base with 3986 Insert-Ir-194.ms7
134	LS-3979A-Base with 3986 Insert-Kr-79.ms7
135	LS-3979A-Base with 3986 Insert-Lu-177.ms7
136	LS-3979A-Base with 3986 Insert-Mo-99.ms7
137	LS-3979A-Base with 3986 Insert-Na-24.ms7
138	LS-3979A-Base with 3986 Insert-Np-237.ms7
139	LS-3979A-Base with 3986 Insert-P-32 - Brem.ms7
140	LS-3979A-Base with 3986 Insert-P-33 - Brem.ms7
141	LS-3979A-Base with 3986 Insert-Pb-203.ms7
142	LS-3979A-Base with 3986 Insert-Pb-210.ms7
143	LS-3979A-Base with 3986 Insert-Pd-109.ms7
144	LS-3979A-Base with 3986 Insert-Pu-238.ms7
145	LS-3979A-Base with 3986 Insert-Pu-239.ms7
146	LS-3979A-Base with 3986 Insert-Pu-240.ms7
147	LS-3979A-Base with 3986 Insert-Pu-241.ms7
148	LS-3979A-Base with 3986 Insert-Ra-223.ms7
149	LS-3979A-Base with 3986 Insert-Ra-224.ms7
150	LS-3979A-Base with 3986 Insert-Ra-226.ms7
151	LS-3979A-Base with 3986 Insert-Re-186.ms7
152	LS-3979A-Base with 3986 Insert-Re-188.ms7
153	LS-3979A-Base with 3986 Insert-Rh-105.ms7
154	LS-3979A-Base with 3986 Insert-Se-75.ms7
155	LS-3979A-Base with 3986 Insert-Sm-153.ms7
156	LS-3979A-Base with 3986 Insert-Sr-89.ms7
157	LS-3979A-Base with 3986 Insert-Sr-90 - Brem.ms7
158	LS-3979A-Base with 3986 Insert-Tb-161.ms7
159	LS-3979A-Base with 3986 Insert-Th-227.ms7
160	LS-3979A-Base with 3986 Insert-Th-228.ms7
161	LS-3979A-Base with 3986 Insert-Tl-201.ms7
162	LS-3979A-Base with 3986 Insert-U-235.ms7
163	LS-3979A-Base with 3986 Insert-W-187.ms7
164	LS-3979A-Base with 3986 Insert-W-188.ms7
165	LS-3979A-Base with 3986 Insert-Xe-133.ms7
166	LS-3979A-Base with 3986 Insert-Y-90 - Brem.ms7
167	LS-3979A-Base with 3986 Insert-Yb-169.ms7
168	LS-3979A-Base with 3986 Insert-Yb-175.ms7

#	Microshield File Ref.
	No Insert
169	LS-3979A-Base withou Insert-Ac-227.ms7
170	LS-3979A-Base without Insert-Ac-225.ms7
171	LS-3979A-Base without Insert-Ac-228.ms7
172	LS-3979A-Base without Insert-Am-241.ms7
173	LS-3979A-Base without Insert-As-77.ms7
174	LS-3979A-Base without Insert-Au-198.ms7
175	LS-3979A-Base without Insert-Ba-131.ms7
176	LS-3979A-Base without Insert-C-14 - Brem.ms7
177	LS-3979A-Base without Insert-Co-60.ms7
178	LS-3979A-Base without Insert-Cs-131.ms7
179	LS-3979A-Base without Insert-Cs-134.ms7
180	LS-3979A-Base without Insert-Cs-137.ms7
181	LS-3979A-Base without Insert-Cu-67.ms7
182	LS-3979A-Base without Insert-Hg-203.ms7
183	LS-3979A-Base without Insert-Ho-166.ms7
184	LS-3979A-Base without Insert-I-125.ms7
185	LS-3979A-Base without Insert-I-129 - Brem.ms7
186	LS-3979A-Base without Insert-I-131.ms7
187	LS-3979A-Base without Insert-In-111.ms7
188	LS-3979A-Ir192-t0-Base without Insert.ms7
189	LS-3979A-Base without Insert-Ir-194.ms7
190	LS-3979A-Base without Insert-Kr-79.ms7
191	LS-3979A-Base without Insert-Lu-177.ms7
192	LS-3979A-Base without Insert-Mo-99.ms7
193	LS-3979A-Base without Insert-Na-24.ms7
194	LS-3979A-Base without Insert-Np-237.ms7
195	LS-3979A-Base without Insert-P-32 - Brem.ms7
196	LS-3979A-Base without Insert-P-33 - Brem.ms7
197	LS-3979A-Base without Insert-Pb-203.ms7
198	LS-3979A-Base without Insert-Pb-210.ms7
199	LS-3979A-Base without Insert-Pd-109.ms7
200	LS-3979A-Base without Insert-Pu-238.ms7
201	LS-3979A-Base without Insert-Pu-239.ms7
202	LS-3979A-Base without Insert-Pu-240.ms7
203	LS-3979A-Base without Insert-Pu-241.ms7
204	LS-3979A-Base without Insert-Ra-223.ms7
205	LS-3979A-Base without Insert-Ra-224.ms7
206	LS-3979A-Base without Insert-Ra-226.ms7
207	LS-3979A-Base without Insert-Re-186.ms7
208	LS-3979A-Base without Insert-Re-188.ms7
209	LS-3979A-Base without Insert-Rh-105.ms7
210	LS-3979A-Base without Insert-Se-75.ms7
211	LS-3979A-Base without Insert-Sm-153.ms7
212	LS-3979A-Base without Insert-Sr-89.ms7
213	LS-3979A-Base without Insert-Sr-90 - Brem.ms7
214	LS-3979A-Base without Insert-Tb-161.ms7
215	LS-3979A-Base without Insert-Th-227.ms7
216	LS-3979A-Base without Insert-Th-228.ms7
217	LS-3979A-Base without Insert-Tl-201.ms7
218	LS-3979A-Base without Insert-U-235.ms7
219	LS-3979A-Base without Insert-W-187.ms7
220	LS-3979A-Base without Insert-W-188.ms7
221	LS-3979A-Base without Insert-Xe-133.ms7
222	LS-3979A-Base without Insert-Y-90 - Brem.ms7
223	LS-3979A-Base without Insert-Yb-169.ms7
224	LS-3979A-Base without Insert-Yb-175.ms7